

Environment-dependent crystal-field tight-binding
based on density-functional theory

*Umgebungsabhängiges Kristallfeld-Tight-Binding
basierend auf Dichtefunktionaltheorie*

Der Naturwissenschaftlichen Fakultät
der Friedrich–Alexander–Universität Erlangen–Nürnberg

zur

Erlangung eines Doktorgrades Dr. rer. nat.

vorgelegt von

Alexander Urban

aus Duisburg



FRIEDRICH–ALEXANDER
UNIVERSITÄT
ERLANGEN–NÜRNBERG

Als Dissertation genehmigt von der Naturwissenschaftlichen Fakultät
der Friedrich–Alexander–Universität Erlangen–Nürnberg

Datum der mündlichen Prüfung:	14. Dezember 2012
Vorsitzender der Promotionskommission:	Prof. Dr. Johannes Barth
Erstberichterstatter:	Prof. Dr. Bernd Meyer
Zweitberichterstatter:	Prof. Dr. Christian Elsässer

Meiner geliebten Oma

Kurzzusammenfassung

Elektronenstrukturechnungen basierend auf Kohn–Sham Dichtefunktionaltheorie (DFT) erlauben genaue Vorhersagen von chemischem Verhalten und Materialeigenschaften von Strukturen bis zu einer Größe von einigen hundert Atomen, was einer Längenskala von wenigen Nanometern entspricht. Viele technologisch relevante Prozesse, zum Beispiel im Bereich der Nanoelektronik, werden jedoch entscheidend von Phänomenen beeinflusst, die auf einer größeren Längenskala von bis zu 100 Nanometern auftreten und von der Beteiligung zehntausender Atome abhängen. Die Berechnung der Elektronenstruktur derart großer Systeme ist möglich mit der semiempirischen Slater–Koster Tight-Binding (TB) Methode. Im Gegensatz zu der auf *first-principles* basierenden DFT, die universell auf beinahe jedes chemische Element anwendbar ist, beruht TB auf parametrisierten Modellen, welche in der Regel auf eine bestimmte Anwendung oder Stoffklasse spezialisiert sind. Die Anpassung der Modellparameter (Slater–Koster Tabellen) erfolgt üblicherweise empirisch, wobei entweder experimentell ermittelte Materialeigenschaften (Geometrien, elastische Konstanten), oder Ergebnisse von *first-principles* Methoden wie DFT als Zielwerte herangezogen werden. Das Erstellen eines neuen TB Modells ist daher mit einem hohen Aufwand verbunden, dem oft eine geringe Übertragbarkeit der Parametrisierung gegenübersteht.

In dieser Arbeit entwickeln wir eine systematische Herangehensweise, um akkurate und übertragbare TB Modelle aus DFT-Rechnungen abzuleiten. Hierbei wird die formelle Beziehung der beiden Methoden ausgenutzt, wonach die TB Gesamtenergie als Approximation des Kohn–Sham Energiefunktionalen verstanden werden kann. Unser Vorgehen unterscheidet sich hierbei konzeptionell von früheren Ansätzen wie der DFTB Methode, da die TB Parameter aus den konvergierten DFT Wellenfunktionen und Hamiltonmatrizen beliebiger Referenzstrukturen ermittelt werden können.

Ableitung von Tight–Binding Parametern aus Dichtefunktionaltheorie

Wir beschreiben eine neue Herangehensweise zur Ableitung von Slater–Koster Parametern aus den Ergebnissen von DFT Rechnungen. In unserer Methode werden DFT

Wellenfunktionen (Kohn–Sham Orbitale) beliebiger Referenzstrukturen, die bezüglich einer numerisch konvergierten Basis aus atomzentrierten Funktionen und ebenen Wellen dargestellt sind, mithilfe eines Projektionsverfahrens auf eine minimale Basis von Atomorbitalen (AOs) abgebildet. Anschließend können die Matrixelemente der Minimalbasisdarstellung des Hamiltonoperators aus den DFT-Ergebnissen berechnet werden. Dreizentrenbeiträge werden hierbei gemittelt erfasst, da diese in der TB Methode nicht explizit beschrieben sind. Anhand der Beispiele Kohlenstoff und Titan wird das Projektionsverfahren vorgestellt und die Genauigkeit der resultierenden TB Parameter demonstriert.

Optimierung von minimalen Atomorbitalbasissätzen

Die Qualität der mithilfe des Projektionsverfahrens ermittelten TB Parameter hängt entscheidend von der Wahl der verwendeten minimalen AO Basis ab. Die Darstellung der DFT Wellenfunktionen in einer AO Minimalbasis ist in der Regel nicht vollständig; folglich gehen bei der Projektion Informationen verloren. Wir haben mehrere Verfahren zur Optimierung von AO Basissätzen entwickelt, die es ermöglichen, diesen Verlust zu minimieren. Nicht nur die Qualität des Basissatzes, sondern auch die Ausdehnung der AOs beeinflusst die Übertragbarkeit und Strukturabhängigkeit der Bindungsintegrale. Wir verwenden daher die neuen Optimierungsverfahren, um die bestmögliche AO-Basis zu einer vorgegebenen Reichweite zu ermitteln. Anhand der Fallbeispiele Kohlenstoff und Titan illustrieren wir die erreichte Verbesserung der Minimalbasisdarstellung, sowie die Übertragbarkeit der optimierten AOs auf verschiedene Strukturen.

Beschreibung von Kristallfeldaufspaltung in der Tight–Binding Methode

Der Projektionsformalismus erlaubt nicht nur die Berechnung konventioneller TB Parameter, also der Bindungs- und Überlappintegrale über zwei an unterschiedlichen Atomzentren lokalisierte Orbitale, sondern ermöglicht es darüber hinaus, die Diagonalelemente (*On-Site* Elemente) der Hamiltonmatrizen zu analysieren. Die *On-Site* Elemente beinhalten die Wechselwirkung zweier an dem selben Atomzentrum lokali-

sierter Orbitale mit dem effektiven Gesamtpotential aller Atome, dem Kristall- oder Ligandenfeld. Diese *Kristallfeldwechselwirkung* führt in Strukturen nichtsphärischer Symmetrie zu einer (spektroskopisch messbaren) Aufspaltung der atomaren Eigenzustände. In konventionellen TB Modellen ist diese Art der Wechselwirkung nicht erfasst, da die On-Site Elemente als strukturunabhängige Konstanten behandelt werden. Wir stellen eine verallgemeinerte TB Methode vor, das Crystal-Field Tight-Binding (CF-TB), welches eine umgebungsabhängige Parametrisierung der On-Site Elemente beinhaltet. Es wird gezeigt, dass CF-TB die Genauigkeit der TB Methode insbesondere für Strukturen niedriger Symmetrie, wie sie zum Beispiel bei Molekulardynamiksimulationen auftreten, erheblich verbessert.

Eichung von Eigenwerten und Bindungsintegralen

Um die Hamiltonmatrizen und Eigenwerte verschiedener atomarer oder molekularer Strukturen vergleichen zu können, muss eine einheitliche Potentialreferenz gewährleistet sein. Bei isolierten Systemen ist die potentielle Energie des Vakuums eine praktikable Wahl für den Energienullpunkt. Im Falle dreidimensionaler periodischer Kristalle ist das Vakuumniveau jedoch nicht direkt verfügbar. Wir demonstrieren, dass die strukturabhängige On-Site Parametrisierung der CF-TB Methode für die Eichung von Eigenwerten und Bindungsintegralen verschiedener Referenzstrukturen geeignet ist. Wir beobachten, dass eine günstige Wahl des Potentialnullpunkts zu einer verminderten Strukturabhängigkeit der Bindungsintegrale, und somit zu übertragbareren TB Parametern führt.

Bandsommen und Kohäsionsenergie

Die Berechnung von Kohäsionsenergien und atomaren Kräften mit der TB Methode erfordert nebst der Slater-Koster Parametrisierung der Bandstruktur noch die Beschreibung der Kern-Kern Abstoßung und des *Double-Counting* Beitrags. In der Regel erfolgt dies durch empirische, atomare Wechselwirkungspotentiale. Verschiedene Eigenwerteichungen und daraus resultierende Bindungsintegrale führen jedoch zu unterschiedlichen Bandsommen, sodass die Wahl des Wechselwirkungspotentials

nicht eindeutig ist. Es ist allerdings möglich, geeignete Energiebeiträge zwischen der Bandsumme und dem empirischen Potential umzuverteilen, und die Qualität eines TB Gesamtenergiemodells kann entscheidend von dieser Energieaufteilung abhängen. Wir haben verschiedene Möglichkeiten zur Energieaufteilung berücksichtigt und deren Anwendbarkeit in Verbindung mit Kohlenstoff CF-TB Modellen untersucht. Unser Ergebnis zeigt, dass es ausgehend von CF-TB Parametern nicht möglich ist, ein einfaches TB *Band* Modell zu konstruieren. Es ist vielmehr notwendig, eine TB *Bond* Beschreibung einzuführen.

Abstract

Electronic structure calculations based on Kohn–Sham density-functional theory (DFT) allow the accurate prediction of chemical bonding and materials properties. Due to the high computational demand DFT calculations are, however, restricted to structures containing at most several hundreds of atoms, i. e. to length scales of a few nanometers. Though, many processes of technological relevance, for example in the field of nanoelectronics, are governed by phenomena that occur on a slightly larger length scale of up to 100 nanometers, which corresponds to tens of thousands of atoms. The semiempirical Slater–Koster tight-binding (TB) method makes it feasible to calculate the electronic structure of such large systems. In contrast to *first-principles*-based DFT, which is universally applicable to almost all chemical species, the TB method is based on parametrized models that are usually specialized for a particular application or for one certain class of compounds. Usually the model parameters (Slater–Koster tables) are empirically adjusted to reproduce either experimental reference data (e. g. geometries, elastic constants) or data from first-principles methods such as DFT. The construction of a new TB model is therefore connected with a considerable effort that is often contrasted by a low transferability of the parametrization.

In this thesis we develop a systematic methodology for the derivation of accurate and transferable TB models from DFT calculations. Our procedure exploits the formal relationship between the two methods, according to which the TB total energy can be understood as a direct approximation of the Kohn–Sham energy functional. The concept of our method is different to previous approaches such as the DFTB method, since it allows to extract TB parameters from converged DFT wave functions and Hamiltonians of arbitrary reference structures.

Derivation of tight-binding parameters from density-functional theory

We introduce a new technique for the systematic derivation of Slater–Koster parameters from the results of DFT calculations. In our approach, the DFT wave functions (Kohn–Sham orbitals) in a numerically converged basis of atom-centered functions and plane waves are mapped onto a minimal basis of atomic orbitals (AOs) using a projection

formalism. This allows the computation of the minimal basis representation of the converged DFT Hamiltonian. Three-center contributions to the Hamilton matrix, which are not treated explicitly in the TB method, are included on average by the methodology. The procedure and the accuracy of the resulting TB parameters is demonstrated for the examples of carbon and titanium.

Optimization of minimal atomic orbital basis sets

The quality of TB parameters obtained using the projection methodology crucially depends on the choice of the minimal AO basis. The minimal basis representation of the Kohn–Sham orbitals is usually not complete, and as a consequence information is lost during the projection. We have therefore developed several schemes for the optimization of AO basis sets that make it possible to minimize this loss. Not only the quality of the basis set, but also the range of the AO basis functions has a significant impact on the transferability and the structure-sensitivity of the bond integrals. We therefore employ the new optimization techniques to determine the best AO basis set for a given cutoff range. The improvement of the minimal basis representation and the transferability of the optimized AOs are validated for carbon and titanium structures as prototypical examples of a covalent main group element and a transition metal.

A tight-binding description of crystal-field splittings

The projection formalism described above is not limited to the calculation of conventional TB parameters, i. e. to bond and overlap integrals over two orbitals that are located at two different atomic sites. It also can be used to analyze the on-site elements of the Hamilton matrix, which contain the interaction of two orbitals at the same atomic site with the effective potential of all atoms in the structure (the *crystal field* or *ligand field*). This crystal field interaction causes the (spectroscopically measurable) splitting of the atomic eigenlevels in structures with non-spherical symmetry. Conventional TB models do not describe such kind of interactions, as the on-site elements are usually treated as structurally independent constants. We introduce an extended crystal-field tight-binding (CF-TB) method, which includes an environment-dependent

on-site parametrization. It is demonstrated that the CF-TB method is substantially more accurate for low-symmetry structures, which, for instance, arise during finite temperature molecular dynamics simulations.

Gauge of eigenvalues and bond integrals

A common potential energy reference is a necessary condition to be able to compare Hamilton matrices and eigenvalues from different structures. For the case of isolated systems, such as molecules or clusters, the potential energy of the vacuum is a convenient choice for the zero point of the potential energy. In three-dimensional periodic crystals the vacuum level is, however, not available. We illustrate that the structure-dependent on-site parameters of a CF-TB model are suitable to gauge eigenvalues and bond integrals of different atomic and molecular structures. Most importantly, with an appropriate choice of potential energy reference, the structure sensitivity of bond integrals can be significantly reduced, thus leading to a substantial increase of the transferability of the TB models.

Band sums and cohesion energy

In addition to the Slater–Koster parametrization of the electronic structure, for the calculation of cohesion energies and atomic forces in TB, a description of the ionic core repulsion and the double-counting corrections is required. Total energy TB implementations usually employ empirical pairwise atomic interaction potentials to account for the missing energy contributions. However, changes in the gauge of the eigenvalues and bond integrals lead to different band sums, so that the choice of the empirical potential is not unique. In fact, it is possible to transfer appropriate energy contributions between the band sum and the empirical pair potential, and the quality of the TB total-energy model may depend upon this energy partitioning. We have considered various options for the energy partitioning and have evaluated their applicability in conjunction with CF-TB total energy expressions. It is shown that it is not possible to construct a simple TB *band* model based on CF-TB parameters, and that it is instead necessary to adopt a tight-binding *bond* description.

Danksagung (Acknowledgment)

Diese Dissertation wäre nicht entstanden ohne die große Unterstützung, die ich durch meine Familie, meine Freunde und Arbeitskollegen erfahren habe.

Allen voran möchte ich mich bei Prof. Dr. Bernd Meyer bedanken, unter dessen Leitung diese Arbeit verwirklicht wurde. Bernd Meyer hatte stets ein offenes Ohr für meine Fragen und wusste diese, oft zu meiner Verwunderung, auch immer sofort zu beantworten. Darüber hinaus hat Bernd Meyer mir immer das Gefühl gegeben, dass er meine Arbeit und meine Pläne unterstützt.

Auch unseren Kooperationspartnern bin ich zu großem Dank verpflichtet. In zahlreichen Projektbesprechungen und Diskussionen sind Ideen entwickelt worden, die letztendlich meine Arbeit beeinflusst und erleichtert haben. Ich bedanke mich daher herzlichst bei (in alphabetischer Reihenfolge) Ralf Drautz, Christian Elsässer, Jan Gehrmann, Paul Kamensky, Aleksey Kolmogorov, Elena Roxana Margine, Matous Mrovec, David Pettifor und Martin Reese.

Prof. Dr. Christian Elsässer danke ich außerdem für das Erstellen des Zweitgutachtens dieser Arbeit. Für die Übernahme des Prüfungsvorsitzes bedanke ich mich bei Prof. Dr. Dirk Zahn, und für seine Arbeit als Zweitprüfer danke ich Prof. Dr. Tim Clark.

Natürlich gebührt auch meinen Kollegen und Freunden im Computer–Chemie–Centrum großer Dank, die während der Monate des Schreibens meinen Launen ausgesetzt waren und mich dennoch durch zum Beispiel Korrekturlesen und Kaffeekochen unterstützt haben. Besonders möchte ich mich bei meinen Bürogefährten Christina Ebensperger, Pawel Rodziewicz und Konstantin Weber für die vielen anregenden Gespräche und Diskussionen bedanken; ebenso bei meinen *Nachbarn* Patrick Duchstein, Philipp Ectors, Theodor Milek und Dirk Zahn. Erwähnt sei noch die *Darts-Connection*, Christof Jäger, Sebastian Schenker, Andreas Krause und Thilo Bauer, die sehr hilfreich dabei war, sich auch mal vor der Arbeit zu drücken. Vielen Dank auch Nadine Scharrer, Isabelle Schraufstetter und Nico van Eikema Hommes, ohne die keine Arbeit am CCC möglich wäre. Für die vielen guten Anregungen und Ratschläge und speziell für das

angenehme Arbeitsklima gilt auch den Kollegen, die hier nicht namentlich erwähnt werden mein Dank.

Bei der Graduate School Molecular Science und bei PD Dr. Norbert Jux bedanke ich mich für die Möglichkeit an Tagungen und Workshops teilnehmen zu können. Den Fonds der Chemischen Industrie danke ich für ein Kekulé Stipendium, welches nicht nur meinen Lebensunterhalt über den Großteil meiner Promotionszeit gesichert hat, sondern auch wichtige Sachmittel zur Verfügung gestellt hat.

Mein spezieller Dank (*Grazie mille!*) gebührt Prof. Dr. Nicola Marzari und seiner Arbeitsgruppe – insbesondere Oliviero Andreussi, Andrea Cepellotti, Daniele Dragoni und David O'Regan. In den drei Monaten in Lausanne, habe ich nicht nur vieles gelernt, sondern auch Freundschaften geschlossen.

Für ihre unbedingte Unterstützung und für das Gefühl, dass alles einen Sinn ergibt, muss ich mich bei meiner Freundin Nong bedanken. Ohne ihre anhaltende Motivation und ohne ihre Liebe wäre vieles nicht möglich gewesen.

Mein größter Dank gilt abschließend jedoch meiner Familie, der ich ob meiner Arbeit in den letzten Jahren leider viel zu wenig Zeit gewidmet habe. Trotzdem konnte ich mich immer auf den Rückhalt in meiner Familie verlassen.

Notation and constants

A scalar	a
The complex conjugate of a	a^*
The real part of a	$\text{Re}(a)$
The imaginary part of a	$\text{Im}(a)$
A vector	\mathbf{c}
The zero vector	$\mathbf{0}$
The i -th component of \mathbf{c}	c_i
A normalized vector	$\hat{\mathbf{n}}$
A matrix	\mathbf{A}
The (i, j) -th matrix element of \mathbf{A}	$A_{ij} = (\mathbf{A})_{ij}$
The transposed of \mathbf{A}	\mathbf{A}^T
The inverse of \mathbf{A}	\mathbf{A}^{-1}
The conjugate transposed of \mathbf{A}	$\mathbf{A}^\dagger = (\mathbf{A}^*)^T$
The determinant of \mathbf{A}	$\det(\mathbf{A})$
The trace of \mathbf{A}	$\text{tr}(\mathbf{A})$
The identity matrix	\mathbf{I}
The identity operation	$\mathbb{1}$
An operator	\hat{O}

Where not explicitly stated, all equations are given in Hartree atomic units (a.u.):

Electronic charge	$e = 1$ a.u.
Reduced Planck constant	$\hbar = 1$ a.u.
Mass of the electron	$m_e = 1$ a.u.

Contents

Kurzzusammenfassung	i
Abstract	v
Danksagung (Acknowledgment)	ix
Notation and constants	xi
I. Introduction	1
I.1. Atomistic simulations on different scales	1
II. Electronic structure theory	9
II.1. Wave mechanics	10
II.2. Hartree–Fock theory	17
II.3. Density-functional theory	24
II.4. Numerical calculations	31
III. The tight-binding method	33
III.1. Non-self-consistent DFT	33
III.2. The tight-binding method	37
III.3. Implementations of the TB method	42
IV. From DFT to tight-binding	53
IV.1. Computational set-up	54
IV.2. Minimal AO basis representation	55
IV.3. Optimization of AO basis sets	58
IV.4. Optimized minimal basis sets	65
IV.5. Derivation of tight-binding parameters	75

V. Crystal-field interactions in tight-binding	85
V.1. Crystal-field interactions	86
V.2. Parametrization of crystal-field interactions	88
V.3. A crystal-field tight-binding model for carbon	95
V.4. A crystal-field tight-binding model for titanium	104
VI. Total energy and CF-TB models	111
VI.1. The invariance of the total energy	111
VI.2. Energy partitioning	113
VI.3. Crystal-field tight-binding band sums	115
VII. Summary and Outlook	119
A. Additional derivations	123
A.1. Orbital dependent electron density	123
A.2. Analytic rotation of two-center integrals	125
A.3. Radial Schrödinger equation	126
A.4. Confinement potential	128
B. Tight-binding parameters	131
Bibliography	148
Curriculum vitae	149

List of Figures

I.1.	Schematic comparison of atomistic simulation methods	3
I.2.	Splitting of the d level in an octahedral ligand field	6
II.1.	Flow chart of the Kohn–Sham algorithm	30
III.1.	The real valued spherical harmonics	39
III.2.	Schematic of the Slater–Koster reference s and p bonds	40
III.3.	Schematic of the Slater–Koster reference d bonds	41
IV.1.	Contracted carbon s radial function	60
IV.2.	Carbon $2s$ radial functions (confinement potential)	62
IV.3.	Auxiliary basis for carbon radial functions.	63
IV.4.	Optimized carbon radial functions for different cutoff radii	67
IV.5.	Change of the electronic spillage with the range of the AO basis	68
IV.6.	Comparison of optimized carbon radial functions	68
IV.7.	Optimized radial functions for different carbon structures	71
IV.8.	Electronic spillage using an optimized carbon basis	72
IV.9.	Energy spillage in carbon structures using optimized AO basis sets . .	72
IV.10.	Radial basis for titanium atomic orbitals	74
IV.11.	Optimized basis for the titanium $3d$ and $4s$ orbitals	75
IV.12.	Overlap matrix elements of an optimized carbon basis	80
IV.13.	Periodic slab models of the diamond (100) and (111) surfaces	81
IV.14.	Carbon Hamilton matrix elements (vacuum reference)	82
IV.15.	Carbon TB band structures densities of states (vacuum reference) . . .	84

V.1.	Off-diagonal on-site elements (schematic)	86
V.2.	On-site Hamilton matrix elements of the carbon dimer	87
V.3.	Effective potential of a linear atom chain (schematic)	90
V.4.	Superposition of Coulomb potentials for an atom chain	92
V.5.	Derivation of CF-TB models (flowchart)	94
V.6.	Carbon dimer on-site elements: $2s^1 2p^3$ vs. $2s^2 2p^2$	96
V.7.	Carbon dimer on-site elements for different AO basis sets	97
V.8.	Carbon on-site elements for graphene and the alkyne chain	98
V.9.	Diamond Hamilton matrix elements (on-site gauge)	99
V.10.	Carbon Hamilton matrix elements (on-site gauge)	100
V.11.	Carbon CF-TB band structures densities of states	102
V.12.	Carbon Hamilton matrix elements (gauge comparison)	103
V.13.	Band structures of distorted graphene	104
V.14.	Titanium overlap matrix elements	105
V.15.	Titanium dimer on-site Hamilton matrix elements	106
V.16.	Titanium dimer off-diagonal on-site elements (fit)	107
V.17.	Titanium Hamilton matrix elements	108
V.18.	Carbon CF-TB band structures densities of states	110
VI.1.	Comparison of tight-binding carbon band sums	115
VI.2.	Comparison of corrected tight-binding carbon band sums	117
VII.1.	Band structure and DOS of an infinite alkyne chain (TB vs. CF-TB) . .	121

List of Tables

IV.1. Carbon–carbon distances for different hybridizations 66

IV.2. Parameters of optimized carbon radial functions 69

IV.3. Titanium–titanium distances for different crystal structures 73

IV.4. Parameters of optimized titanium radial functions 76

B.1. Carbon atomic eigenvalues 132

B.2. Carbon–carbon overlap matrix parameters 132

B.3. Carbon–carbon Hamilton matrix parameters (vacuum reference) 133

B.4. Carbon–carbon crystal-field parameters 134

B.5. Carbon–carbon Hamilton matrix parameters (on-site gauge) 135

B.6. Titanium atomic eigenvalues 136

B.7. Titanium–titanium overlap matrix parameters 136

B.8. Titanium–titanium crystal-field parameters (s level gauge) 137

B.9. Titanium–titanium Hamilton matrix parameters (s level gauge) 138

B.10. Titanium–titanium Hamilton matrix parameters (vacuum level gauge) 138

B.11. Titanium–titanium crystal-field parameters (vacuum level gauge) . . . 139

I. Introduction

I.1. Atomistic simulations on different scales

To measure is to know has long been the tenor in natural science.* Nowadays, we have theoretical methods at hand that are based on experimentally determined physical constants and that are able to describe many aspects of nature with an accuracy that is superior to the experimental precision at the time when the theories were developed. Notably, at the atomic and electronic scales the quantum mechanics described by Schrödinger's famous equation has been tremendously successful.¹ Nowadays, if we stay within the experimentally verified bounds of the theory we might therefore also proclaim that *to calculate is to know*.

I.1.1. Scales and approximations

While the last statement is in principle correct, the Schrödinger equations arising from the full electronic description of even simple structures (say small molecules) are utterly complex and it is usually unfeasible to solve them analytically. In practice one has to resort to approximate methods that can be solved in a numerical fashion.

One such approximate method is density-functional theory (DFT),² which has become very popular during the last two decades and is now widely accepted as a tool for quantitative studies on the molecular and atomic levels. DFT is based on *first principles* and its implementations typically depend on just a small number of physically motivated approximations. The method is applicable to almost all chemical elements and

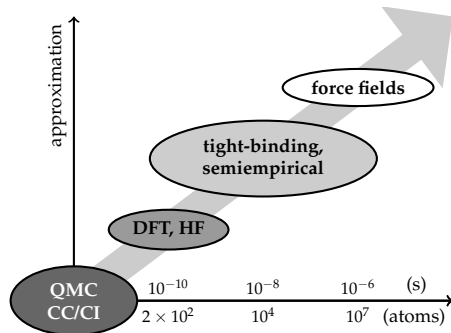
*The German idiom *Messen ist Wissen* is sometimes attributed to Georg Simon Ohm (1789–1854).

can be used to calculate the cohesive energies, the atomic forces and derived quantities for periodic crystals, surfaces, clusters, and molecules. Based on the long experience with the method the error bars of DFT results can also be well estimated. The accuracy of density-functional theory comes, however, at the trade-off to be computationally very demanding. DFT calculations using well-established implementations are on current computing systems therefore limited to a maximum of a few hundred atoms, depending on the chemical species. The simulation of atomic and molecular dynamics using DFT is (depending on the system size) restricted to time scales of much less than one nanosecond. These limitations make it impossible to use DFT to simulate many important phenomena that occur on either larger length or time scales. There are countless examples, such as crystal growth, aggregation of molecules, extended materials defects, phase transitions, and protein folding.

To simulate larger structures of possibly millions of atoms and longer time scales up to microseconds atomic interaction potentials (force fields) are often suitable. Specialized potentials have been developed for the structural optimization and for the simulation of the dynamics of various classes of materials, such as covalent solids and molecules,³⁻⁶ metals,^{7,8} and large organic and biochemical molecules.⁹⁻¹² Although based on various different functional forms, most interaction potentials have in common that they do not provide any information about the electronic structure. Note that especially force fields used in *molecular mechanics* simulations do commonly require atomic bond definitions as input and do not allow for the formation or the cleavage of bonds during a simulation. In general, atomic interaction potentials possess complex functional forms with many empirical parameters, which are adjusted to reproduce either experimental geometries or energies, or data from first principles calculations.

If one is interested in the electronic structure of large systems or if interatomic potentials are not accurate enough for the desired application, one option is to turn to semiempirical methods, which lie conceptually between empirical force fields and *first principles* methods and allow for the treatment of tens of thousands of atoms.¹³⁻¹⁸ Semiempirical electronic structure methods can be understood as direct approximations

Figure I.1. Schematic comparison of atomistic simulation methods. The selected methods for each degree of approximation do not represent an exhaustive set, but are merely examples. Methods referred to by abbreviation in the diagram are quantum Monte-Carlo (QMC), coupled cluster (CC), configuration interaction (CI), density-functional theory (DFT), and Hartree-Fock (HF).



to more accurate methods (usually DFT or Hartree-Fock), but additionally include empirical parameters that can be tuned to reproduce reference data. A schematic comparison of the different approaches is shown in Fig. I.1. One particular example of a semiempirical method is the tight-binding (TB) electronic structure method that is subject of this thesis.^{14,19}

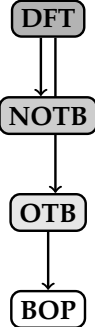
I.1.2. Parametrization and transferability

The common feature of empirical interatomic potentials and semiempirical electronic structure methods is their dependence on an empirical parametrization. Usually the model parameters are adjusted to reproduce either experimental structures and energies or data (energies, forces, eigenvalues, etc.) from more accurate electronic structure methods such as DFT. These have also been the traditional approaches to derive semiempirical tight-binding models.^{20–22} Independent of the origin of the reference data, the resulting parametrization will be most accurate for those structures that are similar to the ones in the reference set and the transferability to structurally or chemically different materials is not *per se* guaranteed. The predictive power of empirical and semiempirical methods is therefore difficult to estimate.

Additionally, parameter fitting is a very time-consuming process that starts with the proper preparation and verification of the reference data. Most atomic interaction potentials and semiempirical electronic structure methods employ pairwise bond pa-

rameters, which means that a model for N chemical elements includes parametrizations for $(N^2 + N)/2 = \mathcal{O}(N^2)$ different atomic interactions.* To name just one example, a typical steel contains ten to fifteen different chemical elements that are all relevant for the mechanical and chemical properties of the material.^{24,25} The simulation of 15 different chemical species would require 120 pairwise parametrizations that in turn all need to be carefully fitted to an exhaustive set of reference data. The resulting force field would, however, be specialized for a single class of materials (steels) and would most certainly not be accurate for the simulation of, for example, molecules. Thus, it is advisable to search for alternative means to derive potential parameters that avoid such a cumbersome manual adjustment.

I.1.3. Parameters based on first principles



Instead of empirically fitting the parameters of interaction potentials and semiempirical electronic structure methods, the relation between methods of different levels of approximation may be exploited. This way each model is hierarchically derived from the next, more accurate one and ultimately from first principles. The formal relation between the tight-binding method and density-functional theory has been established in the 1980s by Harris and Foulkes.^{26–28} By further approximating orthogonal tight-binding models[†] one arrives at reactive bond-order potentials (BOPs), which are interatomic potentials suitable for large-scale simulations.^{6,29,30} Thus, three of the scales depicted in Fig. I.1 are available by systematically approximating density-functional theory and, in principle, extensive fitting of parameters can be avoided.

Various practical ways to derive TB models directly from DFT have been suggested in the literature, a number of which are discussed in Ref. 31. The approaches can be distinguished by the minimal basis sets used for the numerical solution of the Kohn–Sham equations (see also Secs. II.4.1 and II.3.2): the density-functional tight-binding

* Notable exceptions are some semiempirical methods for organic molecules.^{17,18,23}

† See Sec. III.2 for the difference between non-orthogonal and orthogonal TB models.

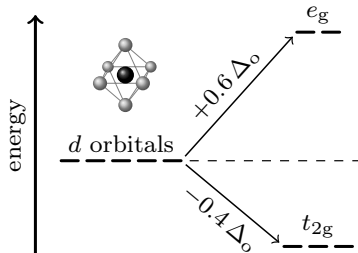
(DFTB) method employs *ad hoc* contracted atomic orbitals as basis functions.³²⁻³⁵ Other schemes employ linear muffin-tin orbitals (LMTOs),³⁶⁻³⁹ quasi-atomic orbitals (QUAMBOs),⁴⁰⁻⁴⁴ or maximally localized Wannier functions (MLWFs).⁴⁵⁻⁴⁷ In the DFTB methodology the TB parameters for each reference bond, the *bond integrals*, are calculated using dimer molecules and incomplete atomic-orbital basis sets; three-center interactions and crystal-field terms can not be taken into account. DFT calculations using LMTO basis sets are, on the other hand, restricted to relatively closed-packed crystal structures. QUAMBOs and MLWFs provide complete minimal basis representations and can be used to calculate very accurate tight-binding models for given structures. They are, however, no eigenfunctions of the angular momentum operator and are therefore not suitable for the analytical Slater–Koster interpolation scheme that is an essential requirement for the transferability of tight-binding integrals (Sec. III.2.2). One goal of this work is to develop a universal methodology for the derivation of tight-binding models from DFT that overcomes the deficiencies of the aforementioned approaches.

I.1.4. Crystal-field tight-binding

From spectroscopic experiments it is known that the local atomic environment of an atom has an influence on the symmetry of the atomic eigenstates and may lead to a splitting of formerly degenerate eigenvalues.⁴⁸ Such effects of the *crystal field* or *ligand field* on the atomic energy levels have been theoretically described by Bethe and van Vleck as early as the 1930s.^{49,50} As an example, the *d*-level splitting in the central atom of an octahedral cluster is shown schematically in Fig. I.2.

By construction, conventional tight-binding models do not describe crystal-field interactions. In fact, the atomic levels in compounds are usually approximated by the eigenvalues of the free atoms and are thus treated as structurally independent constants. Even though approaches to include crystal-field terms in TB models have been suggested in the literature, the additional effort implied by the empirical parametrization has limited practical applications.^{52,53}

Figure I.2. Splitting of the d level in an octahedral ligand field according to the crystal-field theory by Bethe and van Vleck.^{49,50} The notation used for the two-fold degenerate e_g level and the three-fold degenerate t_{2g} level is motivated by group theory. See Refs. 48 and 51 for a in-depth discussions.



In this thesis we attempt to establish a methodology to derive from *first principles* parameters that describe crystal-field splitting depending on the local atomic environment. A straightforward extension of the tight-binding method should allow for the incorporation of such parameters.

I.1.5. The gauge variance of bond integrals

The Hamiltonians of different atomic or molecular structures may only be directly compared, if they share a common *zero point* of the potential energy. The parameters of the tight-binding method, the *bond integrals*, are matrix elements of the discrete representation of the Hamiltonian, and are therefore subject to the same requirement. Usually, the only universal potential energy reference available in electronic structure calculations is the energy of the vacuum. To be able to compare or average the bond integrals of periodic structures without vacuum region, it is therefore necessary to construct artificial surface or cluster models.

We demonstrate that it is possible to *gauge* bond integrals of different structures subsequent to electronic structure calculations. We derive a method that is not restricted to the vacuum level, but can instead be used to impose any desired potential energy reference. An appropriate choice of reference may even result in more transferable tight-binding parameters.

I.1.6. Band sums and cohesive energy

In order to calculate cohesive energies and atomic forces using the tight-binding method, a description of the ion–ion repulsion and of the double-counting contribution is needed in addition to the bond integral parameters. These contributions are usually represented by pairwise empirical atomic interaction potentials. However, the partitioning of the total or cohesive energy is not unique, and the quality of a tight-binding total-energy expression may depend upon the choice of energy terms that enter the empirical potential.

We address this uncertainty with an overview over various energy partitioning schemes that divide the total energy into independent invariant contributions, and discuss their applicability in conjunction with tight-binding models.

I.1.7. Structure and objectives of this thesis

The objectives of this thesis are two-fold: first we seek to improve the versatility of the calculation of tight-binding models from first principles. We present a systematic and universal methodology for the extraction of transferable tight-binding electronic structure models from DFT calculations of arbitrary atomic or molecular reference structures. The method is based on the projection of converged DFT wavefunctions onto optimized minimal atomic-orbital basis sets. After a potential energy reference has been imposed, the bond integrals of a set of reference structures are averaged to achieve transferable bond integrals. The procedure for the construction of new TB models does not require much human intervention and can be automatized to a large extend.

Second, the accuracy of the tight-binding method itself is assessed. In a hierarchy of methods as suggested in Sec. I.1.3 the accuracy on each level of approximation is determined by the errors that were introduced in the more accurate ones. The step from DFT to tight-binding is of crucial importance since it is the foundation of the whole hierarchy. We therefore introduce a straightforward extension to the

tight-binding method that allows for the correct description of crystal-field interactions as discussed in Sec. I.1.4. We argue that the additional crystal-field parameters can be calculated from DFT results using our projection formalism. At the example of carbon and titanium we demonstrate that the first-principles based crystal-field tight-binding (CF-TB) models are able to reproduce the DFT electronic structure with high accuracy.

The thesis is organized as follows: an overview over electronic structure calculations in general and the tight-binding method in particular is provided in Chapters II and III. Our methodology for the derivation of tight-binding models from DFT is introduced in Chapter IV. The crystal-field extension to tight-binding is developed and applied in Chapter V, and in the final Chapter VI the construction of tight-binding total energy expressions and associated pitfalls are discussed.

In our view the systematic derivation of the parameters of approximate atomistic models is a very important step towards the theoretical study of realistic and relevant materials and chemical compounds. We hope, at one point, to be able to say with confidence: *to simulate is to understand*.

II. Electronic structure theory

II.1. Wave mechanics	10
II.1.1. The Born–Oppenheimer approximation	11
II.1.2. Properties of the Hamilton operator	12
II.1.3. The bra–ket notation	14
II.1.4. The variational principle	16
II.2. Hartree–Fock theory	17
II.2.1. Slater determinants	17
II.2.2. The energy expectation value	18
II.2.3. Minimization of the energy functional	20
II.2.4. Orbital energies	22
II.2.5. The spin-restricted case	23
II.3. Density-functional theory	24
II.3.1. The Hohenberg–Kohn theorems	25
II.3.2. The Kohn–Sham density-functional	27
II.4. Numerical calculations	31
II.4.1. Expansion of wave functions	31

The formation and the cleavage of atomic bonds, the chemistry, happens at the level of electrons. For the theoretical exploration of chemical properties we therefore need to use a model that appropriately describes the *electronic structure* of matter. Already for almost 100 years it has been known that electronic properties are governed by the principles of quantum mechanics. In this chapter we will briefly recapitulate the basics of quantum/wave mechanics. Afterwards we will establish a suitable atom model

for the discussion of chemical properties, employing the approximation by Born and Oppenheimer. What follows are a number of approximate theories for the practical evaluation of the intricate quantum mechanical formulas.

II.1. Wave mechanics

Every quantum mechanical system is entirely described by its *Hamiltonian* \hat{H} , which is given as the sum

$$\hat{H} = \hat{T} + \hat{V} \quad (\text{II.1})$$

of the kinetic and the potential energy operators \hat{T} and \hat{V} , respectively. Every measurable state with *wave function* Ψ_i of the quantum system described by \hat{H} obeys the static Schrödinger equation¹

$$\hat{H} \Psi_i = E_i \Psi_i \quad . \quad (\text{II.2})$$

Ψ_i is called an *eigenstate* of the Hamiltonian with an associated energy eigenvalue E_i . Every state Φ that the system can be prepared in, can be expressed as linear combination of eigenstates

$$\Phi = \sum_i c_i \Psi_i \quad . \quad (\text{II.3})$$

The measured energy expectation value for state Φ is given by the scalar product

$$\langle E \rangle = \frac{\int \Phi^* \hat{H} \Phi \, d\tau}{\int \Phi^* \Phi \, d\tau} \quad (\text{II.4})$$

where we introduced the differential $d\tau$ as shorthand for the integration over all spacial and spin coordinates. Equation (II.4) identifies the squared norm $|\Phi|^2 = \Phi^* \cdot \Phi$ of a state as a probability distribution function. If we impose the normalization of the states

$$\int \Phi^* \Phi \, d\tau = 1 \quad (\text{II.5})$$

$|\Phi|^2$ can be directly interpreted as probability amplitude, and the denominator in the expectation value Eq. (II.4) becomes 1.

The concept of operators, states, eigenvalues (\hat{H} , Ψ_i , E_i), and the definition of expectation values is not limited to the energy. Quantum mechanics assigns an operator to every physical observable, such as momentum or spin.

II.1.1. The Born–Oppenheimer approximation

We are, of course, specifically interested in quantum mechanical systems that are built of atoms, such as molecules and crystals. We will treat the atomic core as a single charged particle, so that a neutral atom consists of an atomic core with charge $+Ze$ that is accompanied by Z electrons. The Hamiltonian of an atomic system therefore depends on the sets of electronic and ionic coordinates $\{\mathbf{r}\}$ and $\{\mathbf{R}\}$. Split into the various contributions it can be expressed as

$$\begin{aligned}\hat{H} = & \hat{T}_e(\{\mathbf{r}\}) + \hat{V}_{ee}(\{\mathbf{r}\}) + \hat{V}_{en}(\{\mathbf{r}\}, \{\mathbf{R}\}) \\ & + \hat{T}_n(\{\mathbf{R}\}) + \hat{V}_{nn}(\{\mathbf{R}\}) \quad ,\end{aligned}\tag{II.6}$$

where \hat{T}_e and \hat{T}_n are the kinetic energy operators for the electrons and the nuclei, and the different potential energy terms arise from the electron–electron interaction (\hat{V}_{ee}), the ion–ion interaction (\hat{V}_{nn}), and the electron–ion interaction (\hat{V}_{en}). Naturally, the eigenstates of the Hamiltonian of Eq. (II.6) depend on all ionic and electronic coordinates. For a methane molecule, for example, with one carbon atom and four hydrogen atoms, i.e. five atoms and eight electrons, there are $5 \cdot 3 = 12$ ionic coordinates and $(4 + 4) \cdot 3 = 24$ electronic coordinates, yielding a total of 36 degrees of freedom.

To reduce the coordinate space of the wave function, Born and Oppenheimer suggested to separate the electronic and ionic degrees of freedom in a product ansatz

$$\Psi(\{\mathbf{r}\}, \{\mathbf{R}\}) \approx \Psi_e(\{\mathbf{r}\}) \cdot \Psi_n(\{\mathbf{R}\})\tag{II.7}$$

where Ψ_e and Ψ_n are the electronic and ionic wave functions, respectively.⁵⁴ This approximation can be justified by arguing that the light and fast electrons can adjust adiabatically to a change of the ionic positions. The time-scales of the electronic and the ionic dynamics are very different and therefore the variables can be separated. The

Born–Oppenheimer approximation is found to be very good for most applications. There are, however, situations which demand for a non-adiabatic formulation of the wave function, e. g. in the vicinity of avoided crossings of quantum states.

The product ansatz Eq. (II.7) decouples the electronic and ionic degrees of freedom

$$\hat{H} \Psi = (\hat{H}_e + \hat{T}_e) \Psi_e \Psi_n = (\hat{H}_e \Psi_e) \Psi_n + (\hat{T}_e \Psi_n) \Psi_e \quad , \quad (\text{II.8})$$

so that an electronic Schrödinger equation may be defined as

$$\hat{H}_e \Psi_e = E_e \Psi_e \quad , \quad (\text{II.9})$$

where E_e is the *electronic energy*, and the *electronic Hamiltonian* is

$$\hat{H}_e = \hat{T}_e + \hat{V}_{ee} + \hat{V}_{en} \quad . \quad (\text{II.10})$$

Note, that the evaluation of expectation values of the kind of Eq. (II.4) still requires the integration over the ionic coordinates. In most cases it is, however, sufficient to treat the atomic cores as classical particles because the quantum character of the nuclei may be neglected.*

The remaining part of this thesis is mainly concerned with the solution of the electronic Schrödinger equation (II.9). To ease reading we will therefore from now on drop the index “e” of the electronic Hamiltonian, the electronic energy eigenvalue, and the electronic wave function.

II.1.2. Properties of the Hamilton operator

We have introduced the electronic Hamilton operator \hat{H} in Eq. (II.10), but so far we have not discussed its properties. Certainly, the formal derivation of quantum mechanics is beyond the scope of this thesis and the reader is referred to standard text books on this subject.^{55,56} Here, we will just list a number of properties of the Hamilton operator that will be useful or necessary at later points.

*For small ions, especially for protons, there may occur notable quantum effects.

Differential operator

The Hamilton operator is a differential operator. In its position representation this is due to the kinetic energy operator \hat{T} which is for N electrons given in Hartree atomic units by

$$\hat{T} = \sum_i^N \hat{t}(i) = \frac{1}{2} \sum_i^N \nabla_i^2 \quad . \quad (\text{II.11})$$

As a consequence, the Hamiltonian does (in general) not commute with other operators

$$\hat{H}\hat{A}\Psi \neq \hat{A}\hat{H}\Psi \quad . \quad (\text{II.12})$$

Definiteness

The ionic degrees of freedom are decoupled from the electronic ones in the Born–Oppenheimer approximation introduced in Sec. II.1.1 and the electronic structure is solved in the static external potential

$$V_{\text{ext}}(\{\mathbf{R}\}, \{\mathbf{r}\}) = \sum_i^N v_{\text{ext}}(\{\mathbf{R}\}, \mathbf{r}_i) \quad . \quad (\text{II.13})$$

of the atomic cores. Note that in the absence of external fields $V_{\text{ext}} = V_{\text{en}}$. As obvious from Eq. (II.10), the electronic Hamiltonian is entirely defined by the knowledge of the external potential and the number of electrons N :

$$\{v_{\text{ext}}, N\} \longrightarrow \hat{H} \quad . \quad (\text{II.14})$$

Hermiticity

The Hamiltonian is a hermitian operator^{*}, i. e.

$$\int \Phi^* \hat{H} \Psi \, d\tau = \int \Psi \hat{H} \Phi^* \, d\tau \quad , \quad (\text{II.15})$$

which means that the operator is self-adjoint: $\hat{H} = \hat{H}^\dagger$. The hermiticity implies that (i) all eigenvalues of the Hamilton operator are real, (ii) the eigenstates form a complete

^{*}Note, that this is the case for every quantum mechanical operator that is associated with a physical observable

orthonormal basis in the definition space of \hat{H} , where (iii) degenerate eigenfunctions can be chosen to be orthonormal, so that for every two eigenstates Ψ_i and Ψ_j can be granted that

$$\int \Psi_i^* \Psi_j \, d\tau = \delta_{ij} = \begin{cases} 1 & \text{if } i = j \\ 0 & \text{else} \end{cases} \quad (\text{II.16})$$

where δ_{ij} is the Kronecker delta. Hence, every state or wave function can be expanded in eigenstates of the operator. We have already used this property in Eq. (II.3). This completeness of the basis of eigenfunctions for the space of wave functions can be expressed as

$$\sum_i \Psi_i^*(\tau) \Psi_i(\tau') = \delta(\tau - \tau') \quad . \quad (\text{II.17})$$

II.1.3. The bra-ket notation

Obviously, the central elements in quantum theory are state functions and operators. The expectation value of an operator was defined in Eq. (II.4) as a quotient of two integrals over the abstract differential $d\tau$. Using this trick we avoided the proper definition of the space of the state functions and the Hamiltonian. Even when the coordinate space of the Hamiltonian and the wave functions is known, such as in Eqs. (II.6) and (II.7), there is no unique *representation* of them. The Schrödinger equation could be defined in position (\mathbf{r}) space, but the momentum (\mathbf{k}) space representation, to name just one, is completely equivalent. In fact, the two representations are related via a Fourier transform. For a state function of a single particle, for example, we have

$$\psi(\mathbf{r}) = \int e^{i\mathbf{k}\mathbf{r}} \psi(\mathbf{k}) \, d\mathbf{k} \quad (\text{II.18})$$

where $\psi(\mathbf{r})$ is the representation of the state function in position space and $\psi(\mathbf{k})$ is the momentum space representation. And these are just two examples! However, the

expectation value Eq. (II.4) does not depend on the chosen representation. The reason is that the integral

$$\langle \Phi | \Psi \rangle := \int \Phi^*(\tau) \Psi(\tau) d\tau \quad (\text{II.19})$$

can be identified as a *scalar product* (inner product) between the states Ψ and Φ in the space of state functions, and one property of the scalar product is the invariance with respect to the representation. In contrast to always selecting a certain representation of the state functions, it is often more convenient to work in an equivalent vector space with the same scalar product. For this purpose, we introduce Dirac's bra-ket notation in equation (II.19). The dual space of *bra* vectors $\{\langle \Phi | \}$ and *ket* vectors $\{ | \Phi \rangle \}$ is equivalent to the space of state functions $\{ \Phi(\tau) \}$. The expectation value of Eq. (II.4) can thus be rewritten in a basis-free way as

$$\langle E \rangle = \frac{\langle \Phi | \hat{H} | \Phi \rangle}{\langle \Phi | \Phi \rangle} . \quad (\text{II.20})$$

If one wishes to derive a specific basis representation of a state vector $| \Phi \rangle$, for example the wave function $\Phi(E_i)$ in the basis of energy eigenfunctions $\{ | \Psi_i \rangle \}$, the formal relation is given by the scalar product

$$\Phi(E_i) = \langle \Psi_i | \Phi \rangle \quad \text{with} \quad \hat{H} | \Psi_i \rangle = E_i | \Psi_i \rangle . \quad (\text{II.21})$$

Analogously, the position representation, i. e. the representation in the basis of the eigenfunctions of the position operator \hat{r} , is given by

$$\Phi(\mathbf{r}) = \langle \mathbf{r} | \Phi \rangle \quad \text{with} \quad \hat{r} | \mathbf{r} \rangle = \mathbf{r} | \mathbf{r} \rangle , \quad (\text{II.22})$$

and other representations are derived accordingly. Furthermore, the completeness of the bases formed by eigenstates allows to express the identity operation as a projection operator, for example

$$\mathbb{1} = \sum_i | \Psi_i \rangle \langle \Psi_i | \quad \text{or} \quad \mathbb{1} = \int | \mathbf{r} \rangle \langle \mathbf{r} | d\mathbf{r} , \quad (\text{II.23})$$

which are the state vector equivalents of the completeness relation Eq. (II.17).

In the following we will adapt the bra-ket notation wherever it helps to simplify formulas. Occasionally, we will further employ the following abbreviations for eigenstates of the Hamiltonian:

$$|i\rangle = |\Psi_i\rangle \quad \text{and} \quad \langle i| = \langle \Psi_i| \quad . \quad (\text{II.24})$$

II.1.4. The variational principle

In principle, the electronic Schrödinger equation (II.9) has an infinite number of solutions $\{\Psi_i, E_i\}$. In the absence of external perturbations (for example an electric field) there is, however, always one lowest energy eigenvalue E_0 , the electronic *ground state* energy. The ground state wave functions (there can be several in the case of degeneracy) and the ground state energy are the quantities that we usually seek to calculate.

Recall that any possible state $|\Phi\rangle$ the system resides in can be expanded in the basis of energy eigenstates $\{|\Psi_i\rangle\}$

$$|\Phi\rangle = \left(\sum_i |\Psi_i\rangle \langle \Psi_i| \right) |\Phi\rangle = \sum_i |\Psi_i\rangle \langle \Psi_i | \Phi \rangle = \sum_i c_i |\Psi_i\rangle \quad , \quad (\text{II.25})$$

where $c_i = \langle \Psi_i | \Phi \rangle$ are the expansion coefficients. Inserting this expansion into the energy expectation value Eq. (II.4) and exploiting the orthonormality of the wave functions Eq. (II.16) gives

$$E[\Phi] = \frac{\langle \Phi | \hat{H} | \Phi \rangle}{\langle \Phi | \Phi \rangle} = \frac{\sum_i |c_i|^2 E_i}{\sum_i |c_i|^2} \geq E_0 \quad (\text{II.26})$$

which shows that the expectation value of the Hamilton operator is minimized for the ground state, i. e. there is no state that leads to a lower energy expectation value than the ground state wave functions

$$E[\Phi] = \frac{\langle \Phi | \hat{H} | \Phi \rangle}{\langle \Phi | \Phi \rangle} \geq \frac{\langle \Psi_0 | \hat{H} | \Psi_0 \rangle}{\langle \Psi_0 | \Psi_0 \rangle} = E_0 \quad . \quad (\text{II.27})$$

Consequently, it is possible to determine the ground state by identification of the wave function that minimizes the expectation value of the Hamilton operator

$$E_0 = \min_{\Phi} E[\Phi] \quad . \quad (\text{II.28})$$

Equation (II.28) is the wave function *variational principle*. In practice, the variational principle is applied to a subspace of trial wave functions. In the following section the Hartree–Fock method is discussed, which applies the variational principle on the subspace of Slater determinants.

II.2. Hartree–Fock theory

The Hartree–Fock (HF) method^{55–57} results from the direct application of the wave function variational principle Eq. (II.28). The idea is to start with a trial wave function $\tilde{\Psi} = \Psi(\{c_i\})$, which depends on a set of parameters $\{c_i\}$. These parameters are optimized in order to seize an approximation to the ground state wave function and energy

$$E_0 \approx \min_{\{c_i\}} E[\Psi(\{c_i\})] \quad . \quad (\text{II.29})$$

Obviously, the first challenge is to determine a suitable form for the trial wave function $\Psi(\{c_i\})$.

II.2.1. Slater determinants

Every ansatz for a wave function has to fulfill at least two requirements. First, the wave function of an electronic system has to be antisymmetric with respect to the exchange of two particles*

$$\Psi(\dots, \mathbf{r}_i, \dots, \mathbf{r}_j, \dots) = -\Psi(\dots, \mathbf{r}_j, \dots, \mathbf{r}_i, \dots) \quad . \quad (\text{II.30})$$

Second, it has to be normalizable

$$|\Psi|^2 = \langle \Psi | \Psi \rangle = 1 \quad (\text{II.31})$$

to allow for the interpretation as probability distribution. Equation (II.30) implies in addition that electrons are indistinguishable.

*This is, of course, a condition for any Fermionic system, and electrons are Fermions.

The simplest ansatz for an N -electron wave function that satisfies these conditions is the Slater determinant

$$\Psi^{\text{SD}}(\mathbf{r}_1, \dots, \mathbf{r}_N) = \frac{1}{\sqrt{N!}} \begin{vmatrix} \phi_1(\mathbf{r}_1) & \cdots & \phi_1(\mathbf{r}_N) \\ \vdots & \ddots & \vdots \\ \phi_N(\mathbf{r}_1) & \cdots & \phi_N(\mathbf{r}_N) \end{vmatrix} \quad (\text{II.32})$$

which is constructed from a set of N orthonormal single particle functions $\{\phi_i\}$, the *orbitals*

$$\langle \phi_i | \phi_j \rangle = \delta_{ij} \quad . \quad (\text{II.33})$$

The prefactor $1/\sqrt{N!}$ guarantees the normalization Eq. (II.31). Note that the determinant of Eq. (II.32) can alternatively be expressed using the *antisymmetrizing operator*

$$\hat{A} = \frac{1}{\sqrt{N!}} \sum_p^{\text{permut.}} \text{sgn}(p) \hat{P}_p \quad , \quad (\text{II.34})$$

where the sum runs over all possible permutations p with the *permutation operator*

$$\hat{P}_{ij} \Psi(\dots, \mathbf{r}_i, \dots, \mathbf{r}_j, \dots) = \Psi(\dots, \mathbf{r}_j, \dots, \mathbf{r}_i, \dots) \quad . \quad (\text{II.35})$$

Instead of the explicit determinant of Eq. (II.32) we can therefore write

$$\Psi^{\text{SD}}(\mathbf{r}_1, \dots, \mathbf{r}_N) = \hat{A} \phi_1(\mathbf{r}_1) \dots \phi_N(\mathbf{r}_N) \quad (\text{II.36})$$

or, equivalently, in the *bra-ket* notation

$$|\Psi^{\text{SD}}\rangle = \hat{A} |\phi_1 \dots \phi_N\rangle \quad . \quad (\text{II.37})$$

The application of the variational principle Eq. (II.28) to the space of Slater determinants leads to the Hartree–Fock approximation.

II.2.2. The energy expectation value

Even with an approximate wave function in the form of a Slater determinant Eq. (II.32) it is not an easy task to minimize the energy expectation value

$$E_0^{\text{HF}} = \min_{\{\phi_i\}} E[\Psi^{\text{SD}}] \quad \text{with} \quad E[\Psi^{\text{SD}}] = \langle \Psi^{\text{SD}} | \hat{H} | \Psi^{\text{SD}} \rangle \quad . \quad (\text{II.38})$$

However, the construction of the many-body wave function Ψ from one-electron orbitals $\{\phi_i\}$ reduces the complexity of the problem to the solution of one-electron Schrödinger equations in a mean electronic field. To accomplish this simplification, the Hamiltonian is separated into one-electron operations and two-electron operations

$$\hat{H} = \sum_i \hat{h}(i) + \sum_{j < i} \hat{g}(i, j) \quad , \quad (\text{II.39})$$

where the one-electron Hamilton operator

$$\hat{h}(i) = \hat{t}(i) + v_{\text{ext}}(i) \quad (\text{II.40})$$

describes the kinetic energy of the i -th electron

$$\hat{t}(i) = -\frac{1}{2} \nabla_i^2 \quad (\text{II.41})$$

and the interaction of that electron with the external potentials of the atomic or ionic cores. The two-electron *Coulomb operator* $g(i, j)$ describes the electron–electron repulsion and is given by

$$\hat{g}(i, j) = \frac{1}{||\mathbf{r}_j - \mathbf{r}_i||} \quad . \quad (\text{II.42})$$

We proceed by evaluating the expectation value of the Hamiltonian, Eq. (II.39), for a Slater determinant, Eq. (II.37),

$$\begin{aligned} \langle \Psi^{\text{SD}} | \hat{H} | \Psi^{\text{SD}} \rangle &= \langle \hat{A} \phi_1 \dots \phi_N | \hat{H} | \hat{A} \phi_1 \dots \phi_N \rangle \\ &= \sum_p \text{sgn}(p) \langle \phi_1 \dots \phi_N | \left(\sum_i \hat{h}(i) + \sum_{j < i} \hat{g}(i, j) \right) | \hat{P}_p \phi_1 \dots \phi_N \rangle \\ &= \sum_i \langle \phi_i | \hat{h} | \phi_i \rangle + \frac{1}{2} \sum_{i,j} \left(\langle \phi_i \phi_j | \hat{g} | \phi_i \phi_j \rangle - \langle \phi_i \phi_j | \hat{g} | \hat{P}_{ij} \phi_i \phi_j \rangle \right) \\ &= \sum_i \langle \phi_i | \hat{h} | \phi_i \rangle + \frac{1}{2} \sum_{i,j} \left(J_{ij} - K_{ij} \right) \quad , \end{aligned} \quad (\text{II.43})$$

where we introduced the Coulomb and exchange integrals

$$J_{ij} = \langle \phi_i \phi_j | \hat{g} | \phi_i \phi_j \rangle \quad \text{and} \quad K_{ij} = \langle \phi_i \phi_j | \hat{g} | \phi_j \phi_i \rangle \quad . \quad (\text{II.44})$$

After the resolution of the permutations in Eq. (II.43) only one-electron integrals over \hat{h} and two-electron integrals over \hat{g} remain, so that it is no longer necessary to distinguish the electronic coordinates these operators are acting on. Note, that the sum over i and j in Eq. (II.43) could be rewritten in a symmetrical form because $(J_{ij} - K_{ij})$ vanishes for $i = j$. It is convenient to define two further one-electron operators, the Coulomb operator \hat{j}_j and the exchange operator \hat{k}_j , by means of their action

$$\hat{j}_i(1)|\phi_j(2)\rangle := \langle\phi_i(1)|\hat{g}|\phi_i(1)\rangle|\phi_j(2)\rangle \quad (\text{II.45})$$

$$\hat{k}_i(1)|\phi_j(2)\rangle := \langle\phi_i(1)|\hat{g}|\phi_j(1)\rangle|\phi_i(2)\rangle \quad , \quad (\text{II.46})$$

where we simply enumerate the two different electronic coordinates. The electronic coordinates are given explicitly to underline that the exchange operator actually *exchanges* the electrons in the two orbitals i and j . The expression for the electronic energy eigenvalue in dependence of the orbitals, Eq. (II.43), can thus be rewritten as

$$E[\{\phi\}] = \sum_i \langle\phi_i|\hat{h}|\phi_i\rangle + \frac{1}{2} \sum_{i,j} \left(\langle\phi_j|\hat{j}_i - \hat{k}_i|\phi_j\rangle \right) \quad , \quad (\text{II.47})$$

and we seek a variational minimum of this functional with respect to the set of one-electron orbitals $\{\phi_i\}$.

II.2.3. Minimization of the energy functional

Our objective is the variational minimization of the orbital dependent energy expectation value (II.47) with respect to the one-electron orbitals. We further require the orbitals ϕ_i to remain orthonormal, i.e. that $\langle\phi_i|\phi_j\rangle = \delta_{ij}$. For this constrained minimization problem we resort to the method of *Langrangian multipliers* with the Lagrangian

$$\mathcal{L}[\{\phi\}] = E[\{\phi\}] - \sum_{i,j} \lambda_{ij} \left(\langle\phi_i|\phi_j\rangle - \delta_{ij} \right) \quad . \quad (\text{II.48})$$

For the minimizing set of orbitals the variation $\phi \rightarrow \phi + \delta\phi$ of the Langrangian must vanish

$$\frac{\delta}{\delta\{\phi\}} \mathcal{L}[\{\phi\}] = \frac{\delta}{\delta\{\phi\}} E[\{\phi\}] - \sum_{i,j} \lambda_{ij} \frac{\delta}{\delta\{\phi\}} \langle\phi_i|\phi_j\rangle \stackrel{!}{=} 0 \quad . \quad (\text{II.49})$$

The variation of the orbital overlap in the second term yields

$$\frac{\delta}{\delta\{\phi\}} \langle \phi_i | \phi_j \rangle = \langle \frac{\delta}{\delta\{\phi\}} \phi_i | \phi_j \rangle + \langle \phi_i | \frac{\delta}{\delta\{\phi\}} \phi_j \rangle \quad , \quad (\text{II.50})$$

and the variation of the expectation value (II.47) is given by

$$\begin{aligned} \frac{\delta}{\delta\{\phi\}} E[\{\phi\}] &= \sum_i \left(\langle \frac{\delta}{\delta\{\phi\}} \phi_i | \hat{h} | \phi_i \rangle + \text{c.c.} \right) \\ &+ \frac{1}{2} \sum_{i,j} \left(\langle \frac{\delta}{\delta\{\phi\}} \phi_i \phi_j | \hat{g} | \phi_i \phi_j \rangle + \langle \phi_i \frac{\delta}{\delta\{\phi\}} \phi_j | \hat{g} | \phi_i \phi_j \rangle \right. \\ &\quad \left. + \langle \frac{\delta}{\delta\{\phi\}} \phi_i \phi_j | \hat{g} | \phi_j \phi_i \rangle + \langle \phi_i \frac{\delta}{\delta\{\phi\}} \phi_j | \hat{g} | \phi_j \phi_i \rangle + \text{c.c.} \right) . \end{aligned}$$

A change of indices $(i, j) \rightarrow (j, i)$ in the second Coulomb and the second exchange integral makes it possible to combine two integrals at a time, so that we can get rid of the factor of 1/2:

$$\begin{aligned} \frac{\delta}{\delta\{\phi\}} E[\{\phi\}] &= \sum_i \left(\langle \frac{\delta}{\delta\{\phi\}} \phi_i | \hat{h} | \phi_i \rangle + \text{c.c.} \right) \\ &+ \sum_{i,j} \left(\langle \frac{\delta}{\delta\{\phi\}} \phi_i \phi_j | \hat{g} | \phi_i \phi_j \rangle + \langle \frac{\delta}{\delta\{\phi\}} \phi_i \phi_j | \hat{g} | \phi_j \phi_i \rangle + \text{c.c.} \right) \\ &= \sum_i \langle \frac{\delta}{\delta\{\phi\}} \phi_i | \hat{h} | \phi_i \rangle + \sum_{i,j} \langle \frac{\delta}{\delta\{\phi\}} \phi_i | \hat{j}_j - \hat{k}_j | \phi_i \rangle + \text{c.c.} \quad . \end{aligned}$$

We define the one-electron *Fock operator* \hat{f} as

$$\hat{f} = \hat{h} + \sum_i \left(\hat{j}_i - \hat{k}_i \right) \quad , \quad (\text{II.51})$$

so that we can rewrite the variation of the Lagrangian (II.49) as

$$\frac{\delta}{\delta\{\phi\}} \mathcal{L}[\{\phi\}] = \sum_i \langle \frac{\delta}{\delta\{\phi\}} \phi_i | \hat{f} | \phi_i \rangle - \sum_{i,j} \lambda_{ij} \langle \frac{\delta}{\delta\{\phi\}} \phi_i | \phi_j \rangle + \text{c.c.} \stackrel{!}{=} 0 \quad .$$

Note that the variation of the orbitals ϕ_i and the variation of their complex conjugates ϕ_i^* both must satisfy the stationary condition

$$\langle \frac{\delta}{\delta\{\phi\}} \phi_i | \hat{f} | \phi_i \rangle = \sum_j \lambda_{ij} \langle \frac{\delta}{\delta\{\phi\}} \phi_i | \phi_j \rangle \quad (\text{II.52})$$

$$\text{and} \quad \langle \phi_i | \hat{f} | \frac{\delta}{\delta\{\phi\}} \phi_i \rangle = \sum_j \lambda_{ij} \langle \phi_i | \frac{\delta}{\delta\{\phi\}} \phi_j \rangle \quad . \quad (\text{II.53})$$

By taking the complex conjugate on both sides of equation (II.53) and comparing the result to (II.52) it is evident that $\lambda_{ij} = \lambda_{ij}^*$, i. e. that the Lagrange multipliers form a Hermitian matrix.

The HF equations are the pseudo-eigenvalue expression of the above equations:

$$\hat{f}|\phi_i\rangle = \sum_j \lambda_{ij} |\phi_j\rangle \quad . \quad (\text{II.54})$$

One usually chooses the unitary transformation that diagonalizes the matrix of Lagrange multipliers so that

$$\hat{f}|\tilde{\phi}_i\rangle = \varepsilon_i |\tilde{\phi}_i\rangle \quad , \quad (\text{II.55})$$

in which case the orbitals $\{\tilde{\phi}_i\}$ are called *canonical Hartree–Fock orbitals* and the diagonal Lagrange multipliers ε_i can be interpreted as *orbital energies*. Without loss of generality we shall select the canonical orbitals for the following discussions and refer to them simply as $\{\phi_i\}$.

II.2.4. Orbital energies

The orbital energies ε_i of the canonical HF orbitals can be interpreted as matrix elements of the Fock operator

$$\hat{f}|\phi_j\rangle = \varepsilon_j |\phi_j\rangle \quad \xrightarrow{\langle\phi_i|} \quad \langle\phi_i|\hat{f}|\phi_j\rangle = \delta_{ij} \varepsilon_j \quad . \quad (\text{II.56})$$

Inserting the Fock operator Eq. (II.51) we can find an alternative expression for the Hartree–Fock energy, Eq. (II.43), in terms of the sum of orbital energies

$$\begin{aligned} E^{\text{HF}}[\{\phi\}] &= \sum_i \varepsilon_i - \frac{1}{2} \sum_{i,j} (J_{ij} - K_{ij}) \\ &= \frac{1}{2} \sum_i \left(\varepsilon_i + \langle\phi_i|\hat{h}|\phi_i\rangle \right) \quad . \end{aligned} \quad (\text{II.57})$$

Note, that the second sum in equation (II.57) corrects for the double-counted electron–electron interactions in the sum of orbital energies.

II.2.5. The spin-restricted case

According to Hund's rule every electronic state can be occupied by two electrons with different spins, spin-up and spin-down. For closed-shell systems it is therefore more realistic to construct the all electron wave function from pairs of spacial orbitals that only differ in spin:

$$|\phi_1\rangle = |\chi_1\rangle = |\psi_1\rangle|\uparrow\rangle \quad (\text{II.58})$$

$$|\phi_2\rangle = |\bar{\chi}_1\rangle = |\psi_1\rangle|\downarrow\rangle \quad , \quad (\text{II.59})$$

so that the many-body state can be written as

$$|\chi^{\text{SD}}\rangle = |\chi_1\bar{\chi}_1 \dots \chi_{N/2}\bar{\chi}_{N/2}\rangle \quad . \quad (\text{II.60})$$

The spin eigenfunctions $|\uparrow\rangle$ and $|\downarrow\rangle$ are orthogonal with $\langle\uparrow|\downarrow\rangle = 0$. The restriction to the spin-orbitals simplifies the sum over one-electron integrals in the energy functional (II.47), as the values do not depend on the spin part

$$\sum_i^N \langle\phi_i|\hat{h}|\phi_i\rangle = 2 \sum_i^{N/2} \langle\psi_i|\hat{h}|\psi_i\rangle \quad . \quad (\text{II.61})$$

For two-electron integrals we have to distinguish between the Coulomb integrals, which do not depend on the spin either

$$\begin{aligned} \langle\chi_i\chi_j|\hat{g}|\chi_i\chi_j\rangle &= \langle\chi_i\bar{\chi}_j|\hat{g}|\chi_i\bar{\chi}_j\rangle = \langle\bar{\chi}_i\chi_j|\hat{g}|\bar{\chi}_i\chi_j\rangle = \langle\bar{\chi}_i\bar{\chi}_j|\hat{g}|\bar{\chi}_i\bar{\chi}_j\rangle \\ &= \langle\psi_k\psi_m|\hat{g}|\psi_k\psi_m\rangle \end{aligned} \quad (\text{II.62})$$

and the exchange integrals, which are zero if the two orbitals differ in the spin part. Half of the integrals in the sum over i and j therefore become zero; to provide two examples:

$$\begin{aligned} \langle\chi_i\chi_j|\hat{g}|\chi_j\chi_i\rangle &= \langle\psi_k\psi_m|\hat{g}|\psi_m\psi_k\rangle\langle\uparrow\uparrow|\uparrow\uparrow\rangle = \langle\psi_k\psi_m|\hat{g}|\psi_m\psi_k\rangle \\ \text{but } \langle\chi_i\bar{\chi}_j|\hat{g}|\bar{\chi}_j\chi_i\rangle &= \langle\psi_k\psi_m|\hat{g}|\psi_m\psi_k\rangle\langle\uparrow\downarrow|\downarrow\uparrow\rangle = 0 \quad . \end{aligned}$$

Inserting these simplifications into equation (II.47) yields the spin-restricted energy functional

$$E^{\text{HF}}[\{\psi\}] = 2 \sum_i^{N/2} \langle \psi_i | \hat{h} | \psi_i \rangle + \sum_{i,j}^{N/2} (2J_{ij} - K_{ij}) \quad (\text{II.63})$$

and the Fock operator (II.51) becomes

$$\hat{f} = \hat{h} + \sum_i^{N/2} (2\hat{j}_i - \hat{k}_i) \quad . \quad (\text{II.64})$$

The HF eigenvalue problem remains the same as in the unrestricted case, Eq. (II.55), but is now formulated for space rather than spin orbitals

$$\hat{f}|\psi_i\rangle = \varepsilon_i |\psi_i\rangle \quad . \quad (\text{II.65})$$

II.3. Density-functional theory

As discussed in Sec. II.2, the Hartree–Fock (HF) method is a direct application of the wave function variational principle, Eq. (II.28), to the wave function space of Slater determinants, Eq. (II.32). As it turns out, the description of the many-body wave function by a single Slater determinant is not a very accurate approximation. There are a number of extensions to the HF method, which improve the wave function and thus allow, to some extent, to account for the missing electronic *correlation*. Usually, these methods either include further determinants that correspond to excited states (CI, MC-SCF, CAS-SCF, CC), or add a perturbative correction to the HF energy (MP2, MP4), or combine those two approaches (CASPT2). In every case the computational effort and its scaling with the number of electrons is raised significantly, and these methods are therefore only applicable to relatively small atomic structures of less than 50 atoms.

Electronic density-functional theory (DFT) takes a completely different approach towards the electronic structure problem. Instead of attempting to approximate the

many-body wave function $\Psi(\mathbf{r}_1, \mathbf{r}_2, \dots)$ in DFT the electronic energy expectation value, Eq. (II.4), is directly related to the electron density $n(\mathbf{r})$

$$E^{\text{DFT}}[n(\mathbf{r})] = T[n(\mathbf{r})] + E_{\text{ee}}[n(\mathbf{r})] + E_{\text{ext}}[n(\mathbf{r})] \quad (\text{II.66})$$

where the kinetic energy T , the electron–electron interaction energy E_{ee} , and the external energy E_{ext} are all functionals of the density. The electron density of a system with N electrons is defined as

$$n(\mathbf{r}) := N \int \dots \int \Psi^*(\mathbf{r}, \mathbf{r}_2, \dots, \mathbf{r}_N) \Psi(\mathbf{r}, \mathbf{r}_2, \dots, \mathbf{r}_N) d\mathbf{r}_2 \dots d\mathbf{r}_N \quad (\text{II.67})$$

Note, that $n(\mathbf{r})$ is a function of the three spacial coordinates. In turn, also the energy functional of Eq. (II.66) only depends on three coordinates rather than on the $3N$ electronic coordinates in the wave function case, Eq. (II.4). It is therefore counter-intuitive that a functional of the form of Eq. (II.66) exists. However, Hohenberg and Kohn were able to prove the existence of a density functional of the electronic ground-state energy and that the ground-state electron density minimizes this functional.

II.3.1. The Hohenberg–Kohn theorems

In 1964 Hohenberg and Kohn were able to prove that an exact density functional of the electronic ground state energy, and in fact for every observable, exists.⁵⁸ As discussed in Sec. II.1.2, the Hamilton operator is entirely determined by the knowledge of an external potential v_{ext} and the number of electrons N . The Hamilton operator in turn determines the many-body wave functions, so in particular the ground-state wave function Ψ_0 from which the ground-state electron density n_0 can be derived according to Eq. (II.67):

$$\{v_{\text{ext}}(\mathbf{r}), N\} \rightarrow \hat{H}_e(\mathbf{r}_1, \dots, \mathbf{r}_N) \rightarrow \Psi_0(\mathbf{r}_1, \dots, \mathbf{r}_N) \rightarrow n_0(\mathbf{r}) \quad (\text{II.68})$$

In their first theorem Hohenberg and Kohn showed that *vice versa* a given ground-state electron density $n_0(\mathbf{r})$ can only be the result of exactly one particular external potential

$v(\mathbf{r})$, save an additive constant, and one particular number of electrons N , which again determines the ground-state many-body wave function $\Psi_0(\mathbf{r}_1, \dots, \mathbf{r}_N)$

$$n_0(\mathbf{r}) \rightarrow \{v_{\text{ext}}(\mathbf{r}), N\} \rightarrow \hat{H}_e(\mathbf{r}_1, \dots, \mathbf{r}_N) \rightarrow \Psi_0(\mathbf{r}_1, \dots, \mathbf{r}_N) \quad . \quad (\text{II.69})$$

If the ground-state wave function is uniquely determined by the ground-state electron density, i. e. the wave function is a *functional* of the density, then there must also be a density functional for the expectation value of any operator \hat{O}

$$\langle \Psi_0[n_0(\mathbf{r})] | \hat{O} | \Psi_0[n_0(\mathbf{r})] \rangle = \langle \hat{O} \rangle[n_0(\mathbf{r})] = O[n_0] \quad . \quad (\text{II.70})$$

The proof of relation (II.69) provided by Hohenberg and Kohn is based on *reductio ad absurdum*. Assume that two Hamiltonians \hat{H}_1 and \hat{H}_2 for external potentials that differ by more than a constant

$$\begin{aligned} \hat{H}_1 &= \hat{T} + V_{ee} + V_{\text{ext},1} ; \quad \hat{H}_1 \Psi_1 = E_0^1 \Psi_1 \\ \text{and} \quad \hat{H}_2 &= \hat{T} + V_{ee} + V_{\text{ext},2} ; \quad \hat{H}_2 \Psi_2 = E_0^2 \Psi_2 \end{aligned}$$

would result in the same ground-state electron density $n_0(\mathbf{r})$. If the ground state is not degenerate, the wave function variational principle, Eq. (II.28), states that there is no expectation value smaller than or equal to the ground-state energy

$$\begin{aligned} E_0^1 &< \langle \Psi_2 | \hat{H}_1 | \Psi_2 \rangle = \langle \Psi_2 | \hat{H}_2 | \Psi_2 \rangle + \langle \Psi_2 | \hat{H}_1 - \hat{H}_2 | \Psi_2 \rangle \\ &= E_0^2 + \langle \Psi_2 | V_{\text{ext},1} - V_{\text{ext},2} | \Psi_2 \rangle \end{aligned} \quad (\text{II.71})$$

and equally for the second Hamiltonian

$$\begin{aligned} E_0^2 &< \langle \Psi_1 | \hat{H}_2 | \Psi_1 \rangle = \langle \Psi_1 | \hat{H}_1 | \Psi_1 \rangle + \langle \Psi_1 | \hat{H}_2 - \hat{H}_1 | \Psi_1 \rangle \\ &= E_0^1 + \langle \Psi_1 | V_{\text{ext},2} - V_{\text{ext},1} | \Psi_1 \rangle \quad . \end{aligned} \quad (\text{II.72})$$

Inserting the expression of the electron density (II.67) into equations (II.71) and (II.72) yields

$$E_0^1 < E_0^2 + \int n(\mathbf{r}) [v_{\text{ext},1}(\mathbf{r}) - v_{\text{ext},2}(\mathbf{r})] d\mathbf{r} \quad (\text{II.73})$$

$$\text{and} \quad E_0^2 < E_0^1 - \int n(\mathbf{r}) [v_{\text{ext},1}(\mathbf{r}) - v_{\text{ext},2}(\mathbf{r})] d\mathbf{r} \quad (\text{II.74})$$

with $V_{\text{ext},k} = \sum_i^N v_{\text{ext},k}(\mathbf{r}_i)$. Adding Eqs. (II.73) and (II.74) leads to the contradiction

$$E_0^1 + E_0^2 < E_0^1 + E_0^2 \quad (\text{II.75})$$

and therefore proves that the initial assumption is impossible; two external potentials that differ by more than a constant can not result in the same electron density. Thus, relation (II.69) must be valid and density functionals for the expectation values of all observables, Eq. (II.70), and in particular for the ground-state energy, must exist.

The density variational principle

The second Hohenberg–Kohn theorem derives the applicability of the variational principle to the ground-state electron density. The one-to-one mapping of the electron density and the wave function, which is the result of the first theorem, immediately translates the wave function minimum-energy principle of Eq. (II.28) to the density

$$\begin{aligned} \langle \Psi_0 | \hat{H} | \Psi_0 \rangle &\leq \langle \tilde{\Psi} | \hat{H} | \tilde{\Psi} \rangle \\ \Leftrightarrow \langle \Psi[n_0] | \hat{H} | \Psi[n_0] \rangle &\leq \langle \Psi[\tilde{n}] | \hat{H} | \Psi[\tilde{n}] \rangle \\ \Leftrightarrow E[n_0] &\leq E[\tilde{n}] \quad , \end{aligned} \quad (\text{II.76})$$

where the normalization of the wave function was assumed. For the variational minimization of the energy it is also required that the ground state is a stationary point of the energy functional with respect to the variation of the density. The problem can be formulated as conditional minimization with the additional constraint that the integration of the density over the whole space must yield the number of electrons. Using the Lagrangian formulation the density variational principle can be expressed as

$$\frac{\delta}{\delta n} \left\{ E[n] + \mu \left(\int n(\mathbf{r}) d\mathbf{r} - N \right) \right\} = 0 \quad (\text{II.77})$$

where μ is a Lagrange multiplier.

II.3.2. The Kohn–Sham density-functional

The Hohenberg–Kohn theorems prove the existence of a density functional $E[n]$ of the ground-state energy that is variational with respect to the density. Formally, this

functional can be written as already stated in Eq. (II.66)

$$E[n] = T[n] + E_{ee}[n] + E_{\text{ext}}[n] + E_{\text{nn}} \quad , \quad (\text{II.78})$$

but in fact the exact functional is only known for the external energy where the expectation value of the external potential can be calculated as classical expectation value

$$E_{\text{ext}}[n] = \int n(\mathbf{r}) v_{\text{ext}}(\mathbf{r}) \, d\mathbf{r} \quad . \quad (\text{II.79})$$

The density functionals for the kinetic energy and for the electron–electron repulsive energies are unknown. In an attempt to utilize as much information as is known about those two energy contributions, Kohn and Sham⁵⁹ re-wrote the energy functional Eq. (II.78) into

$$E^{\text{KS}}[n] = T_{\text{s}}[n] + E_{\text{H}}[n] + E_{\text{ext}}[n] + E_{\text{xc}}[n] = E[n] \quad , \quad (\text{II.80})$$

where T_{s} is the kinetic energy of an auxiliary system of non-interacting electrons but with the same electron density. The electron–electron interaction is approximated by the classical Hartree electrostatic energy

$$E_{\text{H}}[n] = \frac{1}{2} \int n(\mathbf{r}) v_{\text{H}}(\mathbf{r}) \, d\mathbf{r} \quad ; \quad v_{\text{H}}(\mathbf{r}) := \int \frac{n(\mathbf{r}')}{|\mathbf{r} - \mathbf{r}'|} \, d\mathbf{r}' \quad , \quad (\text{II.81})$$

which does, however, not distinguish between Coulomb and exchange type interactions, i. e. the integrals of types J_{ij} and K_{ij} in Eq. (II.44). The additional energy term E_{xc} in Eq. (II.80) compensates for the exchange and correlation errors in the electrostatic energy and the missing correlation in the kinetic energy, so that the Kohn–Sham functional – in principle – is no approximation to Eq. (II.78). It rather is formally exact.

The auxiliary Kohn–Sham system

The ground state of a (fictitious) system of non-interacting electrons is exactly described by a single Slater determinant, Eq. (II.32). Note, that in the absence of electron–electron interactions there is no difference between the single particle Hamilton operator and

the Fock operator, Eq. (II.51). The auxiliary Kohn–Sham (KS) system is thus described by a set of one-electron Schrödinger equations

$$\hat{h}|\psi_i\rangle = \varepsilon_i|\psi_i\rangle \quad \text{with} \quad \hat{h} = \hat{t} + v_{\text{eff}}^{\text{KS}} \quad , \quad (\text{II.82})$$

where we introduce the KS orbitals $\{\psi_i\}$ in analogy to the canonical HF orbitals of Eq. (II.55). The energy of the KS system is by construction

$$E_s = T_s + \int n_s(\mathbf{r}) v_{\text{eff}}^{\text{KS}}(\mathbf{r}) d\mathbf{r} \quad \text{with} \quad T_s = \sum_i f_i \langle \psi_i | \hat{t} | \psi_i \rangle \quad (\text{II.83})$$

where $f_i \in [0, 1]$ is the occupation number of state i . The effective KS potential $v_{\text{eff}}^{\text{KS}}$ shall be chosen in such a way that the ground-state electron density n_s of the auxiliary system becomes equal to the density of the real system

$$n_s(\mathbf{r}) = \sum_i f_i |\psi_i(\mathbf{r})|^2 \quad . \quad (\text{II.84})$$

A derivation of the orbital dependent expression of the electron density, Eq. (II.84), is provided in the Appendix A.1. So, the variation of the KS energy functional, Eq. (II.80)

$$\frac{\delta}{\delta n} E^{\text{KS}} = \frac{\delta T_s}{\delta n} + v_{\text{H}} + v_{\text{ext}} + \frac{\delta E_{\text{xc}}}{\delta n} \quad (\text{II.85})$$

and the variation of the energy of the auxiliary system Eq. (II.83)

$$\frac{\delta}{\delta n_s} E_s = \frac{\delta T_s}{\delta n_s} + v_{\text{eff}}^{\text{KS}} \quad (\text{II.86})$$

are required to vanish for the same density n_0 . Setting equal the two variations, Eqs. (II.85) and (II.86), for the common ground state $n = n_s = n_0$

$$\left. \frac{\delta E^{\text{KS}}}{\delta n} \right|_{n=n_0} = \left. \frac{\delta E_s}{\delta n_s} \right|_{n_s=n_0} = 0 \quad (\text{II.87})$$

yields an expression of the effective potential

$$v_{\text{eff}}^{\text{KS}} = v_{\text{ext}} + v_{\text{H}}[n_0] + v_{\text{xc}}[n_0] \quad \text{with} \quad v_{\text{xc}}[n] := \frac{\delta E_{\text{xc}}}{\delta n} \quad , \quad (\text{II.88})$$

where we defined the exchange–correlation potential v_{xc} .

Note, that Eq. (II.88) points out a recursive interdependency: the effective KS potential depends on the ground-state density, which in turn can only be determined for a given

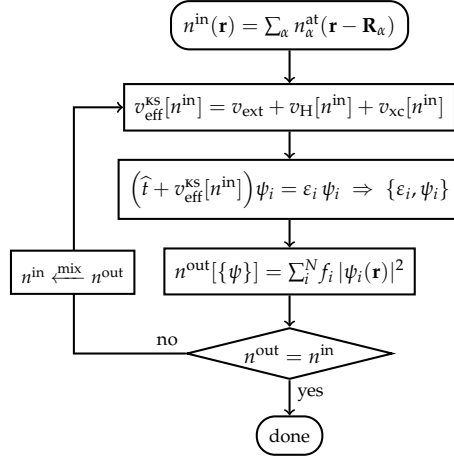


Figure II.1. Flow chart of the self-consistent Kohn-Sham algorithm. In the example, the superposition of electron densities of the free atoms $\{n_a^{\text{at}}\}$ is taken as an initial guess n^{in} of the electron density.

effective potential. The Kohn-Sham equations are therefore usually solved iteratively in a self-consistent procedure starting with either a guess of the electron density n^{in} or the effective potential v^{in} . The electron density n_s of the auxiliary KS system can then be understood as the *output density* n^{out} of the self-consistency iteration, and convergence has been reached when $n^{\text{in}} = n^{\text{out}}$. The flow chart of a possible implementation of the KS algorithm is shown in Fig. II.1.

The underlying idea of the KS scheme is to reduce the value of the *unknown* terms in the density functional of the energy Eq. (II.78). An analytical expression for the exact exchange and correlation energy functional $E_{\text{xc}}[n]$ is, however, not known. Thus, practical use can only be made of the KS algorithm if approximations of this functional are employed.

II.4. Numerical calculations

Neither the Hartree–Fock equation in Eq. (II.55) nor the Kohn–Sham eigenvalue problem of Eq. (II.82) can be solved analytically for general orbitals $\{|\psi\rangle\}$. These one-electron operator eigenvalue problems can, however, be solved numerically, if an ansatz for the wave functions is provided.

II.4.1. Expansion of wave functions

The most common ansatz for the one-electron wave functions $\{|\psi_i\rangle\}$ is an expansion in a suitable basis $\{|\phi_\mu\rangle\}$

$$|\psi_i\rangle \approx \sum_{\mu} c^{i,\mu} |\phi_\mu\rangle \quad . \quad (\text{II.89})$$

Frequent choices for the basis $\{|\phi_\mu\rangle\}$ include atom centered Gauss functions* and hydrogen-like atomic orbitals (Slater functions) for isolated structures, such as molecules and clusters.⁵⁷ For periodic systems, i. e. crystals or super-cells, plane wave basis sets are more appealing. Also grid-based numerical representations of the wave functions are possible. The smallest applicable basis set, a *minimal basis*, comprises just as many functions as needed to describe all occupied atomic eigenstates (1s, 3p, 5d, etc.). Depending on the kind and the number of the basis functions the expansion Eq. (II.89) can be *numerically* exact. However, minimal basis representations are usually a bad approximation for the wave function.

The basis set expansion of the wave functions transforms the operator eigenvalue problems to generalized matrix eigenvalue problems. For the example of the KS one-electron Schrödinger equation the result is

$$\begin{aligned} \hat{h} |\psi_i\rangle = \varepsilon_i |\psi_i\rangle &\Rightarrow \sum_{\nu} \hat{h} |\phi_\nu\rangle c^{i,\nu} = \varepsilon_i \sum_{\nu} |\phi_\nu\rangle c^{i,\nu} \\ &\xrightarrow{\langle \mu | \cdot} \sum_{\nu} H_{\mu\nu} c^{i,\nu} = \varepsilon_i \sum_{\nu} S_{\mu\nu} c^{i,\nu} \leftrightarrow \mathbf{H} \mathbf{c}_i = \varepsilon_i \mathbf{S} \mathbf{c}_i \end{aligned} \quad (\text{II.90})$$

*Often several Gauss functions are combined to form a single atomic-like orbital.

where the elements of the Hamilton matrix \mathbf{H} and the overlap matrix \mathbf{S} are given by

$$H_{\mu\nu} = \langle \phi_\mu | \hat{h} | \phi_\nu \rangle \quad \text{and} \quad S_{\mu\nu} = \langle \phi_\mu | \phi_\nu \rangle . \quad (\text{II.91})$$

The dimension of the Hamilton and overlap matrices is determined by the size of the basis set. The above is completely analogous for the matrix representation of the Fock operator and the Hartree–Fock eigenproblem Eq. (II.55).

A common special case is the use of pairwise orthogonal basis functions, so that the overlap matrix in Eq. (II.90) is the identity matrix

$$S_{\mu\nu} = \langle \phi_\mu | \phi_\nu \rangle = \delta_{\mu\nu} , \quad (\text{II.92})$$

so that the one-electron Schrödinger equation is mapped onto an ordinary matrix eigenvalue problem

$$\mathbf{H} \mathbf{c}_i = \varepsilon_i \mathbf{c}_i . \quad (\text{II.93})$$

III.

The tight-binding method

III.1. Non-self-consistent DFT	33
III.1.1. Expansion about a trial density	35
III.1.2. The Harris–Foulkes functional	37
III.2. The tight-binding method	37
III.2.1. Two-center approximation	38
III.2.2. Slater–Koster interpolation	40
III.3. Implementations of the TB method	42
III.3.1. The tight-binding band model	42
III.3.2. Structural energy difference theorem	43
III.3.3. The tight-binding bond model	45
III.3.4. Self-consistent charge TB	48
III.3.5. The NRL tight-binding method	50

Topic of this chapter is the tight-binding (TB) electronic structure method. The first part of the chapter provides a discussion of the relationship between density-functional theory and TB. The general principles of the semiempirical tight-binding method are introduced. Finally, a number of common implementations of the TB method are compared.

III.1. Non-self-consistent DFT

The self-consistent Kohn–Sham (KS) algorithm outlined in Sec. II.3 of the previous chapter determines the variational ground-state electron density n_0 and the corresponding energy. However, if a good estimate of the ground state density $n^{\text{in}} \approx n_0$ is

available, it might not be desired to go through the entire iterative KS procedure. One might seek instead to calculate an approximate ground-state energy using this density estimate. Going through the flow chart in Fig. II.1 the first step is the construction of the effective potential for the input density

$$v_{\text{eff}}^{\text{KS}}[n^{\text{in}}(\mathbf{r})] = v_{\text{ext}}(\mathbf{r}) + v_{\text{H}}[n^{\text{in}}(\mathbf{r})] + v_{\text{xc}}[n^{\text{in}}(\mathbf{r})] \quad , \quad (\text{III.1})$$

which in the following enters the one-electron Hamiltonian of the KS equations, Eq. (II.82). Successively, the KS kinetic energy can be evaluated as

$$\begin{aligned} \langle \hat{T}_s \rangle &= \sum_i f_i \langle \psi_i | \hat{t} | \psi_i \rangle = \sum_i f_i \langle \psi_i | \hat{h} - v_{\text{eff}}^{\text{KS}} | \psi_i \rangle \\ &= \sum_i f_i \varepsilon_i[n^{\text{in}}] - \int n^{\text{out}}(\mathbf{r}) v_{\text{eff}}^{\text{KS}}[n^{\text{in}}(\mathbf{r})] \, d\mathbf{r} \quad , \end{aligned} \quad (\text{III.2})$$

where $f_i \in [0, 1]$ is the occupation number of state i . Using the expression for the effective potential, Eq. (III.1), yields

$$\begin{aligned} T_s[n^{\text{in}}, n^{\text{out}}] &= \sum_i f_i \varepsilon_i[n^{\text{in}}] - E_{\text{ext}}[n^{\text{out}}] - \int n^{\text{out}} v_{\text{H}}[n^{\text{in}}] \, d\mathbf{r} \\ &\quad - \int n^{\text{out}} v_{\text{xc}}[n^{\text{in}}] \, d\mathbf{r} \quad . \end{aligned} \quad (\text{III.3})$$

Inserting Eq. (III.3) into the KS functional, Eq. (II.80), one arrives at an alternative expression of the KS electronic energy functional

$$\begin{aligned} E^{\text{KS}}[n^{\text{in}}, n^{\text{out}}] &= \sum_i f_i \varepsilon_i[n^{\text{in}}] - \int n^{\text{out}} v_{\text{H}}[n^{\text{in}}] \, d\mathbf{r} - \int n^{\text{out}} v_{\text{xc}}[n^{\text{in}}] \, d\mathbf{r} \\ &\quad + E_{\text{H}}[n^{\text{out}}] + E_{\text{xc}}[n^{\text{out}}] \quad , \end{aligned} \quad (\text{III.4})$$

which still requires a self-consistent solution as it depends on both, the input and the output density. Note that this form of the KS energy functional is the DFT analogue of the Hartree–Fock energy functional of Eq. (II.57), where a double-counting correction is subtracted from the sum of one-electron orbital energies.

The above derivation was provided here for the case of a discrete eigenvalue spectrum $\{\varepsilon_i\}$ and thus the *band energy* was expressed as the sum

$$E_{\text{band}} = \sum_i f_i \varepsilon_i \quad , \quad (\text{III.5})$$

with a discrete occupation function $f_i = f(\varepsilon_i)$. Degenerate eigenvalues are not ruled out by this band sum formulation, hence it is possible that $\varepsilon_i = \varepsilon_{i+1}$. In the case of an infinite crystal the eigenvalue spectrum is, however, continuous. In that case the summation has to be replaced by an integration over the energy

$$E_{\text{band}} = \int f(\varepsilon) g(\varepsilon) \varepsilon \, d\varepsilon \quad (\text{III.6})$$

where we additionally introduced the *density of states* $g(\varepsilon)$, which implicitly accounts for degeneracy. The number of states in the infinitesimal energy interval $[\varepsilon, \varepsilon + \delta\varepsilon]$ is given by $g(\varepsilon) \delta\varepsilon$.

We proceed with the discrete expression while bearing in mind that at certain occasions the sum over states, Eq. (III.5), has to be replaced by the integration of Eq. (III.6).

III.1.1. Expansion about a trial density

Following Harris and Foulkes^{26–28} we express the output density in terms of the input density $n^{\text{out}} = n^{\text{in}} + \Delta n$.*

The Hartree potential, Eq. (II.81), is linear in the density

$$v_{\text{H}}[n^{\text{out}}] = v_{\text{H}}[n^{\text{in}} + \Delta n] = v_{\text{H}}[n^{\text{in}}] + v_{\text{H}}[\Delta n] \quad , \quad (\text{III.7})$$

so that the Hartree energy is given by

$$\begin{aligned} E_{\text{H}}[n^{\text{out}}] &= E_{\text{H}}[n^{\text{in}} + \Delta n] \\ &= E_{\text{H}}[n^{\text{in}}] + E_{\text{H}}[\Delta n] + \int \Delta n(\mathbf{r}) v_{\text{H}}[n^{\text{in}}(\mathbf{r})] \, d\mathbf{r} \quad . \end{aligned} \quad (\text{III.8})$$

In Eq. (III.8) the two mixed integrals over Δn and n^{in} were combined, since with the definition of the Hartree potential, Eq. (II.81), we have the identity

$$\int \Delta n(\mathbf{r}) v_{\text{H}}[n^{\text{in}}(\mathbf{r})] \, d\mathbf{r} = \int n^{\text{in}}(\mathbf{r}') v_{\text{H}}[\Delta n(\mathbf{r}')] \, d\mathbf{r}' \quad .$$

*In-depth discussions of the expansion of the Kohn–Sham functional can be found in Sec. 3.3 of Ref. 19 and in Refs. 60 and 33.

The exchange–correlation potential v_{xc} , defined in Eq. (II.88), is not in general linear in the density and the expansion of the exchange–correlation energy about the trial density is not as trivial as for the Hartree energy in Eq. (III.8). However, if Δn is sufficiently small a truncated Taylor expansion is a good approximation, which is given to first order by

$$\begin{aligned} E_{\text{xc}}[n^{\text{out}}] &= E_{\text{xc}}[n^{\text{in}} + \Delta n] \\ &= E_{\text{xc}}[n^{\text{in}}] + \int \Delta n(\mathbf{r}) v_{\text{xc}}[n^{\text{in}}(\mathbf{r})] \, \mathrm{d}\mathbf{r} + \mathcal{O}(\Delta n^2) \quad , \end{aligned} \quad (\text{III.9})$$

where the definition of v_{xc} of Eq. (II.88) was employed. Inserting the expansions in Eqs. (III.7), (III.8) and (III.9) into the Kohn–Sham functional of Eq. (III.4) yields

$$\begin{aligned} E^{\text{KS}}[n^{\text{in}}, \Delta n] &= \sum_i f_i \varepsilon_i[n^{\text{in}}] - \int n^{\text{in}} v_{\text{H}}[n^{\text{in}}] \, \mathrm{d}\mathbf{r} - \int \Delta n v_{\text{H}}[n^{\text{in}}] \, \mathrm{d}\mathbf{r} \\ &\quad - \int n^{\text{in}} v_{\text{xc}}[n^{\text{in}}] \, \mathrm{d}\mathbf{r} - \int \Delta n v_{\text{xc}}[n^{\text{in}}] \, \mathrm{d}\mathbf{r} \\ &\quad + E_{\text{H}}[n^{\text{in}}] + E_{\text{H}}[\Delta n] + \int \Delta n v_{\text{H}}[n^{\text{in}}] \, \mathrm{d}\mathbf{r} \\ &\quad + E_{\text{xc}}[n^{\text{in}}] + \int \Delta n v_{\text{xc}}[n^{\text{in}}] \, \mathrm{d}\mathbf{r} + \mathcal{O}(\Delta n^2) \quad , \end{aligned}$$

where all first order terms in Δn cancel out. Note, that this is in agreement with the second Hohenberg–Kohn theorem (Sec. II.3.1), i. e. it is a consequence of the ground-state density being a stationary point of the energy functional. After recombination of the Hartree terms one arrives at a first-order expansion of the KS functional

$$\begin{aligned} E^{\text{KS}}[n^{\text{in}}, \Delta n] &= \sum_i f_i \varepsilon_i[n^{\text{in}}] - \int n^{\text{in}} v_{\text{xc}}[n^{\text{in}}] \, \mathrm{d}\mathbf{r} \\ &\quad - E_{\text{H}}[n^{\text{in}}] + E_{\text{xc}}[n^{\text{in}}] + \mathcal{O}(\Delta n^2) \quad , \end{aligned} \quad (\text{III.10})$$

in which $E_{\text{H}}[\Delta n]$ was absorbed in the second order term $\mathcal{O}(\Delta n^2)$.

III.1.2. The Harris–Foulkes functional

As is apparent from the expansion in Eq. (III.10), to first order the Kohn–Sham functional only depends on the input density. We now introduce the approximate Harris–Foulkes functional \mathcal{E}^{HF} by truncating the expansion in Eq. (III.10) after the first order terms

$$\mathcal{E}^{\text{HF}}[n^{\text{in}}] = \sum_i f_i \varepsilon_i[n^{\text{in}}] + \mathcal{D}^{\text{HF}}[n^{\text{in}}] \quad , \quad (\text{III.11})$$

where we additionally define the Harris–Foulkes double counting correction as

$$\mathcal{D}^{\text{HF}}[n^{\text{in}}] := - \int n^{\text{in}} v_{\text{xc}}[n^{\text{in}}] \mathbf{d}\mathbf{r} - E_{\text{H}}[n^{\text{in}}] + E_{\text{xc}}[n^{\text{in}}] \quad . \quad (\text{III.12})$$

The Harris–Foulkes functional, Eq. (III.11), is no longer self-consistent, as it only depends on the input density. However, for the case of KS self-consistency, i. e. for $n^{\text{in}} = n^{\text{out}} = n_0$, both functionals are equal

$$E^{\text{KS}}[n_0] = \mathcal{E}^{\text{HF}}[n_0] \quad , \quad (\text{III.13})$$

as is evident from the comparison with the Kohn–Sham functional, Eq. (III.4). By construction, the difference between the true KS functional and the Harris–Foulkes estimate grows with the second order in the density error $\Delta n = n_0 - n^{\text{in}}$. Note that the functional \mathcal{E}^{HF} is not variational with respect to the density. It has, however, a stationary point at the ground-state density n_0 .^{61,62}

III.2. The tight-binding method

The tight-binding (TB) electronic structure method can be understood as a semiempirical approximation to Kohn–Sham DFT. However, the principles of the method have been introduced already by Slater and Koster in 1954, which predates DFT by one decade.¹⁴ The formal relation between the two methods was established by Foulkes and Haydock in 1989²⁸ and is related to the first order approximation to the Kohn–Sham functional of Sec. III.1.2.

Originally, the TB method was developed to gain insight into the electronic structure of solids by approximating the band energies, i. e. the eigenvalues $\{\varepsilon_i\}$ of the one-electron Hamiltonian of Eq. (II.82). For this purpose the *frozen core* approximation is introduced and only valence electrons are considered. The KS eigenproblem, Eq. (II.82), is solved for a minimal basis representation of the valence wave functions (see Sec. II.4.1) in atom-centered, hydrogen-like *atomic orbitals* (AOs)

$$\sum_{\beta\nu} H_{\alpha\mu,\beta\nu} c^{i,\beta\nu} = \varepsilon_i \sum_{\beta\nu} S_{\alpha\mu,\beta\nu} c^{i,\beta\nu} \leftrightarrow \mathbf{H} \mathbf{c}_i = \varepsilon_i \mathbf{S} \mathbf{c}_i \quad . \quad (\text{III.14})$$

The indices α and β of the basis functions enumerate the atomic centers, μ and ν are combined indices for the angular momentum ℓ and the magnetic quantum number m of the corresponding AO. In tight-binding calculations the matrix elements of the Hamilton and overlap matrices, Eq. (II.91), are, however, not explicitly calculated. The integrals are instead parametrized in dependence of the interatomic distance for reference dimer orientations. The matrix elements for arbitrary structures and molecules can then be estimated in a two-center approximation using the Slater–Koster interpolation rules.

III.2.1. Two-center approximation

The eigenfunctions of the atomic Hamiltonian, atomic orbitals (AOs), are given by a radial function $f_{\alpha\ell}$ times a spherical harmonic function $Y_{\ell m}$

$$\begin{aligned} \phi_{\alpha\ell m}(\mathbf{r} - \mathbf{R}_\alpha) &= f_{\alpha\ell}(r) Y_{\ell m}(\widehat{\mathbf{r} - \mathbf{R}_\alpha}) \\ \text{with } r &= |\mathbf{r} - \mathbf{R}_\alpha| \quad \text{and} \quad \widehat{\mathbf{r} - \mathbf{R}_\alpha} = \frac{\mathbf{r} - \mathbf{R}_\alpha}{r} \quad , \end{aligned} \quad (\text{III.15})$$

where α enumerates the atomic centers and chemical species, ℓ is the magnitude of the angular momentum, and m is the magnetic quantum number (the z component of the angular momentum). Unless the explicit values are needed we will in the following combine the ℓ and m quantum numbers in joined indices μ or ν in order to enhance the readability. The real valued radial functions $f(r)$ are usually chosen to decay

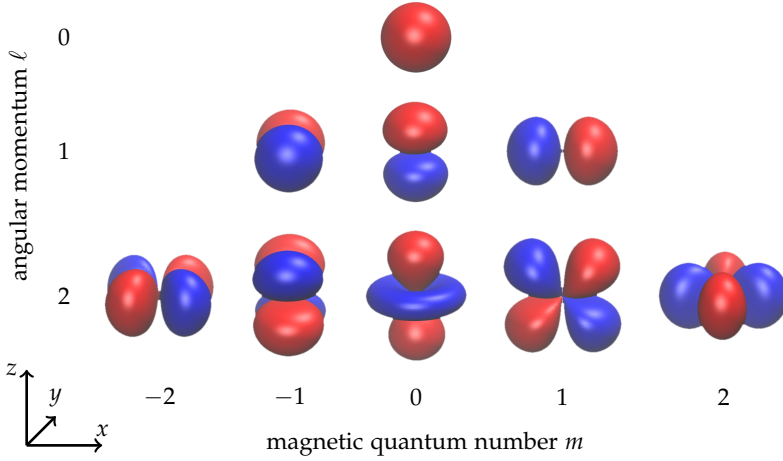


Figure III.1. The real valued spherical harmonic functions (cubic harmonics) $Y_{\ell m}$ for angular momenta $0 \leq \ell \leq 2$ (corresponding to s , p and d orbitals).

exponentially with r , as do the analytical solutions for the hydrogen atom. Note that here and elsewhere in this thesis $Y_{\ell m}$ refers to the *real valued* spherical harmonics (as opposed to the complex spherical harmonics). The spherical harmonics for $\ell \leq 2$ are depicted in Fig. III.1.

A matrix element of an operator \hat{o} in the basis of AOs is given by

$$O_{\alpha\mu,\beta\nu} = \langle \alpha\mu | \hat{o} | \beta\nu \rangle = \int \phi_{\alpha\mu}(\mathbf{r}) \hat{o} \phi_{\beta\nu}(\mathbf{r} - \mathbf{R}_{\alpha\beta}) d\mathbf{r} \quad , \quad (\text{III.16})$$

where $\hat{o} = \hat{h}$ for the Hamilton matrix and $\hat{o} = \mathbb{1}$ for the overlap matrix and $\mathbf{R}_{\alpha\beta} = \mathbf{R}_\beta - \mathbf{R}_\alpha$ is the connecting vector between the two atomic centers α and β . Since the external potential of all nuclei, Eq. (II.13), enters the effective KS potential, the one-electron Hamilton operator of Eq. (II.82)

$$\hat{h}(\mathbf{r}, \{\mathbf{R}\}) = \hat{t}_s(\mathbf{r}) + v_{\text{eff}}^{\text{KS}}(\mathbf{r}, \{\mathbf{R}\})$$

in principle depends on all atomic coordinates $\{\mathbf{R}\}$. However, the values of the AOs, Eq. (III.15), decay exponentially with distance from their origins and the atomic

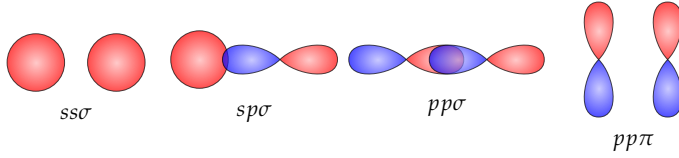


Figure III.2. Schematic of the Slater–Koster reference bonds for s and p orbitals. The cartoons refer to the real valued spherical harmonics depicted in Fig. III.1. The labels correspond to the classic notation of Ref. 14. See Fig. III.3 for the additional bonds for the case that d orbitals are present.

Coulomb potentials decay with r^{-1} . The interaction between a potential at one atomic site with orbitals at two other atomic sites, i. e. *three-center* interactions, are therefore much smaller than two-center interactions.* Motivated by this argumentation, three-center interactions are neglected in the TB method. A special case are those integrals over two orbitals at the same center, the on-site matrix elements $O_{\alpha\mu,\alpha\nu}$. In traditional TB these on-site elements are set to their values in the corresponding free, unbound atoms. For the Hamilton matrix this means the diagonal on-site matrix elements are set to the atomic eigenvalues and the off-diagonal on-site Hamilton matrix elements are set to zero. However, depending on the actual TB implementations the on-site elements might be parametrized as well. See also Sec. III.3 for some examples and Chapter V for our own approach to an on-site parametrization.

III.2.2. Slater–Koster interpolation

Slater and Koster realized that the functional form of the atomic orbitals, Eq. (III.15), makes it possible to analytically expand arbitrary two-center integrals $O_{\alpha\ell_1 m_1, \beta\ell_2 m_2}(\mathbf{R}_{\alpha\beta})$ as of Eq. (III.16) in distance-dependent contributions $O_{\alpha\ell_1, \beta\ell_2}^m(R_{\alpha\beta})$ for a chosen reference orientation.¹⁴ The Slater–Koster reference bonds for systems involving s , p , and d orbitals ($\ell = 0, 1, 2$) are shown in Figs. III.2 and III.3. Selecting the Cartesian $\hat{\mathbf{z}}$ -direction

*Although the individual three-center contributions are small, already Slater and Koster noted that the sum of all three-center terms may indeed be quite significant.¹⁴

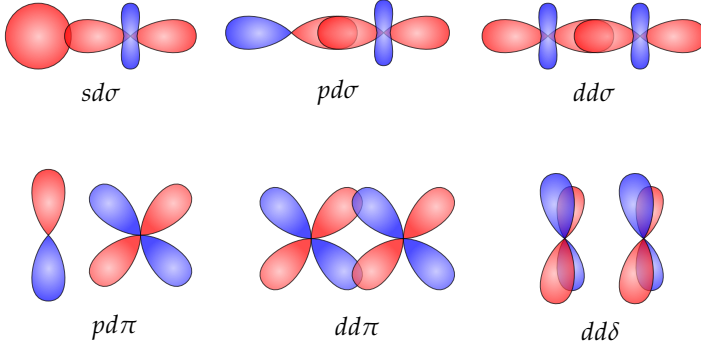


Figure III.3. Schematic of the additional Slater–Koster reference bonds arising from the d orbitals. See Fig. III.2 for the s and p bonds.

as reference we have

$$O_{\alpha\ell_1, \beta\ell_2}^m(R_{\alpha\beta}) = \int \phi_{\alpha\ell_1 m}(\mathbf{r}) \hat{o} \phi_{\beta\ell_2 m}(\mathbf{r} - R_{\alpha\beta} \hat{\mathbf{z}}) d\mathbf{r} \quad , \quad (\text{III.17})$$

and the expansion of general matrix elements can be written as

$$O_{\alpha\ell_1 m_1, \beta\ell_2 m_2}(\mathbf{R}_{\alpha\beta}) = \sum_m^{\min(m_1, m_2)} c_{\ell_1, \ell_2}^m(\hat{\mathbf{R}}_{\alpha\beta}) O_{\alpha\ell_1, \beta\ell_2}^m(R_{\alpha\beta}) \quad . \quad (\text{III.18})$$

The coefficients c_{ℓ_1, ℓ_2}^m in Eq. (III.18) only depend on the angular part of the connecting vector between the two atomic centers. In fact, the expansion in Eq. (III.18) corresponds to the rotation of the matrix element from the local orientation of the reference bond (the $\hat{\mathbf{z}}$ direction) into the actual orientation in the global coordinate system, and the c_{ℓ_1, ℓ_2}^m are elements of rotation matrices. Slater and Koster derived explicit expressions for these rotation matrices for angular momenta $\ell \leq 2$. An analytical formula for arbitrary angular momenta was derived by Podolskiy and Vogl and is reproduced in Appendix A.2.^{14,63,64}

III.3. Implementations of the TB method

The previous section exclusively dealt with the TB approximation to the electronic structure. Despite that, it is usually desired to calculate total energies. There are a number of total energy TB implementations that differ in the way how the total TB energy is defined.

In general, TB models can be divided into two classes: (1) non-self-consistent models that are closely related to the Harris–Foulkes functional, Eq. (III.11), and (2) self-consistent models that incorporate features of the Kohn–Sham functional, Eq. (III.4). Apart from this difference, a common additional approximation to the electronic structure is to require the orthogonality of the atomic orbitals, i. e. to imply Löwdin’s orthogonalized orbitals.⁶⁵ One therefore further distinguishes between orthogonal TB (OTB) models and non-orthogonal TB (NOTB) models.

The common starting point for all TB models discussed in this section is the expression of the total electronic energy as sum over one-electron eigenvalues E_{band} plus double counting \mathcal{D} and the electrostatic repulsion of the ions E_{nn}

$$E_{\text{tot}} = E_{\text{band}} + \mathcal{D} + E_{\text{nn}} = \sum_i f_i \varepsilon_i + \mathcal{D} + E_{\text{nn}} \quad , \quad (\text{III.19})$$

which was derived for the (formally exact) Kohn–Sham functional and the approximate Harris–Foulkes functional in Sec. III.1. In tight-binding models the parametrization of the double-counting \mathcal{D} and the ion–ion repulsion E_{nn} is often combined, so that it is more convenient to discuss the total energy (of static atoms) in the following, rather than the electronic energy only. The eigenvalues $\{\varepsilon_i\}$ of the one-electron Hamiltonian are calculated from approximate TB Hamilton matrices that are based on the Slater–Koster interpolation method of Sec. III.2.2.

III.3.1. The tight-binding band model

The simplest, and historically first TB approximation of the total energy is the tight-binding *band* model.⁶⁶ Here, the double counting term and the ion–ion repulsion are

combined in a single interatomic pair-potential v_{pp} , so that the total energy is given as

$$E_{\text{tot}}^{\text{TB}} = \sum_i f_i \epsilon_i + \sum_{\alpha, \beta} v_{pp}(R_{\alpha\beta}) \quad . \quad (\text{III.20})$$

This approach has, at a later time, been justified by Foulkes and Haydock, who showed that at the ground state the double counting term can be well approximated by pairwise interactions.²⁸ Thus, in the TB band model self-consistent convergence of the ground state density is assumed.

III.3.2. Structural energy difference theorem

The *structural energy difference theorem* (SEDt) and its more general predecessor, the *force theorem*, both derived by Pettifor, are very helpful to understand and analyze total energy differences (and therefore stabilities) of different compounds.^{19,67–70} The theorems relate the total energy difference of two structures to the difference in their bond energies. Here we will give a brief summary of the implications of the SEDt for tight-binding implementations. For in-depth discussions of the subject the reader is referred to Refs. 70 and 19.

Let us for a moment forget about the tight-binding approximation and consider the properties of the true total (electronic) energy. Though, usually we are interested not in the total energy, but in the possibly small energetic difference of structures that determine the structural stability. Since the calculation of the small difference of two large numbers is challenging, it is helpful to further subdivide the total energy as we have already done in Eq. (III.19). Assume, that we can always express the total energy as the sum of a bonding and a repulsive contribution

$$E_{\text{tot}} = E_{\text{bond}} + E_{\text{rep}} \quad . \quad (\text{III.21})$$

Pettifor provides a suitable definition of the bond energy E_{bond} as the difference of the band energy Eq. (III.6) of the compound and the free atoms^{67,69,70}

$$E_{\text{bond}} = \int f(\epsilon) g(\epsilon) \epsilon \, d\epsilon - \sum_{\alpha} \sum_{\mu} f_{\alpha\mu}^{\text{at}} \epsilon_{\alpha\mu}^{\text{at}} \quad , \quad (\text{III.22})$$

which is guaranteed to be negative if the compound is stable. However, alternative definitions might also be appropriate. Let x be a universal structural parameter (for crystals this could be the unit cell volume or the nearest-neighbor distance) and let us consider the energies E_{tot}^1 and E_{tot}^2 of two different structures as functions of x . The minimum geometries shall correspond to x_1 and x_2 , so that

$$\left. \frac{dE_{\text{tot}}^1(x)}{dx} \right|_{x=x_1} = \left. \frac{dE_{\text{tot}}^2(x)}{dx} \right|_{x=x_2} = 0 \quad . \quad (\text{III.23})$$

Now choose \tilde{x}_1 so that the repulsive fraction of the total energy, Eq. (III.21), of the first structure is identical to that one of the second structure at its minimum

$$E_{\text{rep}}^1(\tilde{x}_1) = E_{\text{rep}}^2(x_2) \quad . \quad (\text{III.24})$$

The Taylor expansion of the total energy of the first structure at the chosen value of x is given by

$$E_{\text{tot}}^1(\tilde{x}_1) = E_{\text{tot}}^1(x_1) + \left. \frac{dE_{\text{tot}}^1(x)}{dx} \right|_{x=x_1} \Delta x_1 + \mathcal{O}(\Delta x_1^2) \quad (\text{III.25})$$

$$\text{with } \Delta x_1 = \tilde{x}_1 - x_1$$

where the first order term vanishes because of the minimum condition in Eq. (III.23). Combining the Eqs. (III.21), (III.24) and (III.25) the total energy difference of the two structures at their minimum geometry

$$\Delta E_{\text{tot}} = E_{\text{tot}}^1(x_1) - E_{\text{tot}}^2(x_2)$$

can thus be expressed as

$$\Delta E_{\text{tot}} = E_{\text{bond}}^1(\tilde{x}_1) - E_{\text{bond}}^2(x_2) - \mathcal{O}(\Delta x_1^2) \quad . \quad (\text{III.26})$$

So the total energy difference of two structures is, to first order, given by the change in the bond energy. Note, that the theorem is independent of the actual partitioning of the total energy in Eq. (III.21). The comparison of the energy of two structures according to the SEDT (III.26) has to proceed in two steps: (1) the parameter \tilde{x}_1 is

to be determined, for which the desired part of the total energy cancels out. (2) The remaining parts of the total energies can be compared.

It is simple to come up with two structures, for which the repulsive energy of the TB band model, Eq. (III.20), is the same. Pettifor has, however, shown that the difference in the band energy of two structures does not provide first-order estimate of the change in total energy.⁶⁹ The SEDT is therefore not fulfilled by the TB band model.

III.3.3. The tight-binding bond model

The TB band model of Sec. III.3.1 provides an approximation of the *total* energy. One is, however, usually interested in the energetic *difference* of two systems, for example, to estimate the relative stability. Motivated by this fact and by the considerations that lead to the SEDT in the previous section, Sutton et al. chose the *cohesive energy* as central quantity of their TB *bond* model (TBBM).⁷¹ The cohesive energy is defined as difference of the total energies of the compound and the free atoms*

$$E_{\text{coh}} = \mathcal{E}^{\text{HF}}[n^{\text{in}}] - \sum_{\alpha} E_{\alpha}^{\text{at}} + E_{\text{nn}} \quad , \quad (\text{III.27})$$

where \mathcal{E}^{HF} is the Harris–Foulkes functional, Eq. (III.11), and E_{α}^{at} is the energy of the free, unbound atom α . Choosing the atomic Kohn–Sham orbitals as the TB atomic orbital basis, the atomic energies are given by

$$E_{\alpha}^{\text{at}} = \sum_{\mu} f_{\alpha\mu}^{\text{at}} \epsilon_{\alpha\mu}^{\text{at}} + \mathcal{D}[n_{\alpha}^{\text{at}}] \quad (\text{III.28})$$

where $\{\epsilon_{\alpha\mu}^{\text{at}}\}$ are the atomic eigenvalues, n_{α}^{at} is the atomic electron density and the double counting term \mathcal{D}^{HF} is defined in Eq. (III.12).

Next we construct an input density n^{in} as superposition of the atomic densities

$$n^{\text{in}}(\mathbf{r}) = \sum_{\alpha} n_{\alpha}^{\text{at}}(\mathbf{r} - \mathbf{R}_{\alpha}) \quad . \quad (\text{III.29})$$

*Sutton et al. use the term *binding energy* rather than cohesive energy, but I find that easily to be confused with the covalent *bond energy*.

With this ansatz for the density the Hartree potential Eq. (II.81) of the compound is simply the sum of the atomic potentials

$$v_{\text{H}}[n^{\text{in}}] = \sum_{\alpha} v_{\text{H}}[n_{\alpha}^{\text{at}}] \quad , \quad (\text{III.30})$$

but the Hartree energy, Eq. (II.81), additionally contains a sum over off-diagonal terms

$$\begin{aligned} E_{\text{H}}[n^{\text{in}}] &= \frac{1}{2} \int n^{\text{in}}(\mathbf{r}) v_{\text{H}}[n^{\text{in}}(\mathbf{r})] \, d\mathbf{r} \\ &= \sum_{\alpha} E_{\text{H}}[n_{\alpha}^{\text{at}}] + \underbrace{\sum_{\alpha \neq \beta} \frac{1}{2} \int n_{\alpha}^{\text{at}}(\mathbf{r}) v_{\text{H}}[n_{\beta}^{\text{at}}(\mathbf{r})] \, d\mathbf{r}}_{\Delta E_{\text{H}}} \quad . \end{aligned} \quad (\text{III.31})$$

As discussed in Sec. III.1.1, the exchange-correlation potential $v_{\text{xc}}[n^{\text{in}}]$, Eq. (II.88), is a non-linear functional of the density and an analytical expansion in atomic contributions of the remaining differences of the double counting corrections of the compound and the free atoms is therefore not possible. We thus simply define the difference

$$\Delta E_{\text{xc}} := \mathcal{D}[n^{\text{in}}] - \sum_{\alpha} \mathcal{D}[n_{\alpha}^{\text{at}}] + \Delta E_{\text{H}} \quad . \quad (\text{III.32})$$

Inserting Eqs. (III.28), (III.31) and (III.32) into the expression of the cohesive energy, Eq. (III.27), yields

$$\begin{aligned} E_{\text{coh}} &= \sum_{\alpha\mu} \sum_{\beta\nu} \left(P^{\beta\nu, \alpha\mu} H_{\alpha\mu, \beta\nu} - \delta_{\alpha\beta} \delta_{\mu\nu} f_{\alpha\mu}^{\text{at}} \epsilon_{\alpha\mu}^{\text{at}} \right) \\ &\quad - \Delta E_{\text{H}} + \Delta E_{\text{xc}} + E_{\text{nn}} \quad , \end{aligned} \quad (\text{III.33})$$

where we introduce the *density matrix* as*

$$P^{\beta\nu, \alpha\mu} := \sum_i f_i (c^{i, \alpha\mu})^* c^{i, \beta\nu} \quad . \quad (\text{III.34})$$

Again, $\{c^{i, \alpha\mu}\}$ are the eigenvectors of the TB eigenvalue problem of Eq. (III.14). With this definition we can rewrite the band sum of Eq. (III.5) as

$$\sum_i \epsilon_i = \sum_{\alpha\mu, \beta\nu} P^{\alpha\mu, \beta\nu} H_{\beta\nu, \alpha\mu} \quad , \quad (\text{III.35})$$

which is the trace over the matrix product of the density matrix and the Hamiltonian.

*Here, P is the capital Greek letter ρ .

The double sum in Eq. (III.33) can be partitioned further in order to relate the cohesive energy to more physically motivated quantities. Sutton et al. define the covalent *bond energy* as all contributions to the band sum that arise from integrals with orbitals at two different centers

$$E_{\text{bond}} = \sum_{\substack{\alpha\mu, \beta\nu \\ \alpha \neq \beta}} P^{\beta\nu, \alpha\mu} H_{\alpha\mu, \beta\nu} = E_{\text{band}} - \sum_{\alpha} \sum_{\mu\nu} P^{\alpha\nu, \alpha\mu} H_{\alpha\mu, \alpha\nu} \quad . \quad (\text{III.36})$$

This definition is consistent with the bond energy of Eq. (III.22). The remaining on-site terms are grouped with their atomic counterparts in the *promotion energy*

$$E_{\text{prom}} = \sum_{\alpha} \sum_{\mu\nu} \left(P^{\alpha\nu, \alpha\mu} H_{\alpha\mu, \alpha\nu} - P^{\alpha\nu, \alpha\mu, \text{at}} H_{\alpha\mu, \alpha\nu} \right) \quad , \quad (\text{III.37})$$

which describes the change of the atomic charges upon condensation of the free, infinitely separated atoms to the compound. Note, that in the case of an orthogonal basis the diagonal elements of the density matrix directly correspond to Mulliken's orbital populations $q_{\alpha\mu} = P^{\alpha\mu, \alpha\mu}$ (Mulliken charges).⁷² The atomic density matrix in the AO basis (which consists of atomic eigenstates) is diagonal with $P^{\beta\nu, \alpha\mu, \text{at}} = \delta_{\mu\nu} f_{\alpha\mu}^{\text{at}}$, so that the promotion energy can be equivalently expressed as

$$E_{\text{prom}} = \sum_{\alpha} \sum_{\mu\nu} \left(P^{\alpha\nu, \alpha\mu} H_{\alpha\mu, \alpha\nu} - \delta_{\mu\nu} f_{\alpha\mu}^{\text{at}} H_{\alpha\mu, \alpha\nu} \right) \quad . \quad (\text{III.38})$$

As briefly discussed in Sec. III.2.1, the on-site elements of the Hamilton matrix are commonly set to their corresponding atomic values in conventional TB parametrizations. In such cases the promotion energy, Eq. (III.38), simplifies to

$$E_{\text{prom}} = \sum_{\alpha\mu} \left(P^{\alpha\mu, \alpha\mu} - f_{\alpha\mu}^{\text{at}} \right) \epsilon_{\alpha\mu}^{\text{at}} \quad \text{and} \quad H_{\alpha\mu, \alpha\nu} = \delta_{\mu\nu} \epsilon_{\alpha\mu}^{\text{at}} \quad . \quad (\text{III.39})$$

In Ref. 71 Sutton et al. also argue that both, ΔE_{H} and ΔE_{xc} , can be well approximated by pair-wise interactions. The TBBM cohesive energy is therefore defined as

$$E_{\text{coh}}^{\text{TBBM}} = E_{\text{bond}} + E_{\text{prom}} + \sum_{\alpha, \beta} v_{\text{pp}}(R_{\alpha\beta}) \quad , \quad (\text{III.40})$$

where the distance dependent pair potential v_{pp} also includes the ionic repulsion E_{nn} .

The tight-binding bond model as constructed in Ref. 71 requires additionally the *local charge neutrality* (LCN) of all atoms. This condition is especially met in metals, in which charges can redistribute freely, but it is also a good approximation for semiconductors.⁷³ In practice, LCN is established by applying a common constant shift to all diagonal elements $H_{\alpha\mu,\alpha\mu}$ of the Hamilton matrix in such a way that Mulliken's orbital populations⁷²

$$q_{\alpha\mu} = \sum_{\beta\nu} P^{\alpha\mu,\beta\nu} S_{\beta\nu,\alpha\mu} = P^{\alpha\mu}_{\alpha\mu} \quad (\text{III.41})$$

become equal to the atomic orbital occupations $f_{\alpha\mu}^{\text{at}}$. Note that this implies a self-consistent adjustment of the on-site levels, as the density matrix depends on the eigenvectors of the Hamilton matrix that is modified. The motivation for the LCN condition arises from the expression of the atomic forces, where it becomes evident that the SEDT of Sec. III.3.2 is only fulfilled upon LCN. The reader is referred to Ref. 71 for a detailed derivation.

III.3.4. Self-consistent charge TB

To improve on the requirement of local charge neutrality Elstner and coworkers suggested to go beyond the first-order expansion of the Kohn–Sham energy functional (Sec. III.1.1) and to include the second order corrections to the exchange–correlation energy.^{33,74} The Taylor expansion of the exchange–correlation energy, Eq. (III.9), up to second order in density fluctuations is given by

$$\begin{aligned} E_{\text{xc}}[n^{\text{in}} + \Delta n] &= E_{\text{xc}}[n^{\text{in}}] + \int \Delta n(\mathbf{r}) \left. \frac{\delta E_{\text{xc}}}{\delta n(\mathbf{r})} \right|_{n^{\text{in}}} d\mathbf{r} \\ &+ \frac{1}{2} \int \int \Delta n(\mathbf{r}) \Delta n(\mathbf{r}') \left. \frac{\delta^2 E_{\text{xc}}}{\delta n(\mathbf{r}) \delta n(\mathbf{r}')} \right|_{n^{\text{in}}} d\mathbf{r} d\mathbf{r}' + \mathcal{O}(\Delta n^3) \quad . \end{aligned} \quad (\text{III.42})$$

The first-order variation of E_{xc} is simply the definition of the exchange–correlation potential of Eq. (II.88), so that the total energy functional, using the results of Sec. III.1.1, becomes

$$\begin{aligned} E_{\text{KS}}[n^{\text{in}}, \Delta n] &= E_{\text{band}}[n^{\text{in}}] - E_{\text{H}}[n^{\text{in}}] + E_{\text{xc}}[n^{\text{in}}] + E_{\text{nn}} \\ &- \int n^{\text{in}} v_{\text{xc}}[n^{\text{in}}] d\mathbf{r} + E^{2\text{nd}}[n^{\text{in}}, \Delta n] + \mathcal{O}(\Delta n^3) \quad , \end{aligned} \quad (\text{III.43})$$

with the second order correction

$$\begin{aligned} E^{\text{2nd}} &= E_{\text{H}}[\Delta n] + \frac{1}{2} \int \int \Delta n(\mathbf{r}) \Delta n(\mathbf{r}') \frac{\delta^2 E_{\text{xc}}}{\delta n(\mathbf{r}) \delta n(\mathbf{r}')}\bigg|_{n^{\text{in}}} \mathbf{d}\mathbf{r} \mathbf{d}\mathbf{r}' \\ &= \frac{1}{2} \int \int \Delta n(\mathbf{r}) \Delta n(\mathbf{r}') \left(\frac{1}{|\mathbf{r} - \mathbf{r}'|} + \frac{\delta^2 E_{\text{xc}}}{\delta n(\mathbf{r}) \delta n(\mathbf{r}')}\bigg|_{n^{\text{in}}} \right) \mathbf{d}\mathbf{r} \mathbf{d}\mathbf{r}' . \end{aligned} \quad (\text{III.44})$$

If the charge fluctuation Δn is partitioned into scalar atomic contributions Δq_{α}

$$\Delta n(\mathbf{r}) = \sum_{\alpha} \Delta q_{\alpha} n_{\alpha}(\mathbf{r}) \quad \text{with} \quad \sum_{\alpha} \Delta q_{\alpha} = \int \Delta n(\mathbf{r}) \mathbf{d}\mathbf{r} \quad \text{and} \quad \int n_{\alpha}(\mathbf{r}) \mathbf{d}\mathbf{r} = 1 \quad (\text{III.45})$$

the second-order correction Eq. (III.44) can be expressed in terms of pairwise interaction parameters $\gamma_{\alpha\beta}$

$$E^{\text{2nd}} = \frac{1}{2} \sum_{\alpha, \beta} \Delta q_{\alpha} \Delta q_{\beta} \gamma_{\alpha\beta} . \quad (\text{III.46})$$

In case of spherical partition functions $n_{\alpha}(\mathbf{r})$ Elstner et al. argue that the interaction parameter $\gamma_{\alpha\beta}$ can be well approximated by

$$\gamma_{\alpha\beta} = \begin{cases} U_{\alpha} & \text{if } \alpha = \beta \\ 1/R_{\alpha\beta} & \text{else} \end{cases} . \quad (\text{III.47})$$

The element specific parameter U_{α} in Eq. (III.47) is the *Hubbard* U , which is related to the chemical hardness.⁷⁵ For the inter-site case $\gamma_{\alpha\beta}$ is equal to the Coulomb potential, while for the on-site case the parameter accounts for the self-interaction.

Combining the results and approximating the double counting term and the ion-ion repulsion by a pairwise interaction potentials as in the TB band model of Sec. III.3.1 the total TB energy expression reads

$$E_{\text{tot}}^{\text{SCC}} = \sum_i f_i \varepsilon_i + \frac{1}{2} \sum_{\alpha} \Delta q_{\alpha}^2 U_{\alpha} + \frac{1}{2} \sum_{\alpha \neq \beta} \frac{\Delta q_{\alpha} \Delta q_{\beta}}{R_{\alpha\beta}} . \quad (\text{III.48})$$

For periodic structures standard methods, such as Ewald summation, can be employed to evaluate the last term in Eq. (III.48), the Coulomb energy.⁷⁶ The atom-centered

charge fluctuations Δq_α may be estimated as difference of the atomic charge q_α^{at} and the charge q_α obtained from Mulliken's population analysis⁷²

$$\Delta q_\alpha = q_\alpha^{\text{at}} - q_\alpha \quad \text{with} \quad q_\alpha = \sum_{\mu \in \alpha} \sum_{\nu \beta} P^{\mu\alpha, \nu\beta} S_{\nu\beta, \mu\alpha} \quad . \quad (\text{III.49})$$

The minimum of the energy expression Eq. (III.48) has to be determined self-consistently, as the atomic Mulliken charges depend on the eigenvectors of the Hamiltonian, which in turn depends on the charges. The second-order corrected elements of the Hamilton matrix are given by

$$H_{\mu\alpha, \nu\beta} = H_{\mu\alpha, \nu\beta}^0 + \frac{1}{2} S_{\mu\alpha, \nu\beta} \sum_{\eta} (\gamma_{\alpha\eta} + \gamma_{\beta\eta}) \Delta q_\eta \quad , \quad (\text{III.50})$$

where $H_{\mu\alpha, \nu\beta}^0$ corresponds to the usual Slater–Koster Hamilton matrix elements.

III.3.5. The NRL tight-binding method

A very successful empirical non-orthogonal tight-binding implementation was developed by Cohen, Papaconstantopoulos and Mehl at the Naval Research Laboratory (NRL).^{21,77,78} The NRL-TB method exploits the fact that the actual value of the band sum, Eq. (III.5), depends upon the arbitrary choice of zero for the effective Kohn–Sham potential (see also Sec. IV.5.2 for a discussion of this gauge invariance). By adjusting the potential reference the shifted band energy E'_{band} can therefore always be chosen to be equal to the total energy

$$E'_{\text{band}} = E_{\text{tot}} \quad . \quad (\text{III.51})$$

For the TB total energy of Eq. (III.19) the corresponding structure dependent shift is formally given by

$$v_0 = \frac{E_{\text{tot}} - E_{\text{band}}}{N_e} = \frac{D + E_{\text{nn}}}{N_e} \quad , \quad (\text{III.52})$$

where N_e is the number of electrons. The shifted eigenvalues $\epsilon'_i = \epsilon + v_0$ then result in the desired band sum

$$E'_{\text{band}} = \sum_i f_i \epsilon'_i = E_{\text{band}} + \sum_i f_i \frac{E_{\text{tot}} - E_{\text{band}}}{N_e} = E_{\text{tot}} \quad .$$

The advantage of this potential energy gauge is that the double counting and the ionic repulsion do not need to be parametrized at all. Also note, that the definition of the shifted eigenvalues is such that it is independent of the method used to determine the eigenvalues. Thus, different electronic structure methods can be used to generate the reference data for an empirical fit.⁵³

The potential energy shift has to be reflected in the bond integrals, as the Kohn–Sham Hamiltonian contains the effective potential. Most notably, the diagonal elements of the Hamilton matrix, the on-site elements, can no longer be treated as structurally independent constants. Papaconstantopoulos et al. use an empirical functional form for the parametrization of the on-site elements that additionally allows to fit crystal-field splitting (see also Secs. I.1.4 and V.1).²¹

IV. From DFT to tight-binding

IV.1. Computational set-up	54
IV.2. Minimal AO basis representation	55
IV.2.1. The tensor notation for non-orthogonal basis functions	55
IV.2.2. Quality of the AO representation	57
IV.3. Optimization of AO basis sets	58
IV.3.1. Contracted atomic wave functions	60
IV.3.2. Confined atomic wave functions	61
IV.3.3. Expansion in an auxiliary basis	62
IV.4. Optimized minimal basis sets	65
IV.4.1. Optimized carbon AO basis	66
IV.4.2. Optimized titanium AO basis	72
IV.5. Derivation of tight-binding parameters	75
IV.5.1. Orthogonal tight-binding models	77
IV.5.2. The gauge freedom of the Hamilton matrix	77
IV.5.3. Continuous representation of the bond integrals	78
IV.5.4. Tight-binding parameters for carbon	80

This chapter presents our methodology for the derivation of tight-binding electronic structure models from density-functional theory. Starting point is a self-consistent DFT calculation, converged with respect to the basis set and the Brillouin zone integration. Using a projection method a representation of the Kohn–Sham orbitals in a minimal atomic orbital basis is determined, in which the Hamilton matrix and the overlap matrix elements are calculated.

In the first parts of the chapter the projection methodology is developed. Next, the optimization of minimal AO basis functions for the use in the projection scheme is discussed. The final two sections apply the basis optimization techniques to the examples of carbon and titanium and demonstrate the projection methodology for the construction of a vacuum level TB model for carbon.

IV.1. Computational set-up

Before we discuss numerical results we should briefly point out the computational set-up:

For all calculations presented in this chapter the pseudopotential DFT program by Meyer et al.^{79,80} was used, which employs a mixed basis of plane waves and local atom-centered functions and normconserving pseudopotentials.^{81,82} We generally used the gradient corrected exchange–correlation functional by Perdew, Burke and Enzerhof (PBE).^{83,84} All calculations were done without spin-polarization; this also includes the DFT calculations of the free atoms.

For carbon a plane wave energy cutoff of 30 Ry and a local $2p$ function with a range of 1.1 Bohr were used as basis set. The plane wave cutoff for titanium was 20 Ry and a local $3d$ function with a range of 2.2 Bohr was included in the basis set. The \mathbf{k} -point density was chosen to converge lattice constants and distances to 10^{-3} Bohr.

Algorithms that realize the projection methodology, the basis optimization techniques and the set-up and the solution of tight-binding eigenvalue problems have been implemented into the mixed basis DFT code. Additionally, a stand-alone tight-binding code has been developed, which allows TB electronic structure calculation as well as band structure and density of states analyses.

IV.2. Minimal AO basis representation

The tight-binding approximation to the electronic structure, as introduced in Sec. III.2, is based on the representation of the Kohn–Sham orbitals in a minimal basis of atomic orbitals (AOs). Therefore, the obvious way to derive TB models from DFT would be to perform a minimal basis DFT calculation and to extract the final matrix elements, Eq. (II.91). However, the representation of the DFT wave functions in a minimal AO basis set is not very accurate, since the AOs do not form a complete basis. Due to the artificially restricted space of trial densities, the self-consistent optimization (Sec. II.3.2) may lead to spurious results.

It is therefore preferable to perform a DFT calculation using a numerically converged basis set before changing the representation of the KS orbitals to the needed minimal AO basis. Let $|\psi^{\text{MB}}\rangle$ be the self-consistent Kohn–Sham functions in the numerically converged mixed basis. We seek the expansion in the minimal AO basis $\{|\phi_\mu\rangle\}$

$$|\psi_i^{\text{AO}}\rangle = \sum_\mu c^{i,\mu} |\phi_\mu\rangle \approx |\psi_i^{\text{MB}}\rangle \quad \text{with} \quad \mu = (\alpha\ell m) \quad . \quad (\text{IV.1})$$

For the moment it is not necessary to distinguish between different atoms, so that we include the atom index α in the combined index μ . As the AO basis is incomplete, the expansion in Eq. (IV.1) is not necessarily exact. Recall that atomic orbitals that are located at two different centers are not orthogonal to each other. In general the scalar product of two AOs is given by a finite overlap $\langle\phi_\mu|\phi_\nu\rangle = S_{\mu\nu}$ as already discussed in Sec. II.4.1. At this point it is convenient to introduce the *tensor notation* to avoid explicitly writing down the overlap matrix in all equations.

IV.2.1. The tensor notation for non-orthogonal basis functions

The tensor notation in matrix algebra renders the distinction between orthogonal and non-orthogonal basis functions unnecessary. In the context of electronic structure calculations, the tensor notation was, to the author’s knowledge, first introduced by Sinanoğlu.⁸⁵ See also Refs. 86–88 for introductions to the subject.

Given the set of (in general) non-orthogonal basis functions $\{|\phi_\mu\rangle\}$. We call these functions *covariant* and we will denote all covariant quantities with subscript indices. The overlap matrix is the *covariant metric*

$$S_{\mu\nu} = (\mathbf{S})_{\mu\nu} = \langle\phi_\mu|\phi_\nu\rangle \quad . \quad (\text{IV.2})$$

We now define a second set of basis functions, the *contravariant* basis $\{|\phi^\mu\rangle\}$, which we denote by superscript indices

$$|\phi^\mu\rangle := \sum_\nu |\phi_\nu\rangle (\mathbf{S}^{-1})^{\nu\mu} \quad \text{and} \quad \langle\phi^\mu| := \sum_\nu (\mathbf{S}^{-1})^{\mu\nu} \langle\phi_\nu| \quad . \quad (\text{IV.3})$$

The contravariant functions are *biorthogonal* to the covariant functions

$$\langle\phi^\mu|\phi_\nu\rangle = \sum_\eta (\mathbf{S}^{-1})^{\mu\eta} \langle\phi_\eta|\phi_\nu\rangle = \sum_\eta (\mathbf{S}^{-1})^{\mu\eta} (\mathbf{S})_{\eta\nu} = \delta_\nu^\mu \quad . \quad (\text{IV.4})$$

Together both sets of functions form a biorthogonal basis system, in which the contravariant functions are the *dual basis* in the dual vector space of the basis. Combining Eqs. (IV.3) and (IV.4) the contravariant metric is given by the inverse overlap matrix

$$S^{\mu\nu} := (\mathbf{S}^{-1})^{\mu\nu} = \langle\phi^\mu|\phi^\nu\rangle \quad . \quad (\text{IV.5})$$

Using this definition, the interconversion between covariant and contravariant quantities can be expressed as

$$|\phi^\mu\rangle = \sum_\nu |\phi_\nu\rangle S^{\nu\mu} \quad \text{and} \quad |\phi_\mu\rangle = \sum_\nu |\phi^\nu\rangle S_{\nu\mu} \quad . \quad (\text{IV.6})$$

The identity operator in the dual vector space can be conveniently expressed as

$$\mathbb{1} = \sum_\mu |\phi^\mu\rangle \langle\phi_\mu| = \sum_\mu |\phi_\mu\rangle \langle\phi^\mu| \quad . \quad (\text{IV.7})$$

However, the minimal atomic orbital basis sets that we discuss in this section do not generally span the whole space of the wave functions (Kohn–Sham orbitals), i. e. the expansion in Eq. (IV.1) is only approximate. For the case of such an incomplete basis the operator of Eq. (IV.7) performs a possibly lossy projection onto the AO basis. We therefore write more generally

$$\hat{P} = \sum_\mu |\phi_\mu\rangle \langle\phi^\mu| \quad (\text{IV.8})$$

for the projection onto the covariant basis functions. The projection operator \hat{P} is *idempotent*

$$\hat{P}^2|\chi\rangle = \hat{P}\hat{P}|\chi\rangle = \sum_{\mu} \sum_{\nu} |\phi_{\mu}\rangle \delta_{\nu}^{\mu} \langle\phi^{\nu}|\chi\rangle = \hat{P}|\chi\rangle \quad (\text{IV.9})$$

and hermitian

$$\begin{aligned} \langle\chi|\hat{P}|\xi\rangle &= \sum_{\mu} \langle\chi|\phi_{\mu}\rangle \langle\phi^{\mu}|\xi\rangle = \sum_{\nu} \langle\chi|\phi^{\nu}\rangle \sum_{\mu} S_{\nu\mu} \langle\phi^{\mu}|\xi\rangle \\ &= \sum_{\nu} \langle\chi|\phi^{\nu}\rangle \langle\phi_{\nu}|\xi\rangle = (\langle\xi|\hat{P}|\chi\rangle)^* \quad . \end{aligned} \quad (\text{IV.10})$$

With the operator \hat{P} the expansion in Eq. (IV.1) is simply given by

$$|\psi_i^{\text{AO}}\rangle = \hat{P} |\psi_i^{\text{MB}}\rangle = \sum_{\mu} |\phi_{\mu}\rangle \langle\phi^{\mu}|\psi_i^{\text{MB}}\rangle \quad , \quad (\text{IV.11})$$

and consequently the expansion coefficients are

$$c^{i,\mu} = \langle\phi^{\mu}|\psi_i^{\text{MB}}\rangle \quad . \quad (\text{IV.12})$$

IV.2.2. Quality of the AO representation

Since the expansion of the DFT wave functions in the incomplete AO basis, Eq. (IV.1), is not exact, it is desirable to quantify the degree of approximation. One measure of the quality of the projection is the *electronic spillage* function^{89,90}

$$\mathcal{S}_e := \frac{1}{N} \sum_i f_i \langle\psi_i^{\text{MB}}|(1 - \hat{P})|\psi_i^{\text{MB}}\rangle \quad , \quad (\text{IV.13})$$

where, again, N is the number of electrons and f_i is the occupation number of state i . Using the hermiticity and the idempotency of the projection operator, Eqs. (IV.10) and (IV.9), the spillage function can equivalently be expressed as

$$\begin{aligned} \mathcal{S}_e &= \frac{1}{N} \sum_i f_i \left(\langle\psi_i^{\text{MB}}|\psi_i^{\text{MB}}\rangle - \langle\psi_i^{\text{MB}}|\hat{P}|\psi_i^{\text{MB}}\rangle \right) \\ &= \frac{1}{N} \sum_i f_i \left(1 - \langle\psi_i^{\text{MB}}|\hat{P}|\psi_i^{\text{MB}}\rangle \right) = \frac{1}{N} \sum_i f_i \left(1 - \langle\psi_i^{\text{AO}}|\psi_i^{\text{AO}}\rangle \right) \quad , \end{aligned} \quad (\text{IV.14})$$

from which it is obvious, that the functions describes the fraction of charge that was *lost* (or *spilled*) during the projection. Above, the norm of the wave functions in the numerically complete mixed basis was replaced by one.

An alternative loss function is the *energy spillage*

$$\begin{aligned} \mathcal{S}_E &= \frac{1}{N} \sum_i f_i \left(\langle \psi_i^{\text{MB}} | \hat{h} | \psi_i^{\text{MB}} \rangle - \langle \psi_i^{\text{AO}} | \hat{h} | \psi_i^{\text{AO}} \rangle \right) \\ &= \frac{1}{N} \sum_i f_i \left(\varepsilon_i - \langle \psi_i^{\text{AO}} | \hat{h} | \psi_i^{\text{AO}} \rangle \right) \quad , \end{aligned} \quad (\text{IV.15})$$

which quantifies the approximation in the band energy. However, the energy spillage is less well comparable over different structures as there is a gauge freedom in the absolute value of the band energies (see Sec. IV.5.2) and the relative spillage is, therefore, arbitrary.

The spillage functions are suitable target functions for the optimization of basis sets, i. e. the closer the spillage is to zero, the better the basis can represent the wave functions.

IV.3. Optimization of AO basis sets

With the loss functions of the previous section at hand, one can think of tuning the shape of the basis functions to optimize the minimal basis representation of the wave functions. Restating Eq. (III.15), the functional form of atomic orbitals is given by the product of a radial function $f_{\alpha\ell}$ times a real spherical harmonic function $Y_{\ell m}$

$$\phi_{\alpha\ell m}(\mathbf{r} - \mathbf{R}_\alpha) = f_{\alpha\ell}(r) Y_{\ell m}(\widehat{\mathbf{r} - \mathbf{R}_\alpha}) \quad .$$

Consequently, the angular part of the AOs is uniquely determined by the angular momentum ℓ and the magnetic quantum number m of the AO and can not be modified without breaking the Slater–Koster interpolation method described in Sec. III.2.2. However, the radial functions are arbitrary and can be adjusted separately for each chemical species and each angular momentum. Note, that all DFT calculations that were carried out for this thesis employed the frozen-core approximation using pseudopotentials.

As a consequence, it is not necessary to keep track of the principal quantum number of the orbitals, as only the valence orbitals were calculated. Additionally, the radial functions of the pseudo wave functions are generally nodeless.

Several approaches towards optimized radial functions for atomic orbital basis sets have been suggested in the literature. For the case of numerical basis functions, i.e. where $f_{\alpha\ell}$ is not restricted to an analytical form, examples of optimization procedures are found in Refs. 89–91 and 92. Optimization techniques for the size reduction of analytical basis sets were, for example, used in Refs. 93 and 94.

We have evaluated four different optimization schemes for the minimization of the electronic spillage function, Eq. (IV.13), which will be described in the following.⁹⁵ The common idea behind all four optimization techniques is to iteratively adjust an initial guess for the AO radial functions in a restricted space that is defined by a small set of parameters $\{p_i\}$. With the electronic spillage as objective function the optimization problem is then given by the minimization

$$\min_{\{p_i\}} \mathcal{S}_e[f_{\alpha\ell}(\{p_i\})] \quad . \quad (\text{IV.16})$$

In condensed phases the potentials of the surrounding atoms will lead to an effective screening of the individual AOs. Compared to the wave functions of free atoms, a contraction of the AOs is therefore expected. Thus, one obvious method for the construction of transferable AO basis functions is to contract the atomic wave functions. The methods described in sections IV.3.1 and IV.3.2 accomplish such a contraction in two different ways. Alternatively, optimized radial function can be represented in an auxiliary radial basis, which is demonstrated in Sec. IV.3.3.

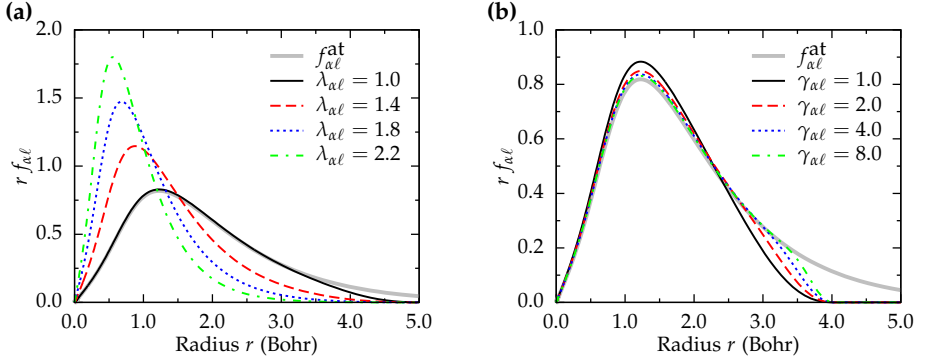


Figure IV.1. (a) Modified carbon 2s radial functions following Eq. (IV.18) for different contraction parameters $\lambda_{\alpha\ell}$. The steepness of the cutoff function was set to $\gamma_{\alpha\ell} = 1.0$ with a cutoff radius of $r_{\alpha\ell}^c = 5.0$ Bohr. (b) The same atomic radial function for various values of $\gamma_{\alpha\ell}$ with a cutoff radius of $r_{\alpha\ell}^c = 4.0$ Bohr and fixed contraction parameter $\lambda = 1.0$. The unmodified atomic radial function is shown as wide gray line in both diagrams.

IV.3.1. Contracted atomic wave functions

Optimized radial functions $f_{\alpha\ell}$ are constructed from the solutions $f_{\alpha\ell}^{\text{at}}$ of the radial Schrödinger equation for isolated atoms*

$$\left(-\frac{1}{2} \frac{1}{r^2} \frac{\partial}{\partial r} r^2 \frac{\partial}{\partial r} + \frac{\ell(\ell+1)}{2r^2} + v_{\text{eff}}^{\text{KS}}(r) \right) f_{\alpha\ell}^{\text{at}}(r) = \epsilon_{\alpha\ell}^{\text{at}} f_{\alpha\ell}^{\text{at}}(r) \quad (\text{IV.17})$$

by contraction by factor $\lambda_{\alpha\ell}$ and multiplication with a smooth cutoff function

$$f_{\alpha\ell}(r) = N f_{\alpha\ell}^{\text{at}}(\lambda_{\alpha\ell} r) \left(1 - e^{-\gamma_{\alpha\ell}(r-r_{\alpha\ell}^c)^2} \right) . \quad (\text{IV.18})$$

The prefactor N has to be chosen such that the radial function remains normalized with

$$\int_0^\infty |f_{\alpha\ell}(r)|^2 r^2 dr = 1 . \quad (\text{IV.19})$$

*In practice the radial Schrödinger equation is usually expressed as quasi 1-d Schrödinger equation (see appendix A.3).

Thus, the parameters $\{p_i\}$ for the minimization, Eq. (IV.16), are $\lambda_{\alpha\ell}$, $\gamma_{\alpha\ell}$ and $r_{\alpha\ell}^c$. As examples for modified atomic radial functions, contracted carbon s orbitals are shown in Fig. IV.1 for different values of the contraction parameter $\lambda_{\alpha\ell}$ and the steepness parameter of the cutoff function $\gamma_{\alpha\ell}$. It is evident from the radial functions in Fig. IV.1, that unfortunate choices of the parameter $\gamma_{\alpha\ell}$ can result in unphysical radial functions. If the parameter is too large, i. e. if the cutoff function is too steep, spurious turning points are introduced in the decaying radial function.

IV.3.2. Confined atomic wave functions

Instead of tinkering with atomic radial functions to imitate the screening by the local atomic environment, another option is to solve the radial Schrödinger equation for an atom in a tuned confinement potential. For this purpose the potential (in Hartree atomic units)*

$$v_{\alpha\ell}^c(r) = \frac{1}{2} \left(\frac{r - r_{\alpha\ell}^0}{r_{\alpha\ell}^c - r_{\alpha\ell}^0} \right)^2 \frac{a_{\alpha\ell}(a_{\alpha\ell} - 1)}{(r_{\alpha\ell}^c - r)^2} \quad \text{for } r_{\alpha\ell}^0 < r < r_{\alpha\ell}^c \quad (\text{IV.20})$$

is added to the effective Kohn–Sham potential in the radial Schrödinger equation, Eq. (IV.17). The parameters of the confinement potential, Eq. (IV.20), are the onset radius $r_{\alpha\ell}^0$, the cutoff radius $r_{\alpha\ell}^c$ and the decay parameter $a_{\alpha\ell}$. The potential is constructed such that the radial function decays with order $(r_{\alpha\ell}^c - r)^{a_{\alpha\ell}}$ at the cutoff, which is shown by a Taylor expansion in Appendix A.4.

The effect of the parameters on the resulting radial function is visualized in Fig. IV.2. Although the impact of the decay order on the final radial function seems marginal in Fig. IV.2 (b), the smoothness of the derivative is much enhanced for $a_{\alpha\ell} > 2$. However, from the depiction it is also noticeable that the confinement potential leads to radial functions that are still very similar to the function of the free atom. The flexibility with changing parameters, i. e. the size of the optimization space, might therefore not be sufficient to minimize the spillage function, Eq. (IV.16), for every structure.

*The expression for the confinement potential in Ref. 95 is given in Rydberg atomic units.

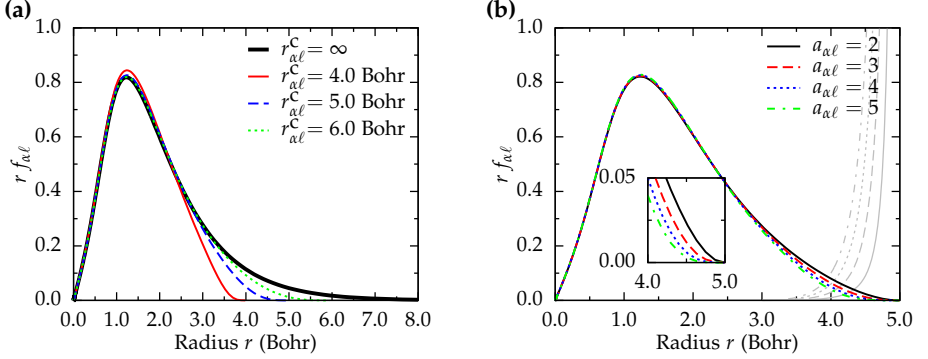


Figure IV.2. (a) Carbon 2s radial function for atoms in confinement potentials $v_{\alpha\ell}^c$ of Eq. (IV.20) for various cutoff radii in comparison to the unconfined atom ($r_{\alpha\ell}^c = \infty$). In all cases the steepness parameter $a_{\alpha\ell}$ was set to 4 with an on-set radius of $r_{\alpha\ell}^0 = 3.0$ Bohr. (b) Carbon 2s radial functions computed for different confinement potentials with cutoff radius $r^c = 5.0$ Bohr and an on-set radius of $r_{\alpha\ell}^0 = 3.0$ Bohr for different values of the steepness parameter $a_{\alpha\ell}$.

IV.3.3. Expansion in an auxiliary basis

In an attempt to combine the advantages of the two former approaches, we have developed an additional optimization scheme based on the expansion of the radial function $f_{\alpha\ell}$ in an auxiliary basis

$$f_{\alpha\ell}(r) = g_{\alpha\ell}^{(0)}(\lambda_{\alpha\ell} r) + c_{\alpha\ell}^{(1)} g_{\alpha\ell}^{(1)}(\lambda_{\alpha\ell} r) + c_{\alpha\ell}^{(2)} g_{\alpha\ell}^{(2)}(\lambda_{\alpha\ell} r) \quad . \quad (\text{IV.21})$$

To limit the number of parameters we have decided to restrict the size of the auxiliary basis to just three functions. Since the final radial function is required to be normalized as in Eq. (IV.19), the optimization parameters $\{p_i\}$ for the minimization, Eq. (IV.16), are the contraction parameter $\lambda_{\alpha\ell}$ and just two expansion coefficients $c_{\alpha\ell}^{(1)}$ and $c_{\alpha\ell}^{(2)}$. The ansatz in Eq. (IV.21) provides the same flexibility for contraction as the contracted atomic functions discussed in Sec. IV.3.1 while a cutoff function can be avoided by using radially confined basis functions.

Two different types of auxiliary basis functions $\{g_{\alpha\ell}^{(i)}\}$ have been evaluated: (1) a set of three atomic radial functions with different radial extensions and (2) a set of three pairwise orthogonal functions.

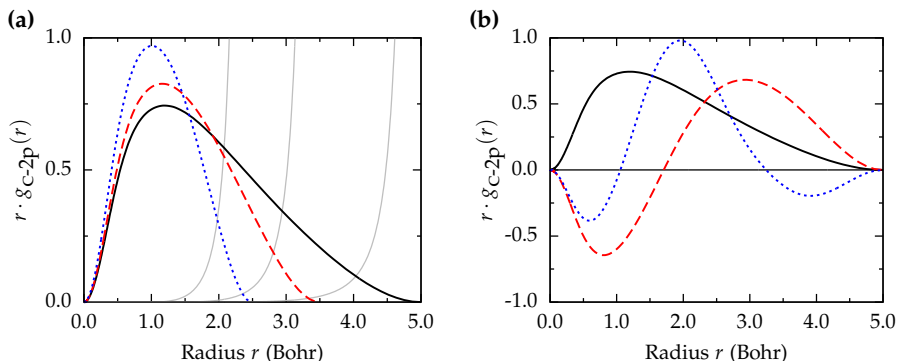


Figure IV.3. Auxiliary bases for the representation of carbon $2p$ radial functions. (a) basis of three functions with different extension (3- ζ basis). The light gray lines are the corresponding confinement potentials. (b) three orthogonal functions constructed following the *energy derivative* procedure. The black radial function is identical in both schemes and corresponds to the solution of the radial Schrödinger equation in a confinement potential with a pole at $r_{\alpha\ell}^c = 5.0$ Bohr.

Downfolding of a *split valence* basis

A common approach for the construction of local basis sets in quantum chemistry is the *split valence* method.⁵⁶ Here, every atomic-like orbital is represented by n local basis functions of an n - ζ (or n -tuple-zeta) basis. The individual basis functions are usually taken as orbitals with different radial extensions. The expansion of the AO radial function of Eq. (IV.21) can be understood as the downfolding of a 3- ζ basis representation to a minimal 1- ζ basis representation, since three basis functions per AO are used to generate a single one.

Various recipes for the choice of suitable orbitals and ranges have been proposed in the literature.^{94,96–99} An example of a split valence 3- ζ basis for the carbon $2p$ orbital is shown in Fig. IV.3 (a). In this case, the three basis functions are the radial functions of isolated atoms in three different confinement potentials of the form of Eq. (IV.20). The cutoff radii $r_{\alpha\ell}^c$ of the confinement potentials were chosen such that the energy eigenvalues of the corresponding $2p$ orbital were increased by steps of 0.4 eV.^{94,96} The on-set radius $r_{\alpha\ell}^0$ was set to 40 % of $r_{\alpha\ell}^c$ and the decay parameter $a_{\alpha\ell}$ was taken to be 2.

Orthogonal radial basis

A completely different approach to generate an auxiliary basis is in a similar spirit as the *energy derivative* of linearized bases in solid state physics.³⁶ Lippert et al. have suggested the use of the derivatives of the wave functions with respect to the occupation number as systematically refinable basis set.¹⁰⁰ The motivation behind this approach is to represent atomic-like orbitals that make up the wavefunctions of molecules and crystals as a Taylor expansions in the corresponding atomic wave function about the occupation numbers

$$f_{\alpha\ell}(r) = \sum_n c_{\alpha\ell}^{(n)} \frac{d^{(n)}}{dN_{\alpha\ell}^{(n)}} f_{\alpha\ell}^{\text{at}}(\mathbf{r}) \quad , \quad (\text{IV.22})$$

where $N_{\alpha\ell}$ is the occupation number of the orbital.* If the wave functions of the simulated molecule or crystal can be well approximated by the superposition of atomic wave functions and successive charge transfer, the expansion in Eq. (IV.22) will rapidly converge. Truncating the Taylor series after the second order yields a basis expansion as in Eq. (IV.21)

$$f_{\alpha\ell}(r) = f_{\alpha\ell}^{\text{at}}(\mathbf{r}) + c_{\alpha\ell}^{(1)} \frac{d}{dN_{\alpha\ell}} f_{\alpha\ell}^{\text{at}}(\mathbf{r}) + c_{\alpha\ell}^{(2)} \frac{d^2}{dN_{\alpha\ell}^2} f_{\alpha\ell}^{\text{at}}(\mathbf{r}) \quad , \quad (\text{IV.23})$$

where the three basis functions are the atomic radial wave function and its first two derivatives with respect to the occupation number. Again, the coefficient of the zeroth order was omitted because of the normalization requirement, Eq. (IV.19). Note, that the basis functions are by construction pairwise orthogonal with an increasing number of nodes.

*In this section we shall denote the occupation numbers by $N_{\alpha\ell}$ instead of $f_{\alpha\ell}$ so not to confuse them with the orbital radial function.

In practice the basis functions $\{g_{\alpha\ell}^{(i)}\}$ are calculated numerically via the following finite difference expressions and subsequent renormalization

$$\begin{aligned} g_{\alpha\ell}^{(0)} &= f_{\alpha\ell}^{\text{at}}(N_{\alpha\ell}) \\ g_{\alpha\ell}^{(1)} &= \frac{f_{\alpha\ell}^{\text{at}}(N_{\alpha\ell} + \Delta N) - f_{\alpha\ell}^{\text{at}}(N_{\alpha\ell})}{\Delta N} \\ g_{\alpha\ell}^{(2)} &= \frac{f_{\alpha\ell}^{\text{at}}(N_{\alpha\ell} + 2\Delta N) - 2f_{\alpha\ell}^{\text{at}}(N_{\alpha\ell} + \Delta N) + f_{\alpha\ell}^{\text{at}}(N_{\alpha\ell})}{\Delta N^2}, \end{aligned} \quad (\text{IV.24})$$

where the atomic radial function $f_{\alpha\ell}^{\text{at}}$ is optionally calculated for the confined radial Schrödinger equation using the potential of Eq. (IV.20). Typically ΔN is chosen to be -0.1 electrons, i. e. slightly cationic configurations are calculated. An example of an orthogonal basis for the carbon $2p$ orbital that was constructed following the above recipe is shown in Fig. IV.3 (b).

A change of ΔN in the occupation number $N_{\alpha\ell}$ will result in a changed atomic eigenvalue $\varepsilon_{\alpha\ell}^{\text{at}} + \Delta\varepsilon$ of the radial Schrödinger equation, Eq. (IV.17). The numerical derivative of the radial function $f_{\alpha\ell}$ with respect to the energy eigenvalue would only require to substitute $\Delta\varepsilon$ for ΔN in Eq. (IV.24). However, since the auxiliary basis functions are renormalized such a relative change does not have any effect, and the actual *energy derivative* would yield the same basis functions.

IV.4. Optimized minimal basis sets

Carbon is a typical covalent main group element and, because of its many natural hybridizations (sp , sp^2 , sp^3), a challenging candidate for the derivation of transferable minimal basis sets. Therefore, we have chosen the carbon $2s$ and $2p$ functions to benchmark the four optimization techniques described in the previous section. Titanium on the other hand is a prototypical example of a d band transition metal and, therefore, well suited to check the applicability of the methods to metallic systems and d orbitals.

Table IV.1. Computed lattice constant a and carbon–carbon distances to the first, second and third neighbor shell in Bohr atomic units for structures with different hybridizations. Details of the computational set-up are given in Sec. IV.1.

structure		a	1st	2nd	3rd
diamond	sp^3	6.715	2.908	4.748	5.568
graphene	sp^2	4.648	2.684	4.648	5.367
alkyne chain	sp	4.850	2.369	2.481	4.850

IV.4.1. Optimized carbon AO basis

The radial cutoff of the basis functions is not among the parameters of the optimization methods of Sec. IV.3.3 that are based on an auxiliary radial basis. To make it possible to compare all four methods of Sec. IV.3 on an equal footing it is therefore necessary to perform the optimization for a number of fixed cutoff values. For the same reason, the contraction factor λ has to be kept fixed for methods C and D, so not to modify the range of the radial functions. Based on the carbon–carbon neighbor distances shown in Table IV.1 we chose cutoff radii between 4.0 Bohr and 6.0 Bohr in increments of 0.5 Bohr. The shortest cutoff of 4.0 Bohr thus corresponds to a nearest neighbor model, the second neighbor shell is included at around 5.0 Bohr and the 6.0 Bohr cutoff reaches, in regular carbon crystals, beyond the third nearest neighbor. Note, however, that this is not the bond interaction radius of two atoms, which is equal to twice the orbital extension (i. e. 8.0, 10.0 and 12.0 Bohr). The optimized $2s$ and $2p$ carbon radial functions for the different cutoff radii and using the *energy derivative* optimization scheme of Sec. IV.3.3 are depicted in Fig. IV.4.

The restricted range of the AO basis functions naturally has an impact on their capability to represent the DFT wave functions, which is reflected in the value of the electronic spillage function \mathcal{S}_e of Eq. (IV.13). Figure IV.5 depicts the change of the electronic spillage for various cutoff radii and over a range of carbon–carbon nearest

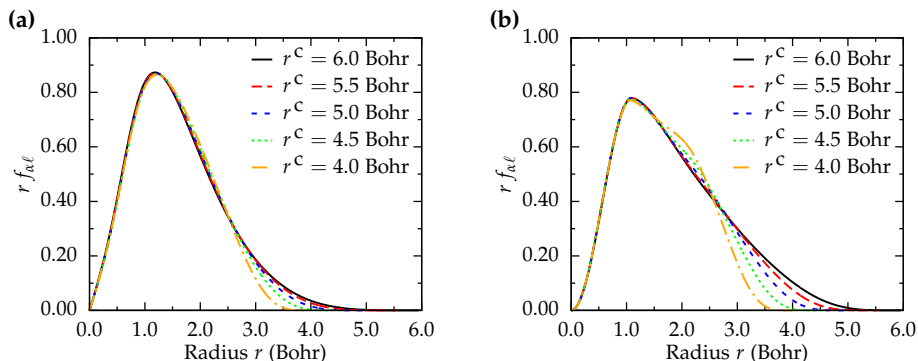


Figure IV.4. Optimized carbon (a) 2s and (b) 2p radial functions for cutoff radii ranging from 4.0 Bohr to 6.0 Bohr. The optimization was done simultaneously for the ground state geometries of diamond, graphene and the infinite alkyne chain. Target function was the electronic spillage of Eq. (IV.13). The radial functions were expanded in a pairwise orthogonal radial basis as described in Sec. IV.3.3. See Table IV.2 for the parameters of that basis.

neighbor distances in the diamond structure. As expected, the spillage becomes larger for shorter ranged AOs, although the absolute value remains relatively small (around 1% of the electrons) even for the shortest cutoff of 4.0 Bohr. More important is, however, that the value of the spillage function stays fairly constant at around 0.2% over the whole a range of $\pm 10\%$ about the minimum nearest neighbor distance. This is except for the 4.0 Bohr case, where it varies considerably from around 0.5% for short carbon-carbon distances to 1.2% for large distances. Since we apt for transferability it is crucial that the AO basis is similarly accurate for varying bonding situations. It is therefore unclear if the 4.0 Bohr basis would be suitable for the calculation of tight-binding parameters.

Now, the performance of the four optimization schemes of Sec. IV.3 shall be compared. To facilitate comprehension we will refer in the following to the four techniques by: **A** for the contracted atomic orbitals of Sec. IV.3.1, **B** for the radial functions of confined atoms of Sec. IV.3.2, **C** for the expansion in a 3- ζ auxiliary radial basis, and **D** for the scheme involving three orthogonal basis functions. As is evident from Fig. IV.6 the

Figure IV.5. Change of the electronic spillage with the range of the AO basis that is used for the representation of the carbon diamond wave functions. The nearest neighbor (NN) distance is varied about $\pm 10\%$ of the minimum geometry. The cutoff radii r^c are given in Bohr units. See Table IV.2 for the parameters of the AO basis functions.

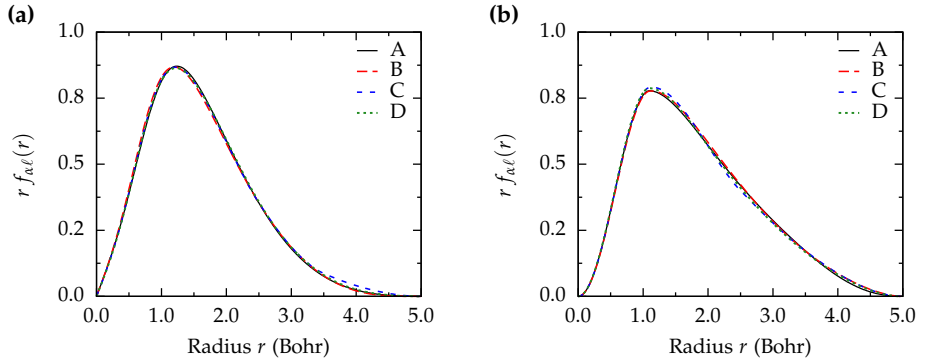
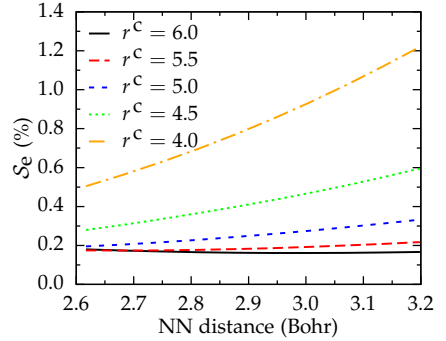


Figure IV.6. Comparison of optimized radial functions for the carbon (a) $2s$ and (b) $2p$ orbitals, as constructed using the four different techniques described in the text. **A:** contracted atomic orbitals (Sec. IV.3.1), **B:** wavefunctions of a confined atom (Sec. IV.3.2), **C** and **D:** expansions of the radial functions using a *triple-zeta* basis and the *energy derivative* approach, respectively (Sec. IV.3.3). Optimized was the electronic spillage function S_e , Eq. (IV.13), at the ground state geometry of diamond, graphene and the infinite alkyne chain. The cutoff radius was in each case $r_{\alpha\ell}^c = 5.0$ Bohr.

Table IV.2. Parameters of optimized carbon radial functions following scheme **D** (see text for details). The auxiliary radial basis functions were computed in a confinement potential with cutoff radius r^c (Bohr units), and the contraction parameter $\lambda_{\alpha\ell} = 1$ was kept constant so not to interfere with the radial extensions. The on-set parameter was in each case $r_{\alpha\ell}^0 = 2.0$ Bohr and the steepness parameter was set to $a_{\alpha\ell} = 5$.

r^c	2s orbital		2p orbital		\mathcal{S}_e (%)
	c_1	c_2	c_1	c_2	
4.0	0.0246	-0.0233	0.1371	-0.1335	1.97
4.5	-0.0253	-0.0004	0.0778	-0.1020	1.23
5.0	-0.0607	0.0062	0.0316	-0.0793	0.82
5.5	-0.0858	0.0052	-0.0031	-0.0632	0.58
6.0	-0.1044	0.0016	-0.0298	-0.0512	0.44

four optimization methods yield almost identical radial functions if the cutoff is chosen manually. However, from our experiences the expansion based methods **C** and **D** have proved to be numerically most stable and therefore well suitable for complete automatization. For method **A** the simultaneous optimization of the three parameters λ , γ and r^c often fails to converge or leads to unphysical radial functions with spurious turning points, as already mentioned in Sec. IV.3.1. Method **B** usually performs worst in terms of the spillage minimization, which had to be expected as it is the least flexible of the four techniques. The decision upon which basis set to use for the expansion of the radial function, i. e. method **C** or **D**, seems to be mostly arbitrary. We have chosen to use the orthogonal radial basis (scheme **D**) in the following, mostly because we like the idea of systematically refinable basis sets of Ref. 100. The optimized expansion coefficients of the carbon 2s and 2p functions for the different cutoff radii are listed in Table IV.2 along with the final value of the electronic spillage \mathcal{S}_e .

Transferability of the optimized basis

Our motivation for the optimization of minimal AO basis sets is, of course, to capture the converged DFT wave functions using the projection formalism of Sec. IV.2 as good as possible before calculating the minimal basis matrix elements, Eq. (II.91), i. e. the tight-binding parameters. The projection procedure will have to be repeated for a number of representative structures and geometries, so that the matrix elements for all relevant interatomic distances can be interpolated. The actual, numerical optimization of the AO basis takes only a short time in comparison to the preceding DFT calculation, so it is in principle feasible to run a basis set optimization for each individual structure. However, the resulting tight-binding parameters could no longer be assigned to one specific set of atomic orbitals. This has the severe disadvantage that discontinuities and scattering will be introduced into the overlap integrals, which exclusively depend on the chosen AO basis.

An alternative is the simultaneous optimization of the AO basis for a representative set of structures at their corresponding minimum geometries. This approach was followed for the optimized radial functions depicted in Fig. IV.6. To estimate how much such concurrently optimized radial functions differ from the structure specific ones, Fig. IV.7 shows the optimized radial functions for the ground state geometries of three very different carbon reference structures along with the result of the combined optimization and the optimized 5.0 Bohr radial function of a free carbon atom. The optimized radial functions of the three reference structures are very similar for the three structures and the simultaneous optimization yields a very good compromise. The optimized 5.0 Bohr radial function for the free carbon atom is instead very different, and would most likely not be a good approximation for carbon atoms in compounds. A comparison of the values of the electronic spillage function for various carbon structures using the simultaneously optimized AO basis in comparison to the results using re-optimized radial functions is shown in Fig. IV.8. As can be seen in Fig. IV.8, the fixed AO basis performs almost equally well as the re-optimization approach for the three reference structures diamond, graphene and the infinite alkyne chain. The spillage for the three

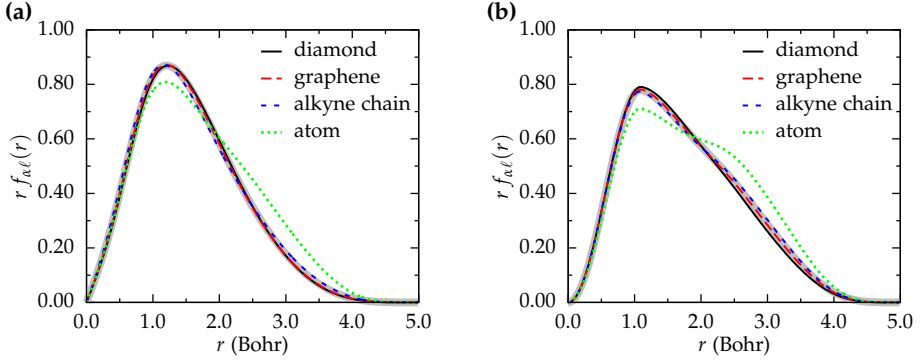


Figure IV.7. Optimized radial functions for different carbon structures. The wide gray radial functions are the result of the simultaneous optimization at the ground state geometry of all of the three structures and using the 5.0 Bohr basis of Table IV.2. The green dotted radial function is the result of the optimization at the free, unbound carbon atom, using the same auxiliary radial basis set.

additional benchmark structures, face-centered cubic (fcc), body-centered cubic (bcc) and simple cubic (sc), is more different for the two approaches, but not larger in value than for the three reference structures. More importantly, the value of the spillage function is relatively constant over the whole nearest neighbor range. We can therefore expect, that tight-binding parameters derived using such a simultaneously optimized, fixed basis are likely to be transferable.

Energy spillage

An alternative target function for the basis optimization is the loss in the band energy, the *energy spillage* \mathcal{S}_E of Eq. (IV.15). As discussed in Sec. IV.2.2 the value of \mathcal{S}_E is not directly comparable over different structures. It is, nevertheless, helpful to look at the *change* of the energy spillage over a range of nearest neighbor distances for each individual structure. For the representative carbon structures diamond, graphene and the infinite alkyne chain the value of the energy spillage function per (valence) electron is shown in Fig. IV.9. The data corresponds to the same fixed optimized AO basis

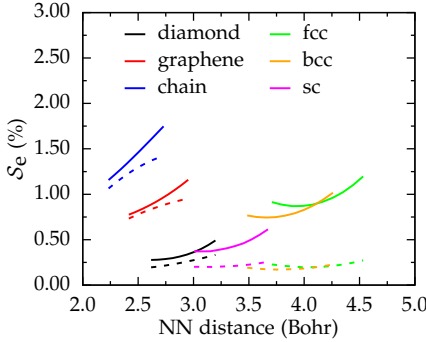


Figure IV.8. Comparison of the values of the electronic spillage function S_e when using a fixed AO basis (solid lines) and a re-optimized AO basis (dashed lines), both with a range of 5.0 Bohr. See Table IV.2 for the parameters of the fixed AO basis.

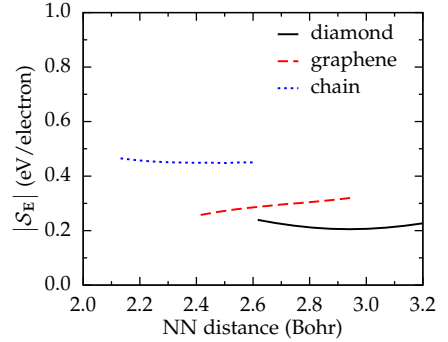


Figure IV.9. The absolute value of the energy spillage function S_E of Eq. (IV.15) for different carbon structures and carbon-carbon distances. The same optimized AO basis as for the solid curves in Fig. IV.8 was used.

as the electron spillage graph in Fig. IV.8. As for the electron spillage, the energy spillage remains fairly constant over the whole range of carbon distances and, thus, also points to a transferable basis set. From our experience it is common that the energy spillage is approximately proportional to the electron spillage and therefore does not provide additional information for the basis optimization. Consequently, we will in the following focus on the more convenient electron spillage and abandon the energy spillage as target function.

IV.4.2. Optimized titanium AO basis

Apart from the additional d orbitals there is no significant difference in the optimization of a minimal AO basis for titanium compared to the procedure described for carbon in the previous Sec. IV.4.1. Following the experiences from the carbon AO basis, we chose the technique described in Sec. IV.3.3 of expanding the radial functions in a pairwise-orthogonal auxiliary basis. In Table IV.3 the computed ground state distances

Table IV.3. Computed lattice constant a and titanium–titanium distances (both in Bohr units) to the first, second and third neighbor shell for different titanium crystal structures. The computational set-up is given in Sec. IV.1.

structure	a	1st	2nd	3rd
hcp	5.544	5.544	7.840	8.803
fcc	7.765	5.491	7.765	9.510
bcc	6.143	5.320	6.143	8.687
A15	9.788	5.471	8.476	8.823
sh	5.162	5.162	7.301	8.941
sc	4.981	4.981	7.044	8.627

of the first three neighbor shells in various titanium crystal structures are listed. We know from the carbon case that the auxiliary radial basis should at least extend far enough to reach the first neighbor shell. For the application of the AO basis sets in actual calculations it is, on the other hand, desirable for the radial functions to be as short-ranged as possible. We therefore chose the cutoff radii 5.0, 5.5 and 6.0 Bohr, as these are close to the average nearest neighbor distance.

As for carbon a number of characteristic reference structures is needed as premise for the optimization. The ground state crystal structure of titanium at ambient conditions is the hexagonal closed packed (hcp) structure. We have instead chosen the fcc structure, as it is topologically very similar to the hcp structure (only the stacking sequence differs), while fcc has a single atom base. With the bcc crystal structure and the simple hexagonal (sh) crystal structure we additionally included very dissimilar structures with reduced coordination in the reference set, so to cover the various bonding situations of titanium.

A technical peculiarity arises from the fact that the $4p$ orbital is not occupied in the titanium atom. The *energy derivative* technique (scheme **D**) of Sec. IV.3.3 would thus require anionic configurations for the p orbital basis. This was avoided by reusing

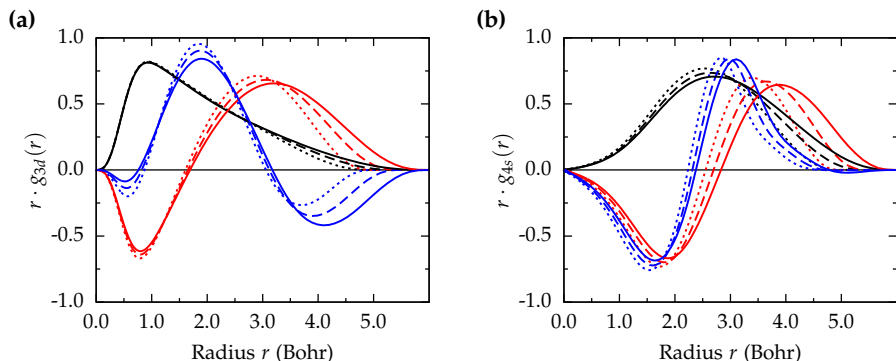


Figure IV.10. Orthogonal radial basis functions for titanium (a) $3d$ and (b) $4s$ atomic orbitals as constructed following the *energy derivative* scheme of Sec. IV.3.3. The s radial basis is also used for the optimization of the p orbitals (see text for details). The figure shows the atomic radial functions (black) and the first (red) and second (blue) derivatives with respect to the occupation numbers. The solid, dashed and dotted functions correspond to cutoff radii of 6.0, 5.5 and 5.0 Bohr, respectively.

the $4s$ basis for the $4p$ orbitals as well. This is merely a technical note since the $4p$ orbitals are high in energy compared to the $3d$ and $4s$ orbitals and contribute little to the binding in typical titanium compounds, as can be seen from local density of states calculations.¹⁰¹ The orthogonal radial basis functions for three different cutoff radii, namely 5.0, 5.5 and 6.0 Bohr, are depicted in Fig. IV.10.

The optimized AO basis functions for the titanium $3d$ and $4s$ orbitals are shown in Fig. IV.11 and their parameters are given in Table IV.4. Even though the maximum of the $3d$ function is at a distance of around 1.0 Bohr close to the atomic core, the decay of the radial function is slow. Thus, even when using the 6.0 Bohr radial basis a spurious turning point is introduced into the decaying branch of the orbital. The $4s$ function adjusts more flexible to the imposed range. The optimization of the $4p$ orbital (not shown in Fig. IV.11) is least stable (but also least important), as the spillage function Eq. (IV.13) does not account for the virtual states. Note, that a range of the radial functions of 5.5 Bohr, i. e. approximately the first nearest neighbor distance, is

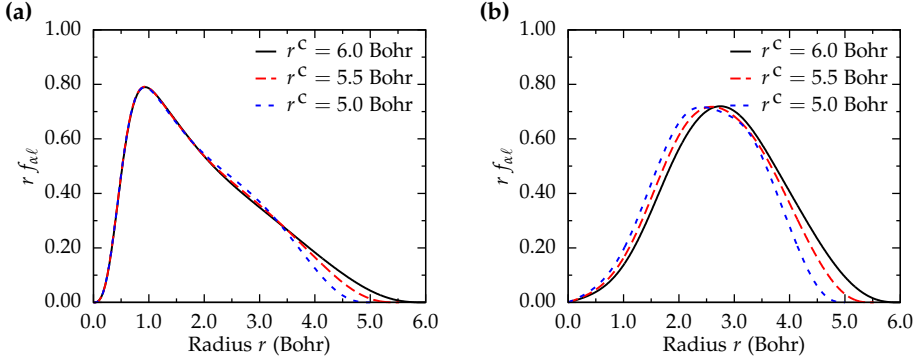


Figure IV.11. Optimized basis functions for the titanium (a) $3d$ and (b) $4s$ orbitals for cutoff radii of 5.0, 5.5 and 6.0 Bohr. The parameters of the basis functions are given in Table IV.4.

already sufficient to construct an accurate AO basis set with a very small electronic spillage value of 0.20 % (Table IV.4).

IV.5. Derivation of tight-binding parameters

With optimized minimal AO basis sets at hand we can now turn back to our original goal, the derivation of tight-binding parameters from DFT calculations. To obtain an electronic structure TB model we now need to

1. perform converged DFT calculations for selected reference structures,
2. change the basis to a minimal AO representation via the projection formalism of Sec. IV.2 and using an optimized basis set as of Sec. IV.3,
3. calculate the matrix elements of Eq. (II.91),
4. average the three-center contributions in the Hamilton matrix elements,
5. decompose the matrix elements to their contributions from the Slater–Koster reference bonds (see Sec. III.2.2), and
6. find a continuous representation of the calculated data points.

Table IV.4. Parameters of optimized titanium radial functions. The radial functions were expanded in an auxiliary basis of three pairwise orthogonal functions as described in Sec. IV.3.3. The basis functions were computed in a confinement potential with cutoff radius r^c (Bohr units), and the contraction parameter was set constant to $\lambda_{\alpha\ell} = 1.0$ so not to interfere with the cutoff radius. The on-set parameter $r_{\alpha\ell}^0 = 3.0$ Bohr and the decay order parameter $a_{\alpha\ell} = 3$ were the same in all cases.

r^c	3d orbital		4s orbital		4p orbital		\mathcal{S}_e (%)
	c_1	c_2	c_1	c_2	c_1	c_2	
5.0	0.0813	-0.0535	0.0964	-0.1127	0.2506	-0.1953	0.54
5.5	0.0598	-0.0375	0.0317	-0.0376	0.1540	-0.0839	0.20
6.0	0.0489	-0.0223	-0.0172	0.0292	0.0689	0.0066	0.08

Steps 1 and 2 have already been discussed in the previous sections. For the evaluation of the necessary integrals, efficient numerical routines based on Fourier transformations have been implemented in the DFT program by Meyer.^{79,80,95} The converged DFT Hamiltonian is used for the calculation of the Hamilton matrix elements in the third step: $H_{\mu\nu} = \langle \phi_\mu | \hat{h}^{\text{DFT}} | \phi_\nu \rangle$. As discussed in Sec. III.2.1 the elements of the Hamilton matrix $H_{\mu\nu}$ implicitly depend on the coordinates of all atoms in the structure because of the environment dependence of the effective Kohn-Sham potential $v_{\text{eff}}^{\text{KS}}(\{\mathbf{R}\})$. In all but trivial structures the potential $v_{\text{eff}}^{\text{KS}}(\{\mathbf{R}\})$ is not radially symmetric in all bond directions $\mathbf{R}_{\alpha\beta}$ between atoms α and β . As a consequence the values of the Hamilton matrix elements depend on the orientation, of the AO basis functions. As a specific example, consider the $pp\pi$ bonds in graphene: the value of a π bond involving two p orbitals that are orthogonal to the graphene plane, i. e. out-of-plane, is very different from an in-plane π bond, due to the different local atomic environments. For reasons explained in detail in Sec. III.2 such three-center terms are neglected in the tight-binding method. We can, however, effectively include the screening effects due to three-center interactions by *averaging* the values of the Hamilton matrix elements over *all possible orientations* of the AO basis. The final step 6. is merely a fit of an analytic function to the calculated data points of matrix element values.

IV.5.1. Orthogonal tight-binding models

As mentioned in Sec. III.3, it is sometimes desirable to go from a non-orthogonal to an orthogonal tight-binding description of the electronic structure, so that the overlap matrix becomes the identity matrix $S_{\mu\nu} = \delta_{\mu\nu}$. Instead of calculating the Hamilton matrix elements *a priori* in an orthogonal Löwdin basis, orthogonal tight-binding (OTB) models can equivalently be constructed *a posteriori* via a symmetric Löwdin transform of the Hamiltonian \mathbf{H} in the non-orthogonal AO basis*

$$\tilde{\mathbf{H}} = \mathbf{S}^{-1/2} \mathbf{H} \mathbf{S}^{-1/2} \quad , \quad (\text{IV.25})$$

so that the energy eigenvalues $\{\varepsilon_i\}$ remain unchanged

$$\begin{aligned} \mathbf{H} \mathbf{c}_i &= \varepsilon_i \mathbf{S} \mathbf{c}_i \\ \Leftrightarrow \mathbf{S}^{-1/2} \mathbf{H} \left(\mathbf{S}^{-1/2} \mathbf{S}^{1/2} \right) \mathbf{c}_i &= \varepsilon_i \mathbf{S}^{-1/2} \mathbf{S} \left(\mathbf{S}^{-1/2} \mathbf{S}^{1/2} \right) \mathbf{c}_i \quad , \quad (\text{IV.26}) \\ \Leftrightarrow \tilde{\mathbf{H}} \tilde{\mathbf{c}}_i &= \varepsilon_i \tilde{\mathbf{c}}_i \end{aligned}$$

and the eigenvectors transform as

$$\tilde{\mathbf{c}}_i = \mathbf{S}^{1/2} \mathbf{c}_i \quad . \quad (\text{IV.27})$$

Note, that the above orthogonalization leads to structure dependent OTB parameters (Hamilton matrix elements). To derive a transferable OTB model it is therefore advisable to average the matrix element values over a set of reference structures.

IV.5.2. The gauge freedom of the Hamilton matrix

The *zero point* of the potential energy is arbitrary and the effective Kohn–Sham potential $v_{\text{eff}}^{\text{KS}}$ of Eq. (III.1) is only defined save an arbitrary constant. This freedom in the Kohn–Sham potential (or the one-electron Hamiltonian) leads to a gauge variance in the band

*The square root of a matrix is defined as the component-wise square root of the diagonal form.

energies, which leaves the wave functions invariant

$$\begin{aligned}
 (\hat{t} + v_{\text{eff}}^{\text{KS}}) \psi_i &= \varepsilon_i \psi_i \\
 \downarrow \quad \hat{v}_{\text{eff}}^{\text{KS}} &= v_{\text{eff}}^{\text{KS}} + \kappa \\
 (\hat{t} + \hat{v}_{\text{eff}}^{\text{KS}}) \psi_i &= (\varepsilon_i + \kappa) \psi_i \quad .
 \end{aligned}
 \tag{IV.28}$$

For the basis representation of the Hamiltonian this means multiples of the overlap matrix elements $S_{\mu\nu}$ may be added to the Hamilton matrix elements $H_{\mu\nu} = \langle \mu | \hat{h} | \nu \rangle$

$$\begin{aligned}
 \langle \phi_\mu | \hat{t} + v_{\text{eff}}^{\text{KS}} | \phi_\nu \rangle &\xrightarrow{v_{\text{eff}}^{\text{KS}} \rightarrow v_{\text{eff}}^{\text{KS}} + \kappa} \langle \phi_\mu | \hat{t} + v_{\text{eff}}^{\text{KS}} | \phi_\nu \rangle + \kappa \langle \phi_\mu | \phi_\nu \rangle \\
 \Leftrightarrow \quad H_{\mu\nu} &\xrightarrow{v_{\text{eff}}^{\text{KS}} \rightarrow v_{\text{eff}}^{\text{KS}} + \kappa} H_{\mu\nu} + \kappa S_{\mu\nu} \quad ,
 \end{aligned}
 \tag{IV.29}$$

without changing the eigenvectors and the electron density.

A consequence of Eqs. (IV.28) and (IV.29) is that Hamilton matrix values from different DFT calculations can only be compared, if the same frame of reference is imposed on the potential energy. Most notably, the common approach of DFT programs to use the structure-dependent average Kohn–Sham potential as zero point for the potential energy will not allow for the comparison of Hamilton matrix elements from different structures. One possible potential reference is the *vacuum level*, i. e. the potential energy within a region of vacuum. However, this approach is obviously not suitable for periodic crystals, which do not contain vacuum regions. The vacuum level gauge is the subject of the following sections of this chapter.

We shall see in Sec. V.2.3 of the following chapter that it is alternatively possible to gauge Hamilton matrices *after* their calculation by a specific choice of the on-site matrix elements.

IV.5.3. Continuous representation of the bond integrals

For tight-binding calculations an analytical representation of the distance-dependent two-center Hamilton and overlap matrix elements is needed. The radial functions of atomic orbitals in principle decay exponentially. Therefore, Slater functions are

commonly used for this purpose, which are exponential functions multiplied by polynomials. An alternative form, which is especially suitable for orthogonal TB models, has been suggested by Goodwin, Skinner and Pettifor (GSP).¹⁰² Both functions, the Slater-type and the GSP-type, have the disadvantage of an infinite range, so that they are usually combined with a multiplicative cutoff function or the functions are simply replaced by polynomials for large atomic separations. Especially the common cutoff functions of the cosine type $f_c(x) = 0.5(\cos x + 1)$ lead to problems when the second derivative is needed. Polynomial tail functions can introduce unphysical forces if they exhibit oscillations.

Therefore we have employed an alternative function type in this work. We construct functions that closely resemble Slater functions while their value and their first and second derivative vanish exactly at a given cutoff. This is achieved by subtracting the second order Taylor expansion $\mathcal{T}_{r^c}^{(2)}[f_s]$ at the cutoff distance r^c from the original Slater type function f_s

$$f(r) = f_s(r) - \mathcal{T}_{r^c}^{(2)}[f_s(r)] \quad , \quad (\text{IV.30})$$

with the second order Taylor expansion

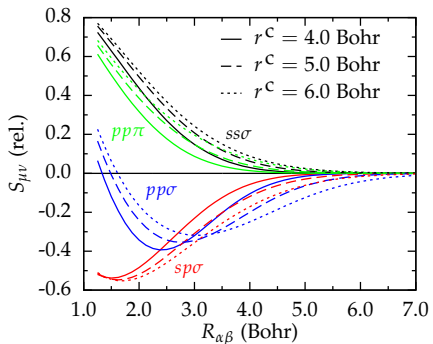
$$\mathcal{T}_{r^c}^{(2)}[f_s(r)] = f_s(r^c) + (r - r^c)f'_s(r^c) + \frac{1}{2}(r - r^c)^2 f''_s(r^c) \quad . \quad (\text{IV.31})$$

The function f_s and its derivatives are given by

$$\begin{aligned} f_s(r) &= \sum_{k=0}^N a_k r^k \cdot e^{-\alpha r} \\ f'_s(r) &= \sum_{k=0}^N a_k k r^{k-1} \cdot e^{-\alpha r} - \alpha f_s(r) \\ f''_s(r) &= \sum_{k=0}^N a_k k(k-1) r^{k-2} \cdot e^{-\alpha r} - 2\alpha f'_s(r) + \alpha^2 f_s(r) \quad , \end{aligned} \quad (\text{IV.32})$$

and the polynomial order N is typically less than three. Computationally, the evaluation of the polynomial derivatives is no obstacle since it can be done in an efficient recursive fashion. The non-linear regression of the matrix element data points using the function type of Eq. (IV.30) was achieved with an implementation of the SIMPLEX algorithm¹⁰³ and using the GNUPLOT software¹⁰⁴.

Figure IV.12. Distance dependent values of the overlap matrix elements for the 4.0, 5.0 and 6.0 Bohr basis sets of Table IV.2. The four Slater–Koster reference bonds referred to in the figure are depicted in Fig. III.2.



IV.5.4. Tight-binding parameters for carbon

The values of the overlap matrix elements $S_{\mu\nu}$ of Eq. (II.91) only depend on the choice of the minimal AO basis. For the 4.0, 5.0 and 6.0 Bohr optimized radial functions from Table IV.2 the distance-dependent values of the overlap matrix elements are shown in Fig. IV.12. The four Slater–Koster reference bonds for the carbon 2s and 2p orbitals are depicted in Fig. III.2 on page 40. As noted before, the maximum range of the matrix elements is two times the cutoff radius of the radial functions. Despite this, all overlap integrals for carbon decay to numerical zero within a range of 7.0 Bohr.

Following the procedure outlined above the Hamilton matrix elements for carbon reference structures were calculated. We selected the diamond structure (sp^3), graphene (sp^2) and the infinite alkyne chain (sp), which are the same structures that were used for the optimization of the AO basis. As reasoned in the previous section, Sec. IV.5.2, it is, however, only meaningful to compare the values of Hamilton matrix elements from different structures, if the same potential energy reference has been imposed. For the one-dimensional alkyne chain and the two-dimensional graphene structures the vacuum level is directly accessible as universal potential zero point. To be able to employ the same reference for the diamond structure, the two slab models depicted in Fig. IV.13 were constructed. Only the two innermost carbon layers of the slabs were used for the calculation of the Hamilton matrix elements. This way the vacuum level is accessible while still a bonding situation close to the ideal diamond structure can be studied.

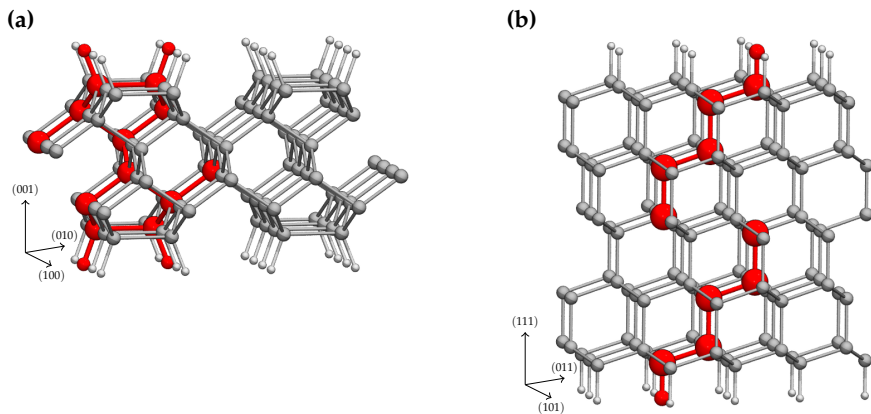


Figure IV.13. Cut-outs of periodic slab models of diamond for (a) the (100) surface and (b) the (111) surface. The periodic units are highlighted in red. In both models the outermost carbon layers (symmetrically on each side of the slab) were allowed to relax. The remaining atoms were retained on the ideal bulk diamond lattice positions. The (100) surface was stabilized by dimerization of the surface atoms in a 1×2 reconstruction. *Dangling bonds* were saturated with hydrogen atoms (smaller spheres).

For each structure geometries within a range of plus/minus ten percent of the minimum nearest neighbor distances of Table IV.1 were calculated. These structures also correspond to the electronic and energy spillage shown in Figs. IV.8 and IV.9 for the optimized carbon AO basis sets. The calculated values of the Hamilton matrix elements using the 4.0, 5.0 and 6.0 Bohr radial functions of Table IV.2 are shown in Fig. IV.14. As visible in the graphs of Fig. IV.14 there is a lack of data for interatomic distances between the first and the second nearest neighbor shells. This bond range is, however, not of great importance in physically relevant structures. Considering that the data points shown in the graphs stem from very different bonding situations in sp , sp^2 and sp^3 structures the scattering of the values for each reference bond is surprisingly small. Note, that with increasing cutoff radius of the AO basis the scattering, especially in the $pp\pi$ bond data, increases as more and more atoms contribute to the three-center interactions. Also, for the longer ranged basis sets the discrepancy between the first

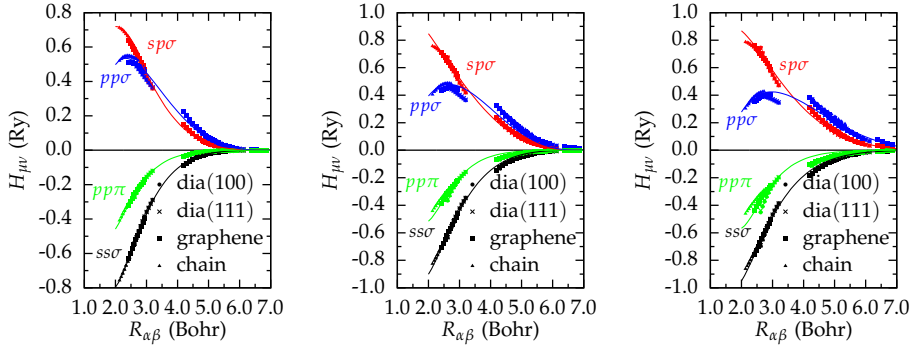


Figure IV.14. Distance and structure dependent values of the Hamilton matrix elements in Rydberg units for the 4.0, 5.0 and 6.0 Bohr basis sets (left to right) of Table IV.2. The four Slater–Koster reference bonds referred to in the figure are depicted in Fig. III.2. The Hamilton matrix elements were calculated for the vacuum level as potential reference. The labels dia(100) and dia(111) refer to the two slab models of Fig. IV.13. The solid lines are continuous bond integral representations with the functional form of Eq. (IV.30). Parameters of these fits are given in Table B.3 in the appendix.

neighbor bond and the second and third neighbors becomes larger for the $pp\sigma$ interaction. It is therefore increasingly challenging to determine a sufficiently accurate continuous representation of the bond integrals, the solid lines in Fig. IV.14. The parameters of the bond integral fits are given in Table B.3 in Appendix B.

Band structures and densities of states

The overlap matrix parameters from Table B.2 and the Hamilton matrix parameters from Table B.3 form complete tight-binding electronic structure models for carbon. We will furthermore introduce the usual TB approximation and treat the on-site elements of the Hamilton matrix as structurally independent values and set them to the atomic eigenvalues.

To assess the accuracy of the tight-binding parameters, TB band structures and densities of states can be compared to their DFT references. The results for the three TB models

of Fig. IV.14 are shown in Fig. IV.15 for the reference structures diamond, graphene and the alkyne chain, along with three benchmark structures (bcc, fcc, sc). In each case the TB model calculated with the shortest ranged basis, the 4.0 Bohr basis (solid black lines), agrees best with the DFT reference. At the first glance it seems counter-intuitive that the most approximate radial basis yields the most accurate electronic structure model. Considering however the increased scattering of the Hamilton matrix elements for the longer ranged basis sets shown in Fig. IV.14 the results can be understood. Obviously, a stable bond integral fit is more important than an AO basis set that yields a very small electronic spillage. Nevertheless, the optimization of the AO basis has a significant impact on the shape of the radial functions.

As defined in Eq. (IV.13), only the occupied states contribute to the electronic spillage function S_e . The radial functions of the minimal basis were therefore not optimized for the representation of the virtual bands, which can be clearly seen in the band structures of Fig. IV.15. However, the occupied bands and the bands close to the Fermi level are overall well captured by the 4.0 Bohr vacuum reference tight-binding model. Even the predicted electronic structure of the three exotic (and unphysical) benchmark systems is very close to the DFT reference.

The largest errors in the tight-binding bands are found for the low symmetry structures graphene and the alkyne chain. In these structures the band energy of the anti-bonding $2s$ band is far too high at the Γ point. The reason for this discrepancy are the effects of the *crystal field*, which are subject of the following Chapter V.

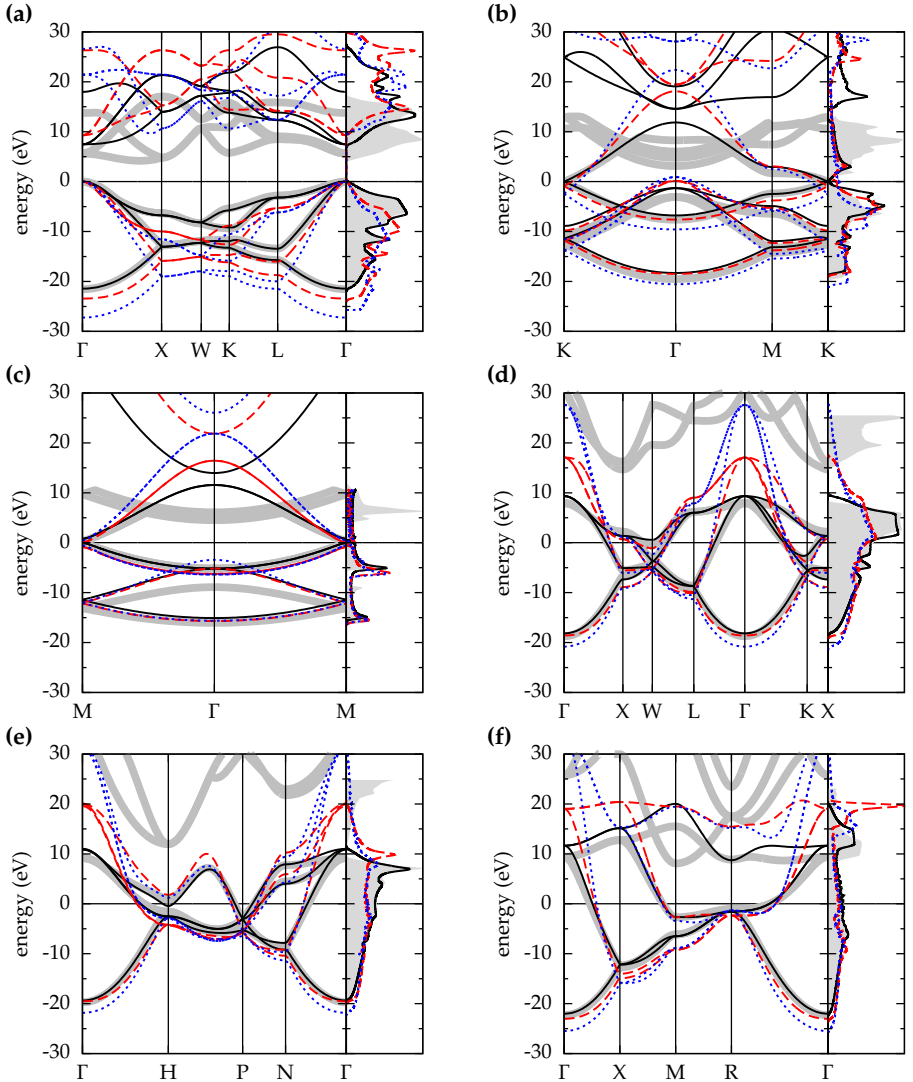


Figure IV.15. DFT and TB band structure plots and densities of states for different carbon structures: (a) diamond, (b) graphene, (c) alkyne chain, (d) fcc, (e) bcc, (f) sc. The gray lines and areas are the DFT reference. The tight binding results were calculated using the TB Hamilton matrix parameters of Fig. IV.14, where the solid black lines, the dashed red lines, and the dotted blue lines correspond to the 4.0 Bohr, the 5.0 Bohr, and the 6.0 Bohr basis sets, respectively. The Fermi levels were shifted to zero to allow for the comparison. Note, that some of the DFT band structures also show virtual $3s/p/d$ bands, which are not included in the TB models.

V Crystal-field interactions in tight-binding

V.1. Crystal-field interactions	86
V.2. Parametrization of crystal-field interactions	88
V.2.1. Partitioning of the Kohn-Sham potential	90
V.2.2. Dimer-based parametrization	92
V.2.3. On-site gauge of the Hamilton matrix	93
V.3. A crystal-field tight-binding model for carbon	95
V.3.1. Dimer-based crystal-field parameters	95
V.3.2. Benchmark of the carbon crystal-field parameters	98
V.3.3. Hamilton matrix gauge	99
V.3.4. Band structures and densities of states	101
V.3.5. Alternative on-site gauges	101
V.3.6. Low-symmetry structures	103
V.4. A crystal-field tight-binding model for titanium	104
V.4.1. Hamilton matrix gauge	106
V.4.2. Band structures and densities of states	109

In conventional tight-binding models the intra-atomic Hamilton matrix elements, the *on-site* elements, are treated as structure independent constants. However, the projection methodology, developed in Chapter IV for the derivation of tight-binding parameters, naturally allows to analyze the on-site Hamilton matrix elements of arbitrary structures. In this chapter the structure dependence and the order of magnitude of such on-site elements of different carbon and titanium structures are discussed. The relation between the on-site elements and the so-called crystal-field interactions is outlined.

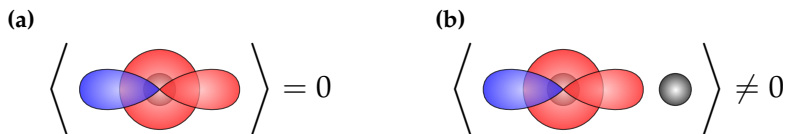


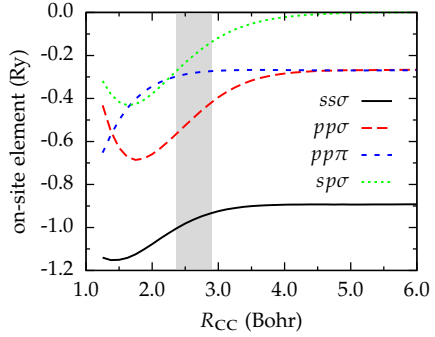
Figure V.1. Schematic of an sp on-site Hamilton matrix element (a) in a free atom and (b) in a dimer molecule. Due to the spherical symmetry, off-diagonal on-site element must vanish on free atoms. In molecules and crystals this symmetry is broken.

An extension of the tight-binding method is presented in which on-site elements are parametrized in a similar fashion as the inter-site bond integrals. The improvement of the crystal-field tight-binding (CF-TB) over conventional tight-binding is demonstrated for band structures and densities of states.

V.1. Crystal-field interactions

As discussed in Sec. III.2, in conventional tight-binding models the intra-atomic matrix elements are usually set to their corresponding atomic values and are thus structure independent constants. As a consequence, the off-diagonal on-site elements, i. e. those matrix elements for two different orbitals at the same atomic site, are set to zero, regardless of the local atomic environment. Additionally, on-site elements that belong to the same angular momentum ℓ are assumed to be equal, as for free atoms the orbitals to the same quantum number ℓ are degenerate. In compounds and crystals the spherical symmetry is, however, broken, and these approximations to the on-site elements may be inappropriate (Fig. V.1). It is well known from spectroscopy that degenerate atomic levels may split due to the interactions with the crystal field. These effects have been described as early as 1929 in the crystal-field theory (CFT) by Bethe and van Vleck.^{49,50} Since TB parameters are usually derived by data fitting, it was merely the number of additional parameters that kept the developers of tight-binding models from including crystal-field interactions.

Figure V.2. The on-site Hamilton matrix elements of the carbon dimer. The bond orientation (σ , π) refers to the vector connecting the two carbon atoms. The gray shaded area corresponds to the nearest neighbor region of Table IV.1. The potential energy reference (zero point) is the vacuum level. The matrix elements were calculated via the projection methodology of Chapter IV using the 4.0 Bohr basis of Table IV.2.



We are in the comfortable situation that the projection methodology of Chapter IV makes it possible to analyze directly the values of the on-site Hamilton matrix elements in any arbitrary crystal structure. Figure V.2 shows the values of the on-site Hamilton matrix elements of the carbon dimer, calculated with the 4.0 Bohr basis of Table IV.2. For carbon–carbon separations of more than around 6 Bohr the atomic levels are recovered, i. e. the diagonal on-site elements adopt the values of the atomic s and p eigenvalues and the off-diagonal sp on-site element becomes zero. For realistic nearest-neighbor distances in carbon compounds (the gray region in Fig. V.2) the picture changes completely: the sp element adopts a large negative value of around -0.2 Ry. Additionally, the three p on-site elements are no longer degenerate, but split into a σ -like and a π -like contribution. When referring to the bond character σ and π we consider the bond vector between the two carbon atoms as reference and name the bond *as if* the two orbitals were located on different centers. The analysis thus shows that the on-site Hamilton matrix elements depend strongly on the local atomic environment and are by no means structurally independent constants, as is assumed in conventional tight-binding models.

Motivated by the above observation, the remainder of this chapter is concerned with the derivation of an efficient and transferable crystal-field parametrization of the Hamilton matrix on-site elements.

V.2. Parametrization of crystal-field interactions

General Hamilton matrix elements were introduced in Eq. (III.16) on page 39

$$H_{\alpha\mu,\beta\nu} = \langle \phi_{\alpha\mu} | \hat{h} | \phi_{\beta\nu} \rangle \quad \text{with} \quad \hat{h} = \hat{t} + v_{\text{eff}}^{\text{KS}} .$$

For the following discussion it is necessary to distinguish between individual atoms, so that we reintroduce the atomic indices α and β of Chapter III. Successively, it was discussed in Sec. III.2.1 that the Hamilton matrix elements can be split into two-center interactions that involve two orbitals at two different atomic sites and three-center interactions that additionally depend on the ionic potentials of all other atoms. This way of thinking implies the partitioning of the effective Kohn–Sham potential into atomic contributions

$$v_{\text{eff}}^{\text{KS}}(\mathbf{r}, \{\mathbf{R}\}) = \sum_{\alpha}^{\text{atoms}} v_{\alpha}(\mathbf{r} - \mathbf{R}_{\alpha}) \quad , \quad (\text{V.1})$$

so that the matrix elements can be expressed as sum of two-center (2c) terms and three-center (3c) terms

$$\begin{aligned} \langle \phi_{\alpha\mu} | \hat{h} | \phi_{\beta\nu} \rangle &= \langle \phi_{\alpha\mu} | \hat{t} + v_{\alpha} + v_{\beta} | \phi_{\beta\nu} \rangle + \sum_{\gamma} \langle \phi_{\alpha\mu} | v_{\gamma} | \phi_{\beta\nu} \rangle \quad \text{with} \quad \gamma \neq \alpha, \beta \\ &= H_{\alpha\mu,\beta\nu}^{2c} + \sum_{\gamma} H_{\alpha\mu,\beta\nu,\gamma}^{3c} . \end{aligned} \quad (\text{V.2})$$

It was then argued in Sec. III.2.1 that the three-center integrals $H_{\alpha\mu,\beta\nu,\gamma}^{3c}$ are small in comparison to the two-center integrals, as they involve the product of three rapidly decaying functions at different centers. Consequently, three-center interactions are neglected in conventional tight-binding models. We also noted that this is a mandatory requirement for the applicability of the Slater–Koster interpolation of Sec. III.2.2.

The on-site elements, on the other hand, are just a special case of the general Hamilton matrix elements, for which $\alpha = \beta$ in Eq. (V.2)

$$\langle \phi_{\alpha\mu} | \hat{h} | \phi_{\alpha\nu} \rangle = \langle \phi_{\alpha\mu} | \hat{t} + v_{\alpha} | \phi_{\alpha\nu} \rangle + \sum_{\gamma} \langle \phi_{\alpha\mu} | v_{\gamma} | \phi_{\alpha\nu} \rangle \quad \text{with} \quad \gamma \neq \alpha . \quad (\text{V.3})$$

Note, however, that on-site elements do not contain *any* three-center interactions! The first term in Eq. (V.3) involves only one atomic center, namely the atom where the two orbitals are located. We will refer to integrals of that kind as *atomic* on-site elements

$$H_{\alpha\mu,\alpha\nu}^{\text{at}} := \langle \phi_{\alpha\mu} | \hat{f} + v_{\alpha} | \phi_{\alpha\nu} \rangle \quad . \quad (\text{V.4})$$

The sum in the second term of the right-hand side of Eq. (V.3) runs over *crystal-field* integrals

$$H_{\alpha\mu,\beta\nu}^{\text{cf}} := \langle \phi_{\alpha\mu} | v_{\beta} | \phi_{\beta\nu} \rangle \quad , \quad (\text{V.5})$$

which describe the interaction of two orbitals located on one atomic site with the Coulomb potential (or pseudopotential) at another site. None of these terms can be neglected based on the argument for three-center interactions in conventional bond integrals. In fact, the environmental dependence of the values of the on-site elements shown in Fig. V.2 is a direct result of the crystal-field terms of Eq. (V.5). It is therefore highly desirable to include the crystal-field interactions in a tight-binding parametrization. In an actual tight-binding calculation the on-site elements have then to be constructed according to Eq. (V.3) as

$$H_{\alpha\mu,\alpha\nu}^{\text{TB}} = H_{\alpha\mu,\alpha\nu}^{\text{at,TB}} + \sum_{\beta \neq \alpha} H_{\alpha\mu,\beta\nu}^{\text{cf,TB}} \quad . \quad (\text{V.6})$$

Note, that the two-center crystal-field integrals of the kind of Eq. (V.5) only need to be known for the same reference orientations as described for the conventional bond integrals in Sec. III.2.2. Only the bond vector has to be defined differently as the connection vector $\mathbf{R}_{\alpha\beta} = \mathbf{R}_{\beta} - \mathbf{R}_{\alpha}$ between the two atoms involved (rather than the vector connecting the orbitals). The Slater–Koster interpolation of Sec. III.2.2 can then be used to calculate analytically the values of arbitrary integrals.

The projection methodology of Chapter IV provides the values of optimal two-center Hamilton matrix elements for any arbitrary structure. There is, however, no obvious method to extract the values of the crystal-field integrals of Eq. (V.5) from the results of the projection; only the entire on-site sum of Eq. (V.3) is available. Intuition suggests to

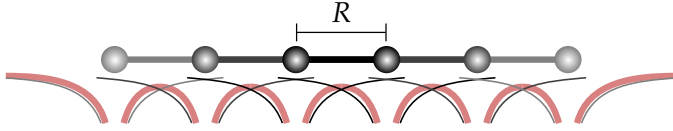


Figure V.3. Schematic depiction of the effective potential of a linear chain of six atoms. The wide red lines stand for the effective potential of the whole molecule. The thin black and gray lines represent the potentials of the free atoms.

tackle this problem by actually performing a partitioning of the Kohn–Sham potential of Eq. (V.1) into atomic contributions and then to calculate the crystal-field integrals Eq. (V.5). Unfortunately, this turns out to be not straightforward.

V.2.1. Partitioning of the Kohn–Sham potential

In order to calculate the crystal-field integrals of Eq. (V.5) a unique and reproducible prescription for a partitioning of the effective Kohn–Sham potential into atomic contributions as in Eq. (V.1) would be needed.

It suggests itself to require each atomic potential $v_\alpha(\mathbf{r} - \mathbf{R}_\alpha)$ to be spherically symmetric about \mathbf{R}_α . We furthermore impose a common frame of reference for the potential energy, e. g. the vacuum level, which is necessary to remove the gauge invariance discussed in Sec. IV.5.2. The potential reference provides the asymptotic value v_0 of the atomic-like potentials. We assume that it is possible to represent entirely the self-consistent effective potential as sum of such atomic-like potentials. These boundaries are, however, still not sufficient to guarantee a unique partitioning.

As an example consider the one-dimensional atom chain of Fig. V.3. According to the boundary conditions outlined above the effective potential of a homonuclear atom chain with an even number of N atoms is, in the direction of the chain, given by

$$v_{\text{eff}}^{\text{KS}} = \sum_{n=1}^{N/2} v\left(r + (2n-1)\frac{R}{2}\right) + v\left(r - (2n-1)\frac{R}{2}\right) \quad \text{with} \quad v(r) = v(-r) \quad , \quad (\text{V.7})$$

where R is the distance between neighboring atoms. Now consider an alternative partitioning with atomic potential contributions \tilde{v} , so that

$$v_{\text{eff}}^{\text{KS}} = \sum_{n=1}^{N/2} \tilde{v} \left(r + (2n-1) \frac{R}{2} \right) + \tilde{v} \left(r - (2n-1) \frac{R}{2} \right) \quad \text{with} \quad \tilde{v}(r) = \tilde{v}(-r) \quad . \quad (\text{V.8})$$

Obviously, the difference between the symmetric potentials $c(r) = v(r) - \tilde{v}(r)$ must be a spherically symmetric function itself. The condition for Eqs. (V.7) and (V.8) to be equally valid is thus given by the difference of the two equations

$$\sum_{n=1}^{N/2} c \left(r + (2n-1) \frac{R}{2} \right) + c \left(r - (2n-1) \frac{R}{2} \right) = 0 \quad \text{with} \quad c(r) = c(-r) \quad . \quad (\text{V.9})$$

Changing the order of the summation, the second term in Eq. (V.9) can be rewritten as

$$\sum_{n=1}^{N/2} c \left(r - (2n-1) \frac{R}{2} \right) = \sum_{n=1}^{N/2} c \left(r - N \frac{R}{2} + (2n-1) \frac{R}{2} \right) \quad . \quad (\text{V.10})$$

Inserting this result into Eq. (V.9) and replacing $r \rightarrow r - (2n-1) \frac{R}{2}$ yields for each summand the condition

$$c(r) = -c \left(r - N \frac{R}{2} \right) \quad ; \quad c(r) = c(-r) \quad , \quad (\text{V.11})$$

which is independent of the summation index. One possible choice for $c(r)$ is thus a cosine function with a periodicity of odd integer fractions of NR

$$c_1(r) = A \cos \left(\frac{2\pi m}{NR} r \right) \quad , \quad m = 1, 3, 5, \dots \quad . \quad (\text{V.12})$$

Thus, we have shown that the partitioning of the effective potential of a symmetric chain of evenly separated atoms into spherical atomic-like potentials is not unique. In the contrary, periodic modulations of the kind of Eq. (V.11) can always be added to the atomic potentials without any effect on the total potential. For a chain of six atoms the situation is exemplified in Fig. V.4, which shows two atomic potentials that lead to identical superpositions.

In numerical optimizations it is hard to avoid the modulations of the atomic potentials. The values of the crystal-field integrals Eq. (V.5) will, however, critically depend on the

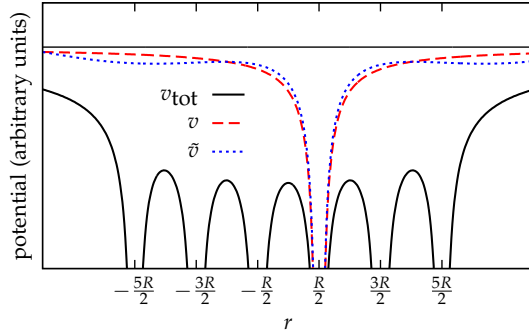


Figure V.4. Analytical superposition of atomic-like potentials for a chain of six atoms. The red dashed curve is an unmodified Coulomb potential $v(r) = -\frac{1}{r}$, whereas the dotted blue potential \tilde{v} is periodically modulated with a cosine function as of Eq. (V.11). The superpositions of six potentials of either kind lead to the same total potential v_{tot} (solid black lines).

chosen partitioning. It is therefore not helpful to proceed with the direct decomposition of crystal-field integrals of complex structures, Eq. (V.3), into individual two-center contributions, Eq. (V.5), unless further boundary conditions are identified that allow for a unique partitioning of the effective potential.

V.2.2. Dimer-based parametrization

Things become much more simple if the dimer molecule is used to derive the values of the crystal-field integrals instead of attempting to calculate them for any arbitrary structure. The expression for the on-site Hamilton matrix elements, Eq. (V.3), simplifies for a dimer to a sum of just two terms

$$H_{\alpha\mu,\alpha\nu}^{\text{dimer}} = \langle \phi_{\alpha\mu} | \hat{h} | \phi_{\alpha\nu} \rangle = H_{\alpha\mu,\alpha\nu}^{\text{at}} + H_{\alpha\mu,\beta\nu}^{\text{cf}} \quad \text{with } \beta \neq \alpha, \quad (\text{V.13})$$

where we used the notation for atomic on-site elements and crystal-field integrals introduced in Eqs. (V.4) and (V.5). The atomic on-site element is only different from zero if the two orbitals ϕ_{μ} and ϕ_{ν} are identical. The limit for large atomic separations

$R_{\alpha\beta} = |\mathbf{R}_\beta - \mathbf{R}_\alpha|$ is given by

$$\lim_{R_{\alpha\beta} \rightarrow \infty} H_{\alpha\mu,\alpha\nu}^{\text{dimer}} = H_{\alpha\mu,\alpha\nu}^{\text{at}} = \begin{cases} \varepsilon_{\alpha\mu}^{\text{at}} & \text{if } \phi_\mu = \phi_\nu \\ 0 & \text{else} \end{cases}, \quad (\text{V.14})$$

with the atomic eigenvalues $\varepsilon_{\alpha\mu}^{\text{at}}$. Assuming that the atomic on-site element $H_{\alpha\mu,\alpha\nu}^{\text{at}}$ is a structure independent atom type specific constant, the distance dependence of the crystal-field integral is simply given by the difference of the dimer on-site matrix element values (e. g. Fig. V.2 for the carbon dimer) and the eigenvalues of the free atom

$$H_{\alpha\mu,\beta\nu}^{\text{cf}} \approx H_{\alpha\mu,\alpha\nu}^{\text{dimer}} - \delta_{\mu\nu} \varepsilon_{\alpha\mu}^{\text{at}}. \quad (\text{V.15})$$

Note, that the reason for Eq. (V.15) being approximate is, again, the ill-defined partitioning of the effective potential. Since the potential contribution v_α of the atomic on-site element, Eq. (V.4), is part of the self-consistent Kohn–Sham potential, it depends in principle on the structure. Approximating the crystal-field integrals as in Eq. (V.15) will thus result in a parametrization that includes the environment dependent modification of the atomic on-site elements.

V.2.3. On-site gauge of the Hamilton matrix

Once a parametrization of the crystal-field integrals is available, the on-site elements can be used for an alternative gauge of the Hamilton matrix elements instead of the approach discussed in Sec. IV.5.2. First, the tight-binding on-site elements $H_{\alpha\mu,\alpha\nu}^{\text{CF-TB}}$ of an arbitrary structure are constructed following Eq. (V.6) using the dimer-based parametrization. Second, the values predicted in such a way are compared to the direct results $H_{\alpha\mu,\alpha\nu}^{\text{AO}}$ of the projection method of Sec. IV. Exploiting the gauge freedom of the Hamilton matrix elements discussed in Sec. IV.5.2, the calculated Hamilton matrix can then be aligned with the predicted on-site elements for one selected on-site level. For the example if the s level is chosen, the appropriate shift is given by

$$H_{\alpha\mu,\beta\nu} = H_{\alpha\mu,\beta\nu}^{\text{AO}} + (H_{s,s}^{\text{CF-TB}} - H_{s,s}^{\text{AO}}) S_{\alpha\mu,\beta\nu}^{\text{AO}}. \quad (\text{V.16})$$

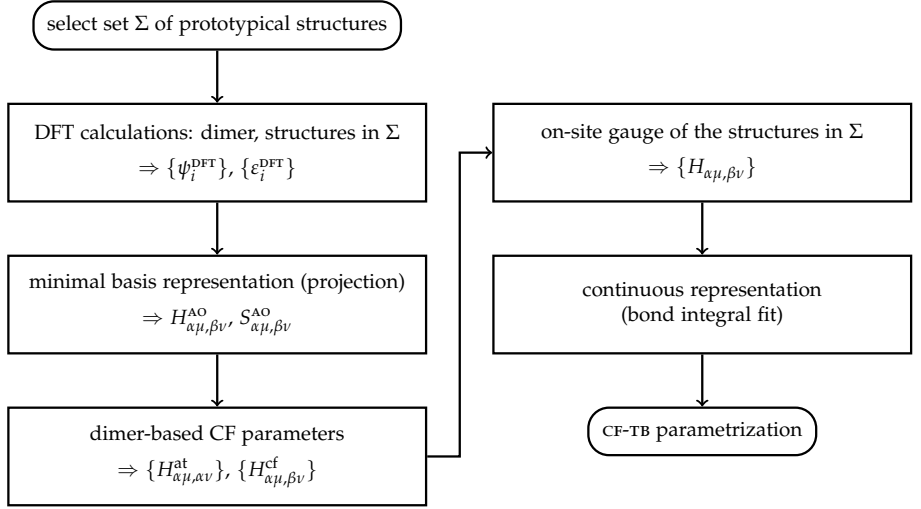


Figure V.5. Flowchart of the procedure for the derivation of crystal-field tight-binding models. The graphic summarizes the methodology discussed in the text. See Sec. IV.2 for details about the minimal AO representation of DFT wave functions. The dimer-based crystal-field parametrization and its use for an on-site gauge of the Hamilton matrix are discussed in Secs. V.2.2 and V.2.3. The functional form used in this work for the final bond integral fit is given in Sec. IV.5.3.

Using the gauged Hamilton matrix elements $H_{\alpha\mu,\beta\nu}$ of several reference structures it can then be proceeded with the derivation of a tight-binding model as described in Sec. IV.5.4. The entire procedure is outlined in a flowchart in Fig. V.5.

Note, that the alignment of the on-site levels, Eq. (V.16), implicitly imposes the potential reference of the crystal-field parametrization to gauge the Hamilton matrix. This technique therefore allows to use the vacuum level as potential reference even in structures without vacuum region.

In the following sections we will go through the procedure outlined in the flowchart in Fig. V.5 to derive crystal-field tight-binding models for carbon and titanium. Starting point are the results of the projection methodology that are already covered by

Sec. IV.5. We refer to tight-binding models as crystal-field tight-binding (CF-TB) if their parametrization includes crystal-field interactions.

V.3. A crystal-field tight-binding model for carbon

For the derivation of crystal-field tight-binding parameters the same set of prototypic carbon structures was used as previously for conventional TB parameters in Sec. IV.5.4, namely the diamond structure, graphene and the infinite alkyne chain. The optimized carbon atomic orbital basis sets of Sec. IV.4.1 were employed in the minimal basis representation of the DFT wave functions.

V.3.1. Dimer-based crystal-field parameters

Two different electronic configurations may be considered for the carbon dimer molecule: the $[\text{He}]2s^22p^2$ configuration corresponds to the atomic occupation and therefore provides the correct dissociation limit. Within crystals and compounds the electronic configuration is closer to $[\text{He}]2s^12p^3$, therefore this occupation might also be a good choice for a transferable TB parametrization. DFT calculations for both configurations were carried out, by using fix molecular orbital occupations for the carbon dimer reflecting the two choices of atomic reference configurations. The corresponding on-site elements were calculated using the projection methodology of Sec. IV.2. The calculated on-site levels are shown in Fig. V.6 (a). At the first glance the results for the two electronic configurations seem to differ significantly. However, as a result of the gauge freedom of the Hamilton matrix elements, discussed in Sec. IV.5.2, only the energy differences between the on-site levels are meaningful. These differences are almost identical for the two configurations, as can be seen in panel (b) of Fig. V.6. Only the off-diagonal $sp\sigma$ element, which is not gauge invariant, shows larger deviations. Since the $[\text{He}]2s^22p^2$ occupation yields the correct asymptotic limit for the free atoms* we decided to use that configuration in the following.

*Note that spin degeneracy was not taken into account for any calculation in this thesis.

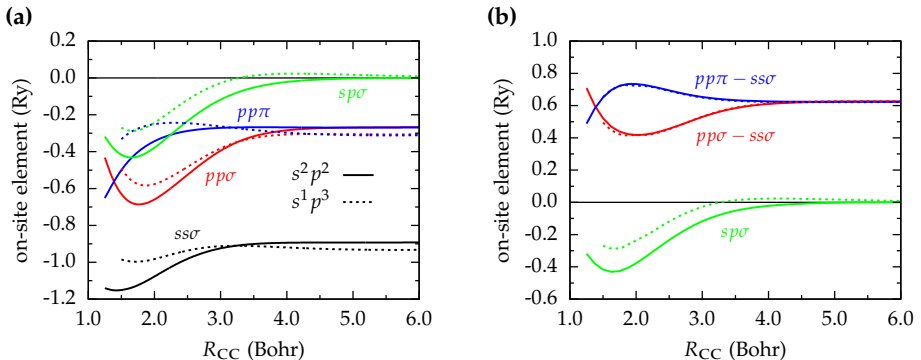


Figure V.6. Carbon dimer on-site elements for the two different electronic configurations $[He]2s^2 2p^2$ (solid lines) and $[He]2s^1 2p^3$ (dotted lines). Panel (a) shows the direct comparison of the on-site elements as calculated with the 4.0 Bohr basis of Table IV.2 and using the vacuum level as potential energy reference. In panel (b) the relative energies of the diagonal on-site elements are compared.

The carbon dimer $[He]2s^2 2p^2$ on-site elements as calculated with the 4.0, 5.0 and 6.0 Bohr basis sets of Table IV.2 are plotted in Fig. V.7. As a result of the energy spillage (Sec. IV.2.2) the values of the on-site elements differ by constant energies for the three basis sets. The comparison of the matrix elements after alignment on the s -level of the 6.0 Bohr basis shows, however, only minor differences. The spillage during the projection thus has only little impact on the structural dependence of the crystal-field integrals. The crystal-field interactions are short ranged, as all on-site elements are essentially converged to the atomic values at a carbon-carbon separation of around 4.5 Bohr. In actual tight-binding calculation we prefer to work with the converged atomic eigenvalues, if they are available. Though, it is only important to use *consistent* eigenvalues for the atomic energy and compound energies. We therefore apply a constant correction to the crystal-field integrals in order to retain the correct atomic levels.

Same as for the conventional bond integrals, for practical applications a continuous analytical representation of the CF integrals is needed. For this purpose the function

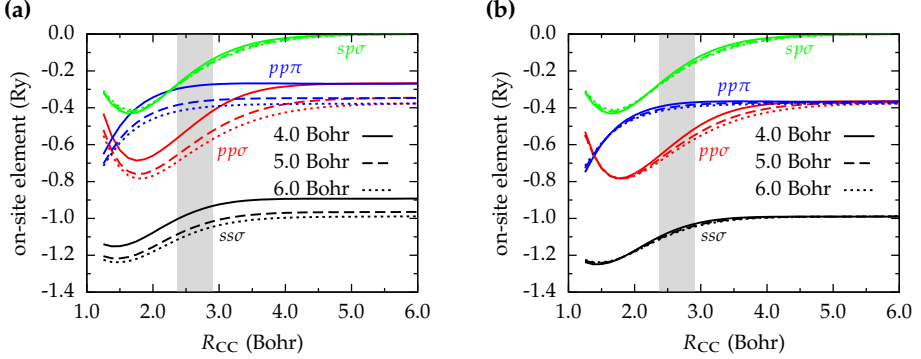


Figure V.7. Carbon dimer on-site elements as calculated using the 4.0, 5.0 and 6.0 Bohr basis sets of Table IV.2 (vacuum reference). In panel (b) the same data is plotted, but the diagonal on-site elements were aligned on the s level. The gray highlighted area corresponds to the nearest neighbor bond region of Table IV.1.

type of Sec. IV.5.3 has been employed. The CF parameters for the three different basis sets are listed in Table B.4 of Appendix B. The dimer-based crystal-field parametrization is subsequently used for the gauging of the Hamilton matrices from different carbon structures.

Finally, note that the vacuum reference on-site integrals used above are not a unique choice for the crystal-field parametrization. The on-site Hamilton matrix elements are subject to the same gauge freedom described in Sec. IV.5.2 as the entire Hamilton matrix. It is therefore always permissible to shift all on-site elements by the same arbitrary constant, even individually for each atomic separation. Upon the Hamilton matrix gauge of Sec. V.2.3 the potential reference of the on-site levels will be implicitly imposed to all Hamilton matrix elements. Other equally systematic and reasonable choices of potential references are (1) to set a selected on-site level to a constant, or (2) to shift the band sum of the dimer molecule to the total energy. These two alternatives are discussed in Sec. V.3.5.

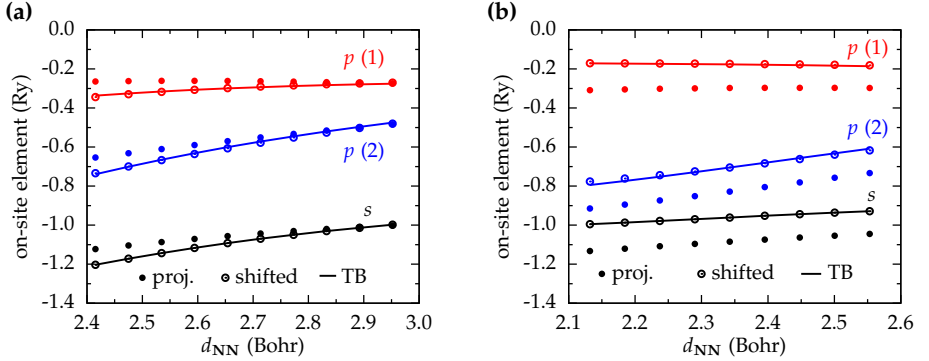
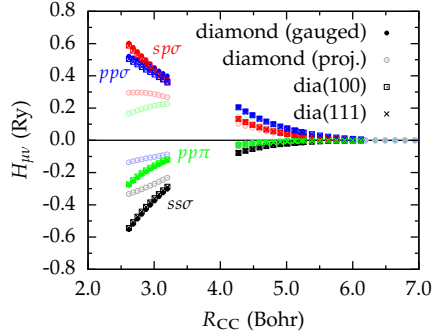


Figure V.8. Comparison of the on-site Hamilton matrix elements for (a) graphene and (b) the infinite alkyne chain as calculated via the projection formalism of Sec. IV.2 (proj.) and as predicted using the dimer-derived crystal-field parametrization (TB). The empty circles represent the projection data after an alignment of the s level with the TB values. The minimal basis representation is achieved using the 4.0 Bohr basis of Table IV.2.

V.3.2. Benchmark of the carbon crystal-field parameters

It is sensible to assess the quality of the dimer approximation for the crystal-field parameters before using them in a Hamilton matrix gauge. For this purpose we compare predicted on-site elements that are calculated according to Eq. (V.6) with the actual results of the projection procedure of Sec. IV.2. Figure V.8 shows the on-site elements of the graphene structure and of the infinite alkyne chain. The relative separation of all levels, and especially the splitting of the p levels, is very well described by the dimer-derived crystal field parameters. Even the absolute energy of the on-site levels is comparable, as for the DFT calculations of all three systems the vacuum level was employed as reference. After applying a constant shift to the projection data to align the s level with the predicted one, the agreement is nearly perfect. The shift determined by this difference is the gauge correction of Eq. (V.16) and has to be applied (scaled by the overlap) to all Hamilton matrix elements.

Figure V.9. Diamond Hamilton matrix elements as calculated using the 4.0 Bohr basis of Table IV.2. The figure shows the vacuum gauge matrix elements obtained from the diamond(100) and diamond(111) surface slab models of Fig. IV.13 in comparison to the on-site gauge matrix elements of the true periodic diamond crystal structure. The unmodified projection results for the diamond structure, which have a different potential reference, are shown as pale empty circles.



Note that the on-site elements of the diamond structure, although well described by the CF parametrization, do not provide any additional insight. Due to the crystal symmetry the p levels do not split in the diamond structure, and the absolute values of the projection data for the on-site elements can not be compared to the predicted levels, as the DFT calculations for the diamond structure were performed with a different potential reference (Sec. IV.5.2).*

V.3.3. Hamilton matrix gauge

In contrast to the vacuum gauge TB model of Sec. IV.5.4 the crystal-field on-site parametrization allows us to use the true periodic diamond crystal structure as reference for the Hamilton matrix parameters. As a proof of concept we can, however, compare the vacuum reference matrix elements of the diamond slabs of Sec. IV.5.4 with the on-site gauged diamond structure matrix elements. Since the DFT calculations for the diamond slabs and the one of the carbon dimer both employ the vacuum level as potential reference, their values should be comparable. The gauged matrix elements are shown in Fig. V.9 along with the un-gauged direct results of the projection. The on-site gauge matrix elements are not only close in value to the slab model based ones,

*When the vacuum level was not available, the structure dependent average effective potential was used as the zero point of the potential energy.

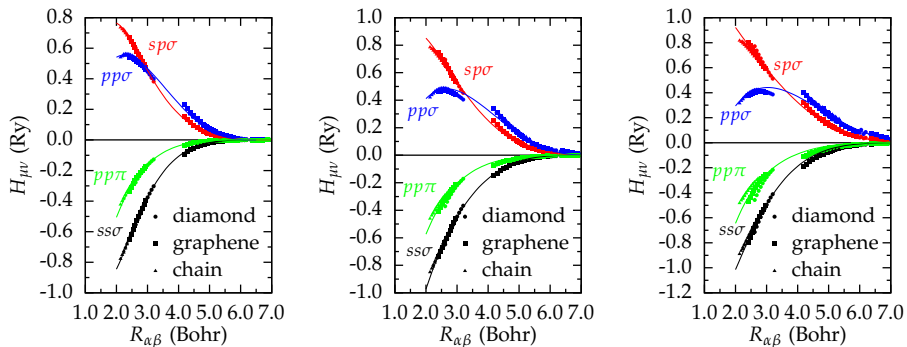


Figure V.10. Distance and structure dependent values of the on-site gauged Hamilton matrix elements in Rydberg units for the 4.0, 5.0 and 6.0 Bohr basis sets (left to right) of Table IV.2. The solid lines are continuous bond integral representations with the functional form of Eq. (IV.30). Parameters of these functions are given in Table B.5 in the appendix. The crystal-field parameters used are the ones given in Table B.4 and depicted in Fig. V.7.

but are virtually identical. This example demonstrates that it is not necessary to spend the effort to construct slab models and to calculate the electronic structure of these larger structures. At least for carbon it is sufficient to use the dimer-based crystal-field parametrization to implicitly gauge arbitrary structures on the vacuum energy level.

The on-site gauge Hamilton matrix elements for all of the three reference structures and the three different basis sets are shown in Fig. V.10. As expected, the on-site gauge bond integrals are very similar to the vacuum reference ones of Fig. IV.14. The small differences that occur even lead to a reduction in the scattering of the data points, i. e. to less environmental dependencies, and the analytic representation of the bond integrals (the bond integral fit) is less arbitrary. The general trends discussed for the conventional TB model in Sec. IV.5.4 still apply: the data calculated with the shortest ranged 4.0 Bohr AO basis set exhibits the least scattering and also allows best for the interpolation between the first and second neighbor bond integrals. See Table B.5 for the parameters of the bond integral fits.

V.3.4. Band structures and densities of states

CF-TB band structures and densities of states for the same set of carbon structures as employed in Sec. IV.5.4 are shown in Fig. V.11. Improvements over the conventional TB model of Sec. IV.5.4 are most apparent for the low-dimensional structures graphene and the infinite alkyne chain. The shape of the band edges and all states below or close to the Fermi level are well described by the CF-TB model. The virtual bands are not expected to be captured particularly well, as the carbon basis sets of Sec. IV.4 were optimized for the occupied bands only. Nevertheless, both the DFT band gap of diamond and the K point in graphene are correctly reproduced by the tight-binding bands.

V.3.5. Alternative on-site gauges

In the previous sections we have demonstrated that a consistent choice of on-site elements is needed to gauge the projected Hamilton matrix elements of different structures. Our choice for the on-site elements in Sec. V.3.1, however, is not unique. The diagonal on-site Hamilton matrix elements are subject to the same gauge invariance described in Sec. IV.5.2 as the inter-site Hamilton matrix elements, i. e. the zero point of the Kohn–Sham energy eigenvalues can be chosen arbitrarily and does not need to be equal to the vacuum level (the choice in Sec. V.3.1). The diagonal elements of the overlap matrix are equal to one so that, according to Eq. (IV.29), any arbitrary shift can be simulataneously imposed upon the on-site levels. Note, that the off-diagonal on-site elements, i. e. integrals over different orbitals at the same site, may not be shifted, as the on-site overlap matrix elements are diagonal $S_{\mu\alpha, \nu\alpha} = \delta_{\mu\nu}$.

Of the infinite possibilities, two further systematic on-site gauges shall be discussed: (1) a constant s level gauge, in which the on-site elements are shifted such that the s level becomes structurally independent, and (2) a total energy gauge, in which the on-site shift renders the band sum equal to the total energy of the dimer molecule. The second choice resembles closely the underlying idea of the NRL tight-binding

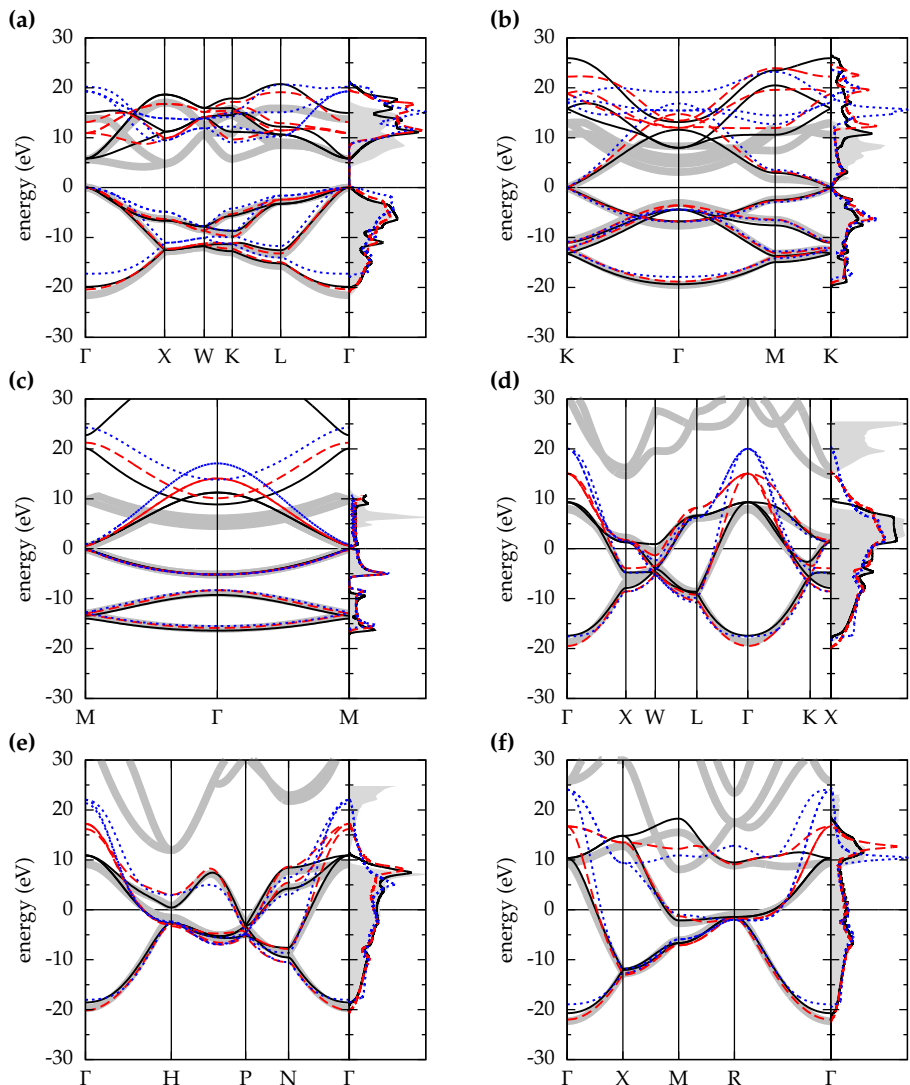


Figure V.11. DFT and CF-TB band structure plots and densities of states for different carbon structures: (a) diamond, (b) graphene, (c) alkyne chain, (d) fcc, (e) bcc, (f) sc. The gray lines and areas are the DFT reference. The tight-binding results were calculated using the TB Hamilton matrix parameters of Fig. V.10, where the solid black lines, the dashed red lines, and the dotted blue lines correspond to the 4.0 Bohr, the 5.0 Bohr, and the 6.0 Bohr basis sets, respectively. The Fermi levels were shifted to zero to allow for the comparison.

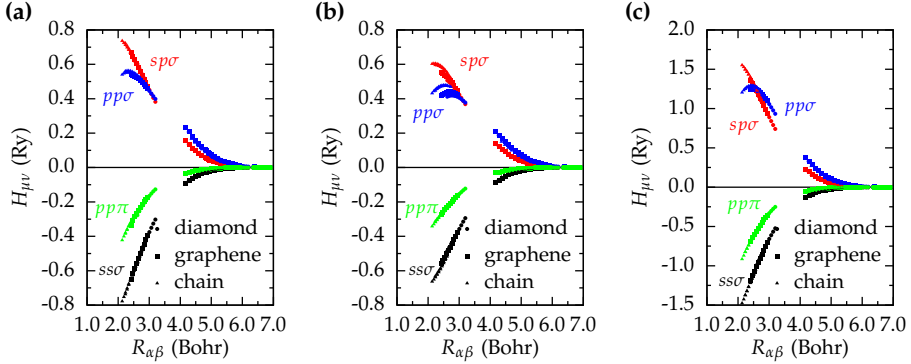


Figure V.12. Comparison of the calculated carbon Hamilton matrix elements for three different on-site gauges: (a) vacuum level gauge, (b) constant s level gauge and (c) total energy gauge. Note the different energy scales.

implementation that is discussed in Sec. III.3.5. However, here we only consider the total energy of the dimer molecule for the gauge instead of the individual energies of all reference compounds, as is done in the NRL model.

The gauged Hamilton matrix elements of the three reference structures resulting from the three different choices of dimer on-site elements are depicted in Fig. V.12. The constant s level gauge results in the largest scattering of the data points and clearly is the worst choice of the three options in the case of carbon. The total energy gauge, on the other hand, yields a scattering that is comparable to the vacuum gauge and might as well be considered for carbon. Note, however, that the energy scale of the bond integrals increases by about a factor of two due to the large shift of the band sum, which also means that the seemingly small scattering in Fig. V.12 (c) still is a factor of two larger than in the vacuum level gauge.

V.3.6. Low-symmetry structures

It might seem a small gain if the improvements of the CF-TB model over the conventional TB model of Sec. IV.5.4 are restricted to low-dimensional and low-symmetry

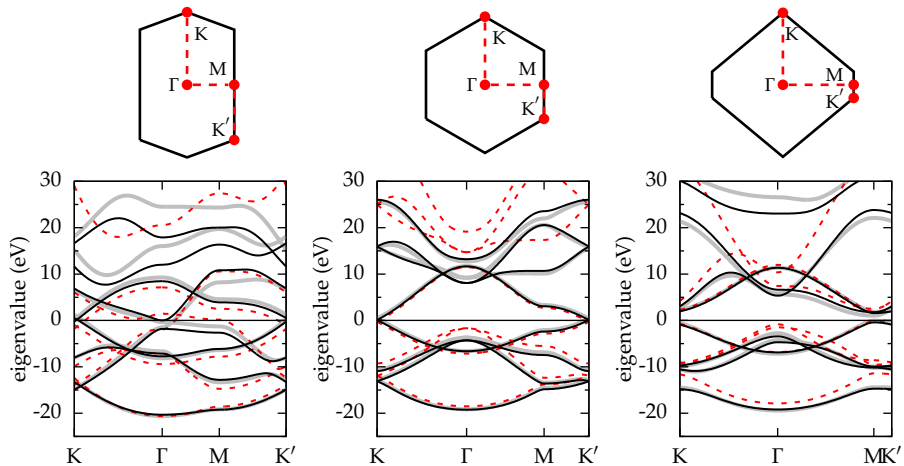


Figure V.13. Band structures of distorted graphene. The CF-TB band structures (black solid lines) are shown along with the DFT references (wide gray solid lines) and the results of the conventional TB model of Sec. IV.5.4 (red dashed lines). Above the diagrams the Brillouin zones of the three structures are sketched. The central band structure corresponds to undistorted, ideal graphene. For all calculations the models based on the 4.0 Bohr AO basis (see the text for details) have been used.

structures. In reality structures of low symmetry are, however, very common even in crystals. It can be expected that crystal-field interactions play an important role in defect structures and distorted structures, in which the symmetry is intrinsically broken. As an example the band structures of distorted graphene are shown in Fig. V.13. For such geometries the CF-TB model yields significantly better results compared to the conventional TB model. Here, neglecting the crystal-field interactions leads to errors in the band curvatures and crossings.

V.4. A crystal-field tight-binding model for titanium

The procedure for the derivation of tight-binding models for the transition metal titanium is, in general, not much different from what has been described for carbon

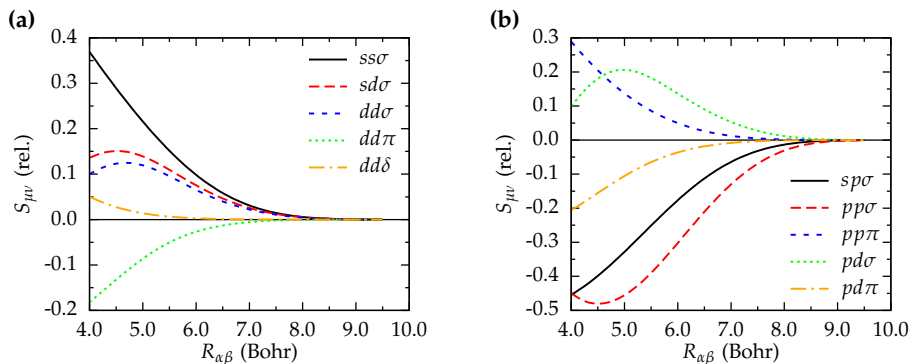


Figure V.14. Distance dependent values of the titanium overlap matrix elements for the optimized 5.5 Bohr AO basis sets of Table IV.4. Panel (a) of the figure shows the matrix elements for the 3d and 4s orbitals only. Those integrals with 4p contributions are shown in panel (b).

in the previous section. There are, of course, six additional bond integrals due to the titanium 3d orbitals as depicted in Fig. III.3. As already reasoned in Sec. IV.4.2, the 4p orbitals are, on the other hand, of low importance for titanium compounds as they are unoccupied in the isolated atom and do not contribute much to the bonding states.

The 5.5 Bohr basis set of Table IV.4 yields very good spillage values while it is at the same time short ranged. Not much can be learned from the comparison of the different basis sets that has not already been discussed for the case of carbon. In the following we will therefore focus on the optimized 5.5 Bohr AO basis set for titanium, which yielded the best results. The overlap matrix elements, as calculated using the projection methodology of Sec. IV.2, are shown in Fig. V.14. For the calculation and comparison of Hamilton matrix elements it is necessary, as it was explained for the carbon case, to introduce a common frame of reference (zero point) for the potential energy. Unlike for carbon there are no physically realistic titanium structures with vacuum regions except for surface models and clusters. It would therefore cause a considerable increase in computational effort to impose the vacuum level as potential reference. Instead, as demonstrated in Sec. V.3.3 for carbon, a dimer-derived crystal-field parametrization can conveniently be used to gauge the Hamilton matrix elements of different structures

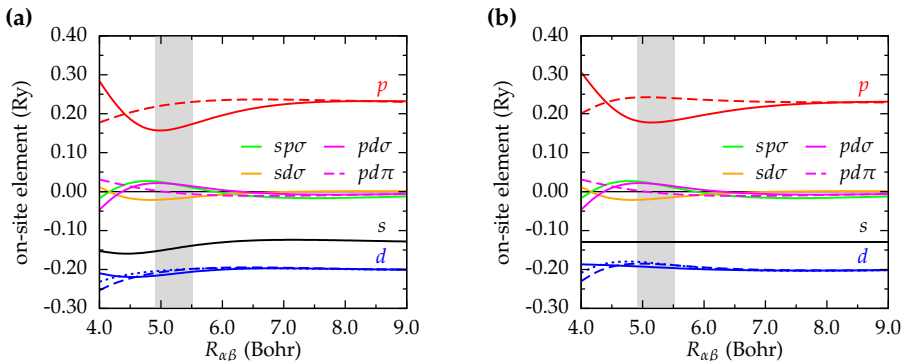


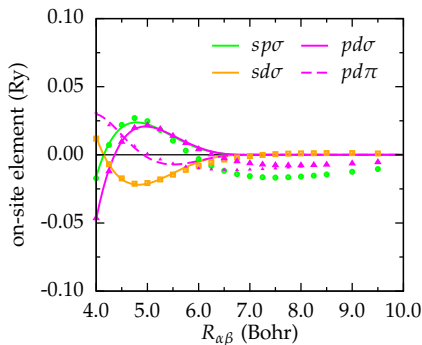
Figure V.15. Titanium dimer on-site Hamilton matrix elements (a) using the vacuum level as potential energy reference and (b) with a constant s level reference. The projection was done on the 5.5 Bohr optimized AO basis of Table IV.4. σ bonds are plotted with solid lines, π bonds and δ bonds with dashed and dotted lines, respectively. The gray region highlights the nearest neighbor shell according to Table IV.3.

and arbitrary potential reference. This way the same reference structures may be employed as used for the optimization of the titanium AO basis sets in Sec. IV.4.2, namely the fcc, bcc and sh crystal structures.

V.4.1. Hamilton matrix gauge

The first step in the construction of a CF-TB model for titanium obviously is to perform DFT calculations for the titanium dimer. In contrast to the carbon dimer of Sec. V.3.1, the electronic configuration of atomic titanium ($[\text{Ar}]3d^34s^2$) can not easily be imposed on the dimer molecule as it would result in a doubly occupied antibonding σ^* orbital. As a compromise, we therefore chose to fully occupy the bonding σ state and to distribute the remaining electrons equally over the five bonding d states. In the dissociation limit this corresponds to a $[\text{Ar}]3d^34s^1$ configuration. As demonstrated for the carbon dimer in Sec. V.3.1, the electronic configuration does not have a large impact on the structure dependence of the crystal-field integrals and the wrong dissociation limit can be cured by an *a posteriori* shift of the atomic eigenvalues.

Figure V.16. Actual values (symbols) and continuous fit (lines) of the titanium dimer off-diagonal on-site elements. Solid lines represent σ bonds, dashed lines stand for π bonds. The off-diagonal on-site elements only depend on the chosen AO basis set (the 5.5 Bohr basis of Table IV.4) and are not subject to a gauge freedom.



The titanium dimer on-site Hamilton matrix elements for the vacuum level as potential energy reference are depicted in Fig. V.15 (a). In comparison to the carbon dimer on-site elements shown in Fig. V.7 the titanium–titanium crystal-field integrals show only a weak structural dependence and are of a much smaller absolute value. Both, the splitting of the d level and the value of the off-diagonal on-site elements are relatively small (around 0.02 Ry or 0.3 eV) in comparison to the expected approximation in the Hamilton matrix parameters. It might therefore be a good approximation to neglect crystal-field interactions in the case of titanium. The on-site parametrization is nevertheless needed to gauge the Hamilton matrix elements of the different reference titanium crystal structures. As an alternative to the vacuum reference on-site integrals, panel (b) of Fig. V.15 shows the values of the on-site elements for a constant s level reference. Here, the gauge freedom of the on-site elements was exploited to shift the diagonal on-site elements in such a way that the s level becomes structure-independent, as previously discussed for carbon in Sec. V.3.5. Such a choice of potential reference for the on-site elements suggests itself if the crystal-field interactions are to be neglected after the Hamilton matrix gauge.

Although the absolute values of the titanium dimer off-diagonal on-site elements is small, they decay slowly and are not converged to zero even for an atomic separation of 10.0 Bohr. The integrals approach, however, approximately constant values at a range of 7.0 Bohr. We therefore decided to impose this radius as a cutoff for the crystal-field

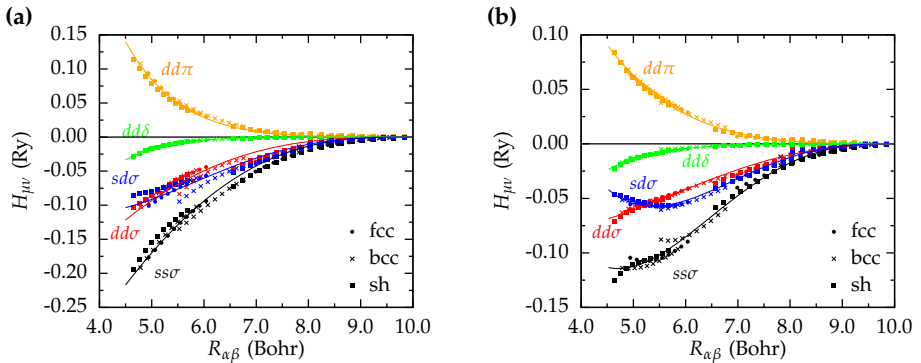


Figure V.17. Titanium Hamilton matrix elements for (a) the vacuum level on-site gauge (Fig. V.15 a.) and (b) for the constant s-level gauge (Fig. V.15 b.). The matrix element data points stem from the fcc, bcc and sh crystal structures and have been calculated using the optimized 5.5 Bohr AO basis set of Table IV.4. The solid lines represent bond integral fits with the functional form of Sec. IV.5.3. Bond integrals with p contribution are omitted for clarity.

interactions (Fig. V.16). For atomic separations larger than 7.0 Bohr a constant, but small error in the crystal-field interactions is therefore to be expected.

The Hamilton matrix elements of the three reference structures for the vacuum level gauge as well as for the constant s-level gauge are depicted in Fig. V.17. Even the seemingly small differences in the on-site values of Fig. V.15 (a) and (b) lead to significantly different Hamilton matrix elements. Especially note the different energy scales in the two diagrams of Fig. V.17. In contrast to carbon, for titanium the constant s level gauge results in a reduced scattering of the data points in comparison to the vacuum level gauge, most notably in the $sd\sigma$ bond integral. The same trend is also observed for those matrix elements with p contribution (not shown in Fig. V.17).

Note, that the constant s level reference might still not be the *ideal* Hamilton matrix gauge for titanium. For this work only the two options shown in Fig. V.15 were compared and the accuracy of the resulting crystal-field tight-binding models is found to be satisfactory. A possible subject for a future study could be the development of a methodology that allows to determine the optimal on-site reference for maximally transferable bond integrals.

V.4.2. Band structures and densities of states

To assess the quality of the titanium CF-TB model let us take a look at the band structures and densities of states for a number of titanium crystal structures. In Fig. V.18 the results for the three reference structures fcc, bcc and sh and for three benchmark structures are shown. Note, that the hcp structure (**d**) is the most stable titanium crystal structure at normal conditions, while the ω Ti structure (**e**) corresponds to a meta-stable high-pressure phase.^{105,106} Overall the constant s -level gauge CF-TB model yields results that are in very good agreement with the DFT references. Especially when comparing the densities of states the s -level gauge (solid black lines) proves, as expected, to be more reliable than the vacuum gauge (red dashed lines).

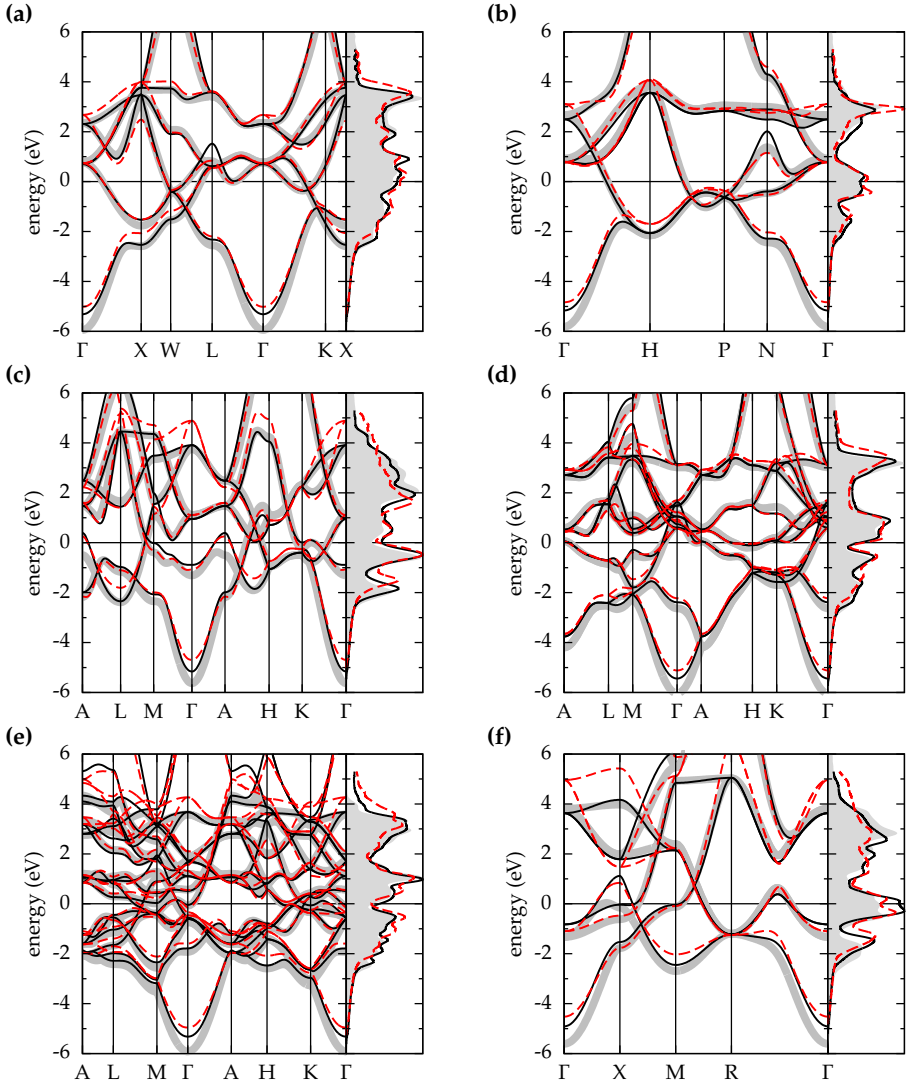


Figure V.18. DFT and CF-TB band structure plots and densities of states for different titanium structures: (a) fcc, (b) bcc, (c) sh, (d) hcp, (e) ω Ti/C32, (f) sc. The gray lines and areas are the DFT reference. The solid black lines are the band structures and densities of states as calculated with the constant s -level CF-TB model, the red dashed lines correspond to the vacuum level CF-TB model. The Fermi levels were shifted to zero to allow for the comparison.

VI.

Total energy and CF-TB models

VI.1. The invariance of the total energy	111
VI.2. Energy partitioning	113
VI.3. Crystal-field tight-binding band sums	115

The crystal-field extension to the tight-binding electronic structure method (Chapter V) has implications on the total energy implementation. In this section the effects of the variable on-site Hamilton matrix elements on the band sum and the total energy are discussed. Consequences for the calculation of tight-binding total energies and cohesive energies using the implementations of Sec. III.3 are estimated.

At the beginning of the chapter a theoretical understanding of the tight-binding total energy functional is established. The later two sections focus on the practical implications for the development of a total energy crystal-field tight-binding implementation and provide a comparison of the DFT cohesive energy with conventional and crystal field tight-binding band energies.

VI.1. The invariance of the total energy

The gauge invariance of the total energy and the change of the one-electron eigenvalues with respect to a shift of the potential energy zero point was subject of Sec. IV.5.2. It can be easily verified that the one-electron kinetic energy t_i of the Kohn–Sham equations,

Eq. (II.82), obeys the same invariance as the total energy

$$t_i = \langle \psi_i | \hat{t}_i | \psi_i \rangle = \varepsilon_i - \langle \psi_i | v_{\text{eff}}^{\text{KS}} | \psi_i \rangle$$

$$\xrightarrow{v_{\text{eff}}^{\text{KS}} \rightarrow v_{\text{eff}}^{\text{KS}} + \kappa} (\varepsilon_i + \kappa) - \langle \psi_i | v_{\text{eff}}^{\text{KS}} + \kappa | \psi_i \rangle = t_i \quad , \quad (\text{VI.1})$$

which is basically another way to express Eq. (IV.28). Note, that the shift of the eigenvalues is compensated by an equal shift of the potential energy expectation value in Eq. (VI.1). The total Kohn–Sham kinetic energy, $T_s = \sum_i f_i t_i$, is therefore invariant with respect to a shift of the effective potential, whereas the band energy changes

$$E_{\text{band}} = \sum_i f_i \varepsilon_i \xrightarrow{v_{\text{eff}}^{\text{KS}} \rightarrow v_{\text{eff}}^{\text{KS}} + \kappa} \sum_i f_i \varepsilon_i + N_e \kappa \quad , \quad (\text{VI.2})$$

with a shift that is proportional to the number N_e of electrons in the system.

Recall from Sec. III.1 that the Harris–Foulkes non-selfconsistent energy functional \mathcal{E}^{HF} of Eq. (III.11) is constructed by evaluating the total single-particle kinetic energy T_s and inserting the result, i. e. the sum over all t_i of Eq. (VI.1), into the Kohn–Sham energy functional. The potential energy contribution $\langle v_{\text{eff}}^{\text{KS}} \rangle$ is in Eq. (III.12) absorbed by the Harris–Foulkes double counting term \mathcal{D}^{HF} to yield

$$\mathcal{E}_{\text{tot}}^{\text{HF}}[n] = \sum_i f_i \varepsilon_i[n] + \mathcal{D}^{\text{HF}}[n] + E_{\text{nn}} \quad , \quad (\text{VI.3})$$

which is the foundation of the tight-binding energy expression, Eq. (III.19),

$$E_{\text{tot}}^{\text{TB}} = E_{\text{band}}^{\text{TB}} + \mathcal{D}^{\text{TB}} + E_{\text{nn}} \quad . \quad (\text{VI.4})$$

For the following discussion it is helpful to consider the total energy of a static structure, instead of the electronic energy only. Therefore the ion–ion interaction energy E_{nn} is included in the equations above. Also the Harris–Foulkes functional is *by construction* invariant with respect to a shift of the Kohn–Sham potential, as a shift of the band sum is compensated by a corresponding inverse shift of the double counting. In principle every total energy tight-binding implementation, Eq. (VI.4), does also have to fulfill this requirement. Even though the Slater–Koster band sum parametrization might be separate from the parametrization of the tight-binding double counting, the two contributions can thus not be considered independently.

Note that the simplest tight-binding total energy implementation, the TB band model discussed in Sec. III.3.1, is not invariant with respect to the choice of the potential zero point. If it is guaranteed that the potential energy reference of the band energy is structurally independent, it is however still possible to determine a matching pair potential parametrization of the double counting. This is in practice realized by enforcing constant on-site Hamilton matrix elements. Since the CF-TB method of Chapter V is *based* on the parametrization of the environmental dependence of the Hamilton matrix on-site elements, a simple CF-TB band model implementation is ruled out.

VI.2. Energy partitioning

As argued in the previous section the partitioning of the total energy into the band sum plus corrections might not be the most fortunate choice for the construction of general tight-binding total energy models. We therefore rewrite the TB energy expression by moving energy contributions from the band sum to the double-counting term

$$E_{\text{tot}}^{\text{TB}} = (E_{\text{band}}^{\text{TB}} - \Delta E) + (\mathcal{D}^{\text{TB}} + \Delta E) + E_{\text{nn}} \quad , \quad (\text{VI.5})$$

where the band sum correction term ΔE is chosen in such a way that it cancels out the energy shift upon change of the potential energy reference:

$$E_{\text{band}} - \Delta E \xrightarrow{v_{\text{eff}}^{\text{KS}} \rightarrow v_{\text{eff}}^{\text{KS}} + \kappa} (E_{\text{band}} + N_{\text{e}} \kappa) - (\Delta E + N_{\text{e}} \kappa) \quad . \quad (\text{VI.6})$$

The *corrected* band sum $(E_{\text{band}} - \Delta E)$ can then be parametrized independently of the remaining terms in the energy expression.

Several approaches towards an energy partitioning as in Eq. (VI.5) into physically motivated terms have been suggested. The tight-binding bond model (TBBM, Sec. III.3.3 and Ref. 71) expresses the total energy as sum of the bond energy E_{bond} , the promotion energy E_{prom} , the energy of the free atoms E_{atoms} , and a pair potential energy E_{pp} that accounts for the remaining terms

$$E_{\text{tot}}^{\text{TBBM}} = E_{\text{bond}} + E_{\text{prom}} + E_{\text{atoms}} + E_{\text{pp}} \quad , \quad (\text{VI.7})$$

which is equivalent to (see Sec. III.3.3 for the definitions of the individual terms)

$$= E_{\text{band}} - \sum_{\alpha\mu} f_{\alpha\mu}^{\text{at}} (H_{\alpha\mu,\alpha\mu} - \epsilon_{\alpha\mu}^{\text{at}}) + E_{\text{pp}} \quad , \quad (\text{VI.8})$$

with atomic occupations $f_{\alpha\mu}^{\text{at}}$ (orbital resolved charges) and atomic eigenvalues $\epsilon_{\alpha\mu}^{\text{at}}$.

The TBBM band sum correction is thus given by

$$\Delta E^{\text{TBBM}} = \sum_{\alpha\mu} f_{\alpha\mu}^{\text{at}} (H_{\alpha\mu,\alpha\mu} - \epsilon_{\alpha\mu}^{\text{at}}) \quad , \quad (\text{VI.9})$$

which possesses the desired transformation behavior, Eq. (VI.6), upon a shift of the Kohn–Sham potential.

Fähnle and coworkers adapted the TBBM for the analysis of general electronic structure calculations,^{107,108} and slightly modified the band sum correction to

$$\Delta E^{\text{A}} = \sum_{\alpha\mu} q_{\alpha\mu} (H_{\alpha\mu,\alpha\mu} - \epsilon_{\alpha\mu}^{\text{at}}) \quad , \quad (\text{VI.10})$$

where $q_{\alpha\mu}$ are Mulliken’s orbital populations of the bound atoms.⁷² Their work furthermore suggest the mixed option

$$\Delta E^{\text{B}} = \sum_{\alpha\mu} (q_{\alpha\mu} H_{\alpha\mu,\alpha\mu} - f_{\alpha\mu}^{\text{at}} \epsilon_{\alpha\mu}^{\text{at}}) \quad . \quad (\text{VI.11})$$

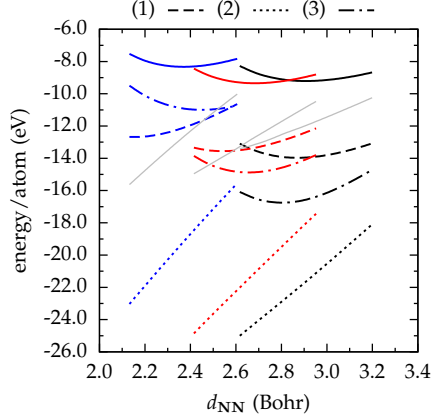
In the spirit of the constant s level Hamilton matrix gauge of Sec. V.4.1 it seems also reasonable to select a reference on-site level for the band sum correction. One possibility, using the valence s level, is

$$\Delta E^{\text{C}} = \sum_{\alpha\mu} f_{\alpha\mu}^{\text{at}} (H_{s \text{ level}} - \epsilon_{s \text{ level}}^{\text{at}}) \quad . \quad (\text{VI.12})$$

We note in passing that all of the above band sum corrections but ΔE^{B} become zero for the case of constant TB on-site elements, in which case $H_{\alpha\mu,\alpha\mu} = \epsilon_{\alpha\mu}^{\text{at}}$. The correction term ΔE^{B} does not (in general) vanish as the Mulliken charge $q_{\alpha\mu}$ is usually not equal to the atomic charge $f_{\alpha\mu}^{\text{at}}$.

Similar as for the choice of an on-site reference the *best* choice of the band sum correction may, unfortunately, depend on the actual tight-binding model. We shall evaluate the above four equally justified approaches in the following section for the concrete example of carbon tight-binding models.

Figure VI.1. Comparison of tight-binding carbon band sums and the DFT cohesive energy. The DFT cohesive energy for the infinite alkyne chain (blue), graphene (red) and diamond (black) are represented by solid lines as function of the nearest neighbor distance d_{NN} . The tight binding band sum differences according to Eq. (VI.13) ($\Delta E = 0$) were obtained using: (1) the conventional carbon TB model of Sec. IV.5.4, (2) the vacuum gauge and (3) the total energy gauge CF-TB models (both derived in Sec. V.3.3) each based on the 4.0 Bohr basis of Sec. IV.4.1. For a comparison the corresponding results obtained with the DFTB model of Ref. 32 are shown in gray.



VI.3. Crystal-field tight-binding band sums

The quantity of interest in atomistic energy calculations usually is not the total energy,^{*} but the cohesive energy E_{coh} of Eq. (III.27)

$$E_{\text{coh}} = E_{\text{tot}} - E_{\text{atoms}} \quad .$$

It is therefore more educative to compare the DFT cohesive energy to the TB band sum, Eq. (III.5), minus the sum of the TB energies of the free atoms, Eq. (III.28), and the band sum correction ΔE

$$E_{\text{band}}^{\text{TB}} - E_{\text{atoms}}^{\text{TB}} - \Delta E = \sum_i f_i \varepsilon_i - \sum_{\alpha\mu} f_{\alpha\mu}^{\text{at}} \varepsilon_{\alpha\mu}^{\text{at}} - \Delta E \quad . \quad (\text{VI.13})$$

In a working tight-binding model the difference between the actual (DFT) cohesive energy and the band sum terms in Eq. (VI.13) should be captured by a pairwise interaction potential or a simple manybody potential.

^{*}If the calculation involved pseudopotentials the total energy is anyway arbitrary and only energy differences are meaningful.

The DFT cohesive energies and the TB band sum differences as of Eq. (VI.13) for $\Delta E = 0$ obtained using three different tight-binding models of this work and the DFTB carbon model of Ref. 32 are depicted in Fig. VI.1. The results for the four tight-binding models are quite different in energy value and trend. The conventional TB model of Sec. IV.5.4 and the total energy gauge CF-TB model yield band sums with minima close to the cohesive energy minima, whereas the band sums of the DFTB model and the vacuum gauge CF-TB model are monotonously rising with increasing nearest neighbor distance. Also note, that the two CF-TB models yield very different band sums and thus there can not exist a common potential to complete the cohesive energy.

Figure VI.2 shows the same band sum differences as Fig. VI.1, but including the four different options of band sum corrections ΔE that were introduced in Sec. VI.2. The correction terms render the band sum difference invariant with respect to the choice of the potential energy zero point. As a consequence the previously very different band sums of the two CF-TB models become very similar upon correction with each of the four options. In any case the CF-TB band sums are, however, shifted to higher energies in such a way that their minima lie at larger nearest neighbor distances than the minima of the DFT cohesive energies. In other words the remaining missing energy contributions, which shall be represented by a (hopefully simple) interatomic potential, have to be attractive rather than repulsive as for the conventional TB models.

From this analysis it is yet uncertain, which of the four band sum corrections would lead to the most transferable cohesive energy parametrization, and the construction of a total energy CF-TB model will therefore be the subject of future studies.

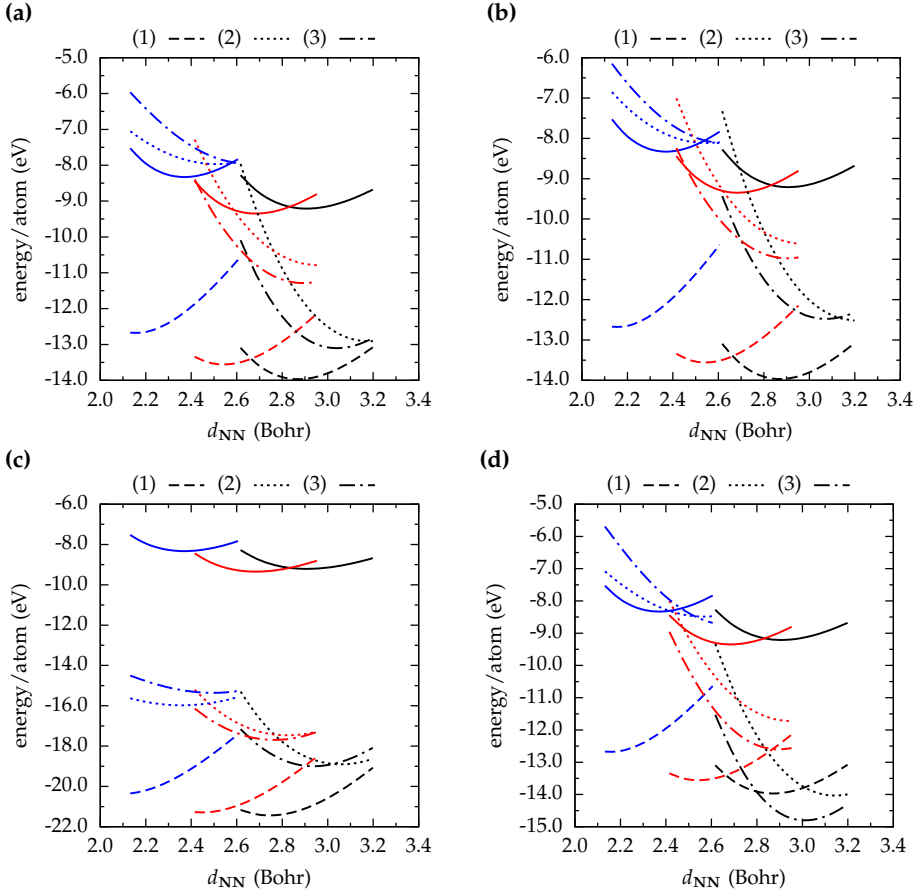


Figure VI.2. Comparison of tight-binding band sums for various correction approaches. The solid curves represent the DFT cohesive energy for the infinite alkyne chain (blue, shortest distances), graphene (red, intermediate distances) and diamond (black, largest distances). The other curves were calculated using (1) the conventional carbon TB model of Sec. IV.5.4, (2) the vacuum gauge CF-TB model of Sec. V.3 and (3) the total energy gauge CF-TB model of Sec. V.3 (in all cases based on the 4.0 Bohr basis set). The figures visualize the effects of the four band sum corrections discussed in the text: (a) ΔE^{TBBM} , (b) ΔE^A , (c) ΔE^B , and (d) ΔE^C .

VII.

Summary and Outlook

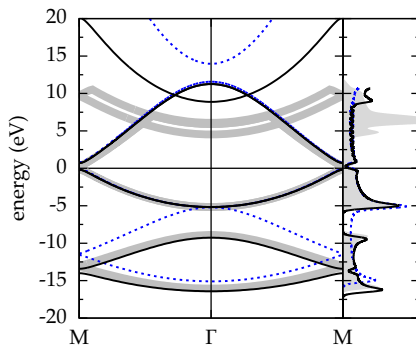
In this thesis we have presented a systematic and universal framework for the derivation of semiempirical electronic structure tight-binding models from density-functional theory (DFT) calculations. A flow-chart of the entire methodology is depicted in Fig. V.5 on page 94 and involves the following steps: first, a set of reference structures for the desired atomic interaction is selected. Second, DFT calculations of these structures for geometries close to the structural equilibrium are performed to obtain the converged Kohn–Sham wave functions and Hamiltonians. Next, minimal basis representations of the wave functions and the Hamilton matrices are determined via a projection of the Kohn–Sham orbitals onto an atomic orbital basis set (Sec. IV.2). Three-center contributions to the Hamilton matrix elements are included on average as the tight-binding method imposes a two-center approximation (Sec. III.2.1 and IV.5). Finally, the tight-binding model is the result of a continuous analytical representation of the overlap matrix elements and the calculated Hamilton matrix elements of all reference structures. For this purpose, we introduced an analytical function in Sec. IV.5.3, which has similar properties as Slater type functions, while its value, the first and the second derivatives vanish exactly at a given cutoff radius.

The reliability of DFT-based tight-binding models crucially depends on the quality of the minimal atomic orbital basis set employed during the projection. In Sec. IV.3 we have therefore developed three different procedures that allow for the optimization of minimal basis sets. The methods were evaluated for carbon and titanium structures in Sec. IV.4, as examples for a covalent main group element and a prototypical transition metal. The optimized basis sets were subsequently used to derive electronic structure

tight-binding models for these two chemical elements in Secs. IV.5.4, V.3 and V.4. We find that a good AO basis set is not the only requirement for well-transferable, structure-independent bond integrals. Instead, the range of the AOs also has a delicate impact on the structure-sensitivity of the Slater–Koster parameters. However, once a suitable range has been determined, optimal basis functions for the given range can be achieved using the new optimization techniques.

An essential conclusion of Chapter IV is the insight that Hamilton matrix elements of different atomic structures may, due to a gauge invariance (Sec. IV.5.2), only be compared, if the same frame of reference for the potential energy had been imposed on them. For the construction of carbon tight-binding models in Sec. IV.5.4 this condition was fulfilled by using the energy of the vacuum as potential zero point. This technique, however, requires to set up surface (slab) models for otherwise periodic reference crystal structures in order to have vacuum regions available. An alternative method to remove the gauge freedom has been developed in Chapter V. It has been shown that a potential reference can be imposed on the Hamilton matrix *a posteriori* by utilizing a crystal-field (CF) parametrization derived from the on-site Hamilton matrix elements of diatomic reference molecules (Sec. V.2.3). Since crystal-field interactions can be straightforwardly calculated using the projection method of Chapter IV, we suggest to include them on a regular basis into DFT-derived tight-binding models and propose a crystal-field tight-binding (CF-TB) extension in Sec. V.2. CF-TB models for carbon and titanium were presented in Secs. V.3 and V.4 and their differences and qualities were discussed in detail in these sections. To give just one example of the effect of crystal-field interactions on the electronic structure, the band structure and the density of states of an infinite alkyne chain is depicted in Fig. VII.1. Both, the conventional tight-binding model as well as the crystal-field tight-binding model correctly describe the π bands, including the band gap due to the Peierls distortion.^{109,110} The crystal-field splitting of the π and the σ bands at the Γ point is, however, only captured by the CF-TB model. As reasoned in Sec. V.3.6, such effects become especially important in low-dimensional geometries and for structures with a low symmetry, which typically arise at finite temperatures, for example, during a molecular dynamics simulation.

Figure VII.1. Band structure and density of states (DOS) of an infinite alkyne chain. The DFT reference is shown as gray lines and regions, the blue dotted curves correspond to the results of the conventional TB model of Sec. IV.5.4, whereas the black solid band structure and DOS were calculated using the CF-TB model of Sec. V.3. The Fermi level was shifted to zero.



Although crystal-field integrals derived from diatomic molecules provide a potential energy reference that may conveniently be imposed to previously calculated Hamilton matrices, the absolute values of the dimer on-site elements are themselves not uniquely defined. As demonstrated for the case of titanium in Sec. V.4.1, the gauge of the dimer on-site Hamilton matrix elements may have a significant impact on the transferability of the resulting tight-binding bond integrals. We have, so far, not undertaken any attempts to remove this gauge invariance entirely. The development of an automatized method for the derivation of ideally gauged on-site integrals that minimizes the structural dependency of the bond integrals might be subject of a future study.

While CF-TB models of the electronic structure are useful tools in combination with classical force fields or for situations where the molecular or crystal geometry is known, it is eventually desirable to have a tight-binding implementation at hand that allows the calculation of cohesive energies and atomic forces. The band energy, i. e. the sum of the one-electron eigenvalues, as calculated with a CF-TB electronic structure model, depends on the potential energy reference that has been imposed upon parametrization of the crystal-field integrals (the bond integral gauge). It is therefore necessary to identify a gauge invariant *bond* energy by removing an appropriate part from the band sum, so that the remaining part of the cohesive energy can be represented by a (hopefully) pairwise atomic interaction potential. The definition of the bond energy is not unique, which introduces an additional degree of freedom. One option is the expression of the tight-binding bond model of Sec. III.3.3. The requirements for a

crystal-field tight-binding total energy functional were elaborated in Chapter VI. More choices for tight-binding total energy expressions have been explored in Sec. VI.2 and their adequacy in conjunction with CF-TB electronic structure models has been estimated in Sec. VI.3. However, the definite construction of total energy CF-TB models will have to be proceeded in a separate work.

A

Additional derivations

A.1. Orbital dependent electron density	123
A.2. Analytic rotation of two-center integrals	125
A.3. Radial Schrödinger equation	126
A.4. Confinement potential	128

A.1. Orbital dependent electron density

We seek an expression for the electron density n , Eq. (II.67), of an N electron Slater determinant wave function, Eq. (II.37),

$$|\Psi^{SD}\rangle = \hat{A}|\phi_1, \dots, \phi_N\rangle \quad . \quad (\text{A.1})$$

The antisymmetrization operator \hat{A} was introduced in Sec. II.2.1 and is given by

$$\hat{A} = \frac{1}{\sqrt{N!}} \sum_p^{\text{permut.}} \text{sgn}(p) \hat{P}_p \quad , \quad (\text{A.2})$$

where \hat{P}_p is the permutation operator associated with the permutation p . It is convenient to define the one-electron density operator as

$$\hat{n}(i) := |\mathbf{r}_i\rangle\langle\mathbf{r}_i| \quad , \quad (\text{A.3})$$

where \mathbf{r}_i is the coordinate vector of the i -th electron, so that we can rewrite the density, Eq. (II.67), without the real space integrals as

$$n(\mathbf{r}) = \sum_i^N \langle \Psi^{SD} | \hat{n}(i) | \Psi^{SD} \rangle \quad . \quad (\text{A.4})$$

We note, that the position representation of the density operator of equation Eq. (A.3) is

$$\hat{n}(\mathbf{r}, i) = \delta(\mathbf{r} - \mathbf{r}_i) \quad , \quad (\text{A.5})$$

so that the expectation value in Eq. (A.4) correctly translates to

$$\sum_{i=1}^N \int d\mathbf{r}_1 \dots \int d\mathbf{r}_N \Psi^*(\mathbf{r}_1, \dots, \mathbf{r}_N) \delta(\mathbf{r} - \mathbf{r}_i) \Psi(\mathbf{r}_1, \dots, \mathbf{r}_N) = n(\mathbf{r}) \quad . \quad (\text{A.6})$$

The individual electrons are indistinguishable, and thus the integration over every electronic coordinate must yield the same result*. We can therefore resolve the sum in Eq. (A.4) and simply express the density as

$$n(\mathbf{r}) = N \langle \Psi^{\text{SD}} | \hat{n}(1) | \Psi^{\text{SD}} \rangle \quad . \quad (\text{A.7})$$

Inserting the expression of the Slater determinant, Eq. (A.1), into Eq. (A.7) yields

$$\begin{aligned} n(\mathbf{r}) &= N \langle \hat{A} \phi_1, \dots, \phi_N | \hat{n}(1) \hat{A} | \phi_1, \dots, \phi_N \rangle \\ &= \frac{1}{(N-1)!} \sum_{p, p'} \text{sgn}(p) \text{sgn}(p') \langle \hat{P}_p \phi_1, \dots, \phi_N | \hat{n}(1) \hat{P}_{p'} | \phi_1, \dots, \phi_N \rangle \quad . \end{aligned} \quad (\text{A.8})$$

Note, that terms with two different permutations $p \neq p'$ under the double sum will always give rise to integrals over two different, orthogonal orbitals $\langle \phi_i | \phi_j \rangle = \delta_{ij}$ and will therefore vanish. Only those $N!$ terms where $p = p'$ remain

$$\begin{aligned} n(\mathbf{r}) &= \frac{1}{(N-1)!} \sum_p \langle \hat{P}_p \phi_1, \dots, \phi_N | \hat{n}(1) \hat{P}_p | \phi_1, \dots, \phi_N \rangle \\ &= \sum_j \langle \phi_j(1) | \hat{n}(1) | \phi_j(1) \rangle \quad , \end{aligned} \quad (\text{A.9})$$

where the square of the permutation parity always gives $\text{sgn}^2(p) = 1$. Finally, evaluating the one-electron integrals of the previous expression in real space we arrive at the orbital dependent expression of the electron density in Eq. (II.84)

$$n(\mathbf{r}) = \sum_j \int \phi_j^*(\mathbf{r}_1) \delta(\mathbf{r} - \mathbf{r}_1) \phi_j(\mathbf{r}_1) d\mathbf{r} = \sum_j |\phi_j(\mathbf{r})|^2 \quad . \quad (\text{A.10})$$

*We have implicitly used this property in Eq. (II.67)

A.2. Analytic rotation of two-center integrals

This section is a brief summary of the analytic rotation formalism for two-center integrals by Podolskiy and Vogl.^{63,64} For a complete discussion and the derivation see the original publications.

Two-center matrix elements of an operator in the basis of atomic orbitals, Eq. (III.16),

$$O_{\ell_1 m_1 \ell_2 m_2}(\mathbf{r}) = \int f_1(|\mathbf{r}'|) Y_{\ell_1 m_1}(\hat{\mathbf{r}}') \hat{o}(\mathbf{r}') f_2(|\mathbf{r}' - \mathbf{r}|) Y_{\ell_2 m_2}(\widehat{\mathbf{r}' - \mathbf{r}}) d\mathbf{r}' \quad (\text{A.11})$$

$Y_{\ell m}$: cubic harmonics (real valued spherical harmonics)

can be analytically expanded in distance dependent reference integrals. For the Cartesian $\hat{\mathbf{z}}$ direction as bond orientation, these reference integrals are given by

$$O_{\ell_1 \ell_2}^m(r) = \int f_1(|\mathbf{r}'|) Y_{\ell_1 m}(\hat{\mathbf{r}}') \hat{o} f_2(|\mathbf{r}' - r \hat{\mathbf{z}}|) Y_{\ell_2 m}(\widehat{\mathbf{r}' - r \hat{\mathbf{z}}}) d\mathbf{r}' \quad (\text{A.12})$$

with $-\min(\ell_1, \ell_2) \leq m \leq \min(\ell_1, \ell_2)$,

and the expansion of the matrix elements is (in spherical coordinates)

$$O_{\ell_1 m_1 \ell_2 m_2}(r, \vartheta, \varphi) = \sum_{m=0}^{\min(m_1, m_2)} c_{\ell_1 \ell_2}^m(\vartheta, \varphi) O_{\ell_1 \ell_2}^m(r) \quad . \quad (\text{A.13})$$

Note that the reference bond integrals, Eq. (A.12), obey the symmetry

$$O_{\ell_1 \ell_2}^m = O_{\ell_1 \ell_2}^{-m} = (-1)^{\ell_1 - \ell_2} O_{\ell_2 \ell_1}^m \quad . \quad (\text{A.14})$$

Podolskiy and Vogl derived the following explicit expression for the expansion coefficients $c_{\ell_1 \ell_2}^m$ of Eq. (A.13):

$$c_{\ell_1 \ell_2}^{m'}(\vartheta, \varphi) = S_{m_1 m'}^{\ell_1}(\vartheta, \varphi) S_{m_2 m'}^{\ell_2}(\vartheta, \varphi) + T_{m_1 m'}^{\ell_1}(\vartheta, \varphi) T_{m_2 m'}^{\ell_2}(\vartheta, \varphi) \quad , \quad (\text{A.15})$$

with the definitions

$$S_{m m'}^{\ell}(\vartheta, \varphi) := A_m(\varphi) \left[(-1)^{m'} d_{|m| m'}^{\ell}(\vartheta) + d_{|m| -m'}^{\ell}(\vartheta) \right] \quad (\text{A.16})$$

$$T_{m m'}^{\ell}(\vartheta, \varphi) := B_m(\varphi) \left[(-1)^{m'} d_{|m| m'}^{\ell}(\vartheta) - d_{|m| -m'}^{\ell}(\vartheta) \right] \quad ,$$

where d is Wigner's (small) d function, and the prefactor A and B are given by

$$A_m(\varphi) := \begin{cases} (-1)^m \sin(-m\varphi) & m < 0 \\ \frac{1}{\sqrt{2}} & m = 0 \\ (-1)^m \cos(m\varphi) & m > 0 \end{cases} \quad (\text{A.17})$$

$$B_m(\varphi) := \begin{cases} (-1)^m \cos(m\varphi) & m < 0 \\ 0 & m = 0 \\ (-1)^m \sin(-m\varphi) & m > 0 \end{cases} . \quad (\text{A.18})$$

Naturally, no expansion/rotation is necessary for $\mathbf{r} = r \hat{\mathbf{z}}$.

An explicit expression of the Wigner d function is, for example, provided in Ref. 64 as

$$d_{mm'}^\ell(\vartheta) = 2^{-\ell} (-1)^{\ell-m'} [(\ell+m)! (\ell-m)! (\ell+m')! (\ell-m')!]^{\frac{1}{2}} \\ \times \sum_{k=k_0}^{k_1} \frac{(-1)^k (1-\cos\vartheta)^{\ell-k-(m+m')/2} (1+\cos\vartheta)^{k+(m+m')/2}}{k! (\ell-m-k)! (\ell-m'-k)! (m+m'+k)!} , \quad (\text{A.19})$$

with the summation boundaries $k_0 = \min(\ell-m, \ell-m')$ and $k_1 = \max(0, -m-m')$.

A.3. Radial Schrödinger equation

Unit conversions can be confusing, especially in conjunction with coordinate transformations. In this section we will therefore deviate from our convention, and we will explicitly write down the reduced Planck constant \hbar and the electron mass m_e (which both are equal to 1 in Hartree atomic units).

For the case of isolated (spherical) atoms, for which $v_{\text{eff}}^{\text{KS}}(\mathbf{r}) = v_{\text{eff}}^{\text{KS}}(r)$, the solutions of the three-dimensional one-electron Schrödinger equation of Eq. (II.82)

$$\left(-\frac{\hbar^2}{2m_e} \nabla^2 + v_{\text{eff}}^{\text{KS}}(r) \right) \psi_n(\mathbf{r}) = \varepsilon_n \psi_n(\mathbf{r}) \quad (\text{A.20})$$

can be more easily determined in spherical coordinates.

The Laplacian ∇^2 in spherical coordinates is given by

$$\begin{aligned}\nabla^2 &= \frac{1}{r^2} \frac{\partial}{\partial r} r^2 \frac{\partial}{\partial r} + \frac{1}{r^2 \sin \vartheta} \frac{\partial}{\partial \vartheta} \sin \vartheta \frac{\partial}{\partial \vartheta} + \frac{1}{r^2 \sin^2 \vartheta} \frac{\partial^2}{\partial \varphi^2} \\ &= \frac{1}{r^2} \left(\frac{\partial}{\partial r} r^2 \frac{\partial}{\partial r} - \frac{1}{\hbar^2} \hat{L}^2 \right) \quad ,\end{aligned}\tag{A.21}$$

where the eigenfunctions of the operator \hat{L}^2 are the spherical harmonics $Y_{\ell m}$, with

$$\hat{L}^2 Y_{\ell m}(\vartheta, \varphi) = \hbar^2 \ell(\ell+1) Y_{\ell m}(\vartheta, \varphi) \quad .\tag{A.22}$$

Inserting the atomic orbital product ansatz, Eq. (III.15),

$$\psi_n(\mathbf{r}) = \psi_{n\ell m}(r, \vartheta, \varphi) = f_{n\ell}(r) \cdot Y_{\ell m}(\vartheta, \varphi)\tag{A.23}$$

and the Laplacian of Eq. (A.21) into the Schrödinger equation, Eq. (A.20), allows to separate the radial and angular degrees of freedom and leaves us with the radial Schrödinger equation, Eq. (IV.17),

$$\left[-\frac{\hbar^2}{2m_e} \left(\frac{1}{r^2} \frac{\partial}{\partial r} r^2 \frac{\partial}{\partial r} - \frac{\ell(\ell+1)}{r^2} \right) + v_{\text{eff}}^{\text{KS}}(r) \right] f_{n\ell}(r) = \varepsilon_n f_{n\ell}(r) \quad .\tag{A.24}$$

The first term in Eq. (A.24) can be rewritten using the identity

$$\frac{1}{r^2} \frac{\partial}{\partial r} r^2 \frac{\partial}{\partial r} g(r) = \frac{1}{r} \frac{\partial^2}{\partial r^2} r g(r)\tag{A.25}$$

to yield the alternative equation

$$-\frac{\hbar^2}{2m_e} \frac{1}{r} \frac{\partial^2}{\partial r^2} r f_{n\ell}(r) + \frac{\hbar^2 \ell(\ell+1)}{2m_e r^2} f_{n\ell}(r) + v_{\text{eff}}^{\text{KS}}(r) f_{n\ell}(r) = \varepsilon_n f_{n\ell}(r) \quad .\tag{A.26}$$

Multiplying both sides of Eq. (A.26) with r and introducing the transformed radial function $u_{n\ell}(r) := r f_{n\ell}(r)$ results in the quasi-1d Schrödinger equation

$$\left(-\frac{\hbar^2}{2m_e} \frac{\partial^2}{\partial r^2} + \tilde{v}_{\text{eff}}(r) \right) u_{n\ell}(r) = \varepsilon_n u_{n\ell}(r) \quad ,\tag{A.27}$$

where a *centrifugal term* is added to the effective potential

$$\tilde{v}_{\text{eff}}(r) = v_{\text{eff}}^{\text{KS}}(r) + \frac{\hbar^2}{2m_e} \frac{\ell(\ell+1)}{r^2} \quad .\tag{A.28}$$

A.4. Confinement potential

We seek to analyze the decay behavior of the solutions of the confined radial Schrödinger equation

$$\left(-\frac{1}{2} \frac{\partial^2}{\partial r^2} + V(r) + v_c(r) \right) f(r) = \varepsilon f(r) \quad (\text{A.29})$$

with $V(r) = \frac{\ell(\ell+1)}{2r^2} + v_{\text{eff}}^{\text{KS}}(r) \quad ,$

where the confinement potential $v_c(r)$ was introduced in Eq. (IV.20) as

$$v_c(r) = \frac{1}{2} \left(\frac{r - r_0}{r_c - r_0} \right)^2 \frac{a(a-1)}{(r_c - r)^2} \quad \text{for } r_0 < r < r_c \quad .$$

Inserting the Taylor expansion of the radial function about the cutoff radius r_c

$$f(r) = \sum_{n=0}^{\infty} c_n (r_c - r)^n \quad (\text{A.30})$$

and its second derivative

$$\begin{aligned} \frac{\partial^2}{\partial r^2} f(r) &= \sum_{n=2}^{\infty} n(n-1) c_n (r_c - r)^{n-2} \\ &= \sum_{n=0}^{\infty} (n+2)(n+1) c_{n+2} (r_c - r)^n \end{aligned} \quad (\text{A.31})$$

into the Schrödinger equation, Eq. (A.29), yields the following condition for the solution:

$$\begin{aligned} &\sum_{n=0}^{\infty} -\frac{1}{2} (n+2)(n+1) c_{n+2} (r_c - r)^n + \sum_{n=0}^{\infty} V(r) c_n (r_c - r)^n \\ &+ \sum_{n=-2}^{\infty} \frac{1}{2} \left(\frac{r - r_0}{r_c - r_0} \right)^2 a(a-1) c_{n+2} (r_c - r)^n - \sum_{n=0}^{\infty} \varepsilon c_n (r_c - r)^n = 0 \quad . \end{aligned} \quad (\text{A.32})$$

Sorting terms by order in $(r_c - r)$ we arrive at the condition

$$\frac{1}{2} \left(\frac{r - r_0}{r_c - r_0} \right)^2 a(a-1) \left(\frac{c_0}{(r_c - r)^2} + \frac{c_1}{r_c - r} \right) = 0 \quad (\text{A.33})$$

for orders (-2) and (-1) and

$$\begin{aligned} \left(V(r) - \varepsilon \right) c_n + \frac{1}{2} \left[-(n+2)(n+1) \right. \\ \left. + \left(\frac{r-r_0}{r_c-r_0} \right)^2 a(a-1) \right] c_{n+2} = 0 \end{aligned} \quad (\text{A.34})$$

for all higher orders. From Eq. (A.33) it is evident that

$$c_0 = c_1 = 0 \quad \text{for } a > 1, \quad (\text{A.35})$$

and for $r \rightarrow r_c$ the second condition, Eq. (A.34), implies

$$c_{n-2} = 0 \quad \Rightarrow \quad c_n = 0 \quad \vee \quad a = n. \quad (\text{A.36})$$

Together, Eqs. (A.35) and (A.36) show that for $a = 2, 3, 4, \dots$ all terms $(r_c - r)^n$ with $n < a$ in the Taylor expansion, Eq. (A.30), vanish, and thus the radial function $f(r)$ decays as $(r_c - r)^a$ at the cutoff radius.

B.

Tight-binding parameters

Tables

B.1. Carbon atomic eigenvalues	132
B.2. Carbon-carbon overlap matrix parameters	132
B.3. Carbon-carbon Hamilton matrix parameters (vacuum reference) . . .	133
B.4. Carbon-carbon crystal-field parameters	134
B.5. Carbon-carbon Hamilton matrix parameters (on-site gauge)	135
B.6. Titanium atomic eigenvalues	136
B.7. Titanium-titanium overlap matrix parameters	136
B.8. Titanium-titanium crystal-field parameters (s level gauge)	137
B.9. Titanium-titanium Hamilton matrix parameters (s level gauge) . . .	138
B.10. Titanium-titanium Hamilton matrix parameters (vacuum level gauge)	138
B.11. Titanium-titanium crystal-field parameters (vacuum level gauge) . .	139

Cutoff radii are given in Bohr units. The bond and crystal-field integrals are parametrized in Rydberg atomic units. See Sec. [IV.5.3](#) for the functional form of the fit.

The derivation of the conventional vacuum gauge carbon tight-binding model is discussed in Sec. [IV.5.4](#). The derivation of the carbon CF-TB model can be found in Sec. [V.3](#). The titanium CF-TB models are discussed in Sec. [V.4](#).

Table B.1. Asymptotic atomic eigenvalues of carbon (Rydberg units) for the different basis sets of Table IV.2. The values listed here are the asymptotic dimer on-site levels.

level	ϵ , 4.0 Bohr (Ry)	ϵ , 5.0 Bohr (Ry)	ϵ , 6.0 Bohr (Ry)
2s	-0.89317700	-0.96566125	-0.98912960
2p	-0.26938440	-0.34745325	-0.37639880

Table B.2. Carbon-carbon overlap matrix parameters for the different basis sets of Table IV.2.

basis	bond	r^c	α	a_0	a_1
4.0	$ss\sigma$	5.5	1.002255	1.240952	3.350085
	$sp\sigma$	5.5	$5.779726 \cdot 10^{-1}$	$-1.050657 \cdot 10^1$	-6.686082
	$pp\sigma$	5.5	$3.501334 \cdot 10^{-2}$	$-6.392817 \cdot 10^5$	$-7.868920 \cdot 10^3$
	$pp\pi$	5.5	1.367029	$-3.563430 \cdot 10^{-2}$	3.554727
5.0	$ss\sigma$	6.5	1.094875	$-2.888173 \cdot 10^{-1}$	3.481373
	$sp\sigma$	6.5	$6.803300 \cdot 10^{-1}$	-2.054825	-4.180914
	$pp\sigma$	6.5	$9.060093 \cdot 10^{-2}$	$-7.270502 \cdot 10^3$	$-2.602056 \cdot 10^2$
	$pp\pi$	6.5	1.173671	$1.270293 \cdot 10^{-1}$	2.655345
6.0	$ss\sigma$	7.5	1.103087	$-4.858043 \cdot 10^{-1}$	3.161910
	$sp\sigma$	7.8	$5.622475 \cdot 10^{-5}$	$6.139577 \cdot 10^7$	$1.884919 \cdot 10^6$
	$pp\sigma$	7.5	$7.796503 \cdot 10^{-2}$	$-6.041538 \cdot 10^3$	$-1.855820 \cdot 10^2$
	$pp\pi$	7.5	$9.574197 \cdot 10^{-1}$	1.011025	1.432654

Table B.3. Carbon–carbon Hamilton matrix parameters for the different basis sets of Table IV.2. The vacuum level was employed as zero point of the potential energy. The on-site elements are set to the atomic eigenvalues.

basis	bond	r^c	α	a_0	a_1
4.0	$ss\sigma$	7.0	1.532366	$2.890974 \cdot 10^1$	$-2.398253 \cdot 10^1$
	$sp\sigma$	7.0	1.180339	$-1.392311 \cdot 10^1$	$1.265912 \cdot 10^1$
	$pp\sigma$	7.0	$6.375224 \cdot 10^{-1}$	$8.323779 \cdot 10^{-1}$	6.784512
	$pp\pi$	7.0	1.834896	$2.672219 \cdot 10^1$	$-2.265520 \cdot 10^1$
5.0	$ss\sigma$	7.0	1.248976	$1.027604 \cdot 10^1$	$-1.212599 \cdot 10^1$
	$sp\sigma$	7.0	$2.263337 \cdot 10^{-1}$	$9.611706 \cdot 10^1$	$1.079882 \cdot 10^1$
	$pp\sigma$	7.0	$2.198934 \cdot 10^{-2}$	$1.344657 \cdot 10^6$	$1.027263 \cdot 10^4$
	$pp\pi$	7.0	1.831334	$4.116994 \cdot 10^1$	$-3.103417 \cdot 10^1$
6.0	$ss\sigma$	9.0	1.308698	$1.157469 \cdot 10^1$	$-1.252540 \cdot 10^1$
	$sp\sigma$	9.0	$8.357621 \cdot 10^{-1}$	-1.497045	3.961358
	$pp\sigma$	9.0	$3.625365 \cdot 10^{-1}$	9.545616	4.555643
	$pp\pi$	9.0	1.775190	$4.187611 \cdot 10^1$	$-3.085336 \cdot 10^1$

Table B.4. Carbon-carbon crystal-field parameters for the different basis sets of Table IV.2. The asymptotic values are the atomic eigenvalues.

basis	bond	r^c	α	a_0	a_1			
4.0	<i>ssσ</i>	5.0	1.941196	-11.402640	29.384335	-23.835826	5.579434	
	<i>spσ</i>	5.0	0.818689	-16.793382	-27.427964	1.532145	-1.810448	
	<i>ppσ</i>	5.0	1.436243	5.177040	2.385771	-7.989710	2.232160	
	<i>ppπ</i>	5.0	0.862586	-1.323592	4.593953	-0.503886	0.229620	
5.0	<i>ssσ</i>	5.5	2.288241	-20.033413	43.793830	-30.610318	4.517683	
	<i>spσ</i>	5.5	0.771053	-13.174289	-22.200573	1.748827	-1.396152	
	<i>ppσ</i>	5.5	0.817502	-2.371913	-19.751405	3.065810	-1.169246	
	<i>ppπ</i>	5.5	0.723603	0.604254	4.984395	-0.515742	0.253756	
6.0	<i>ssσ</i>	6.0	2.542704	-22.681132	44.855680	-25.747600	0.494931	
	<i>spσ</i>	6.0	1.761719	3.877992	-0.367261	-4.657746	-0.048099	
	<i>ppσ</i>	6.0	0.769398	-8.931158	-22.389196	2.444414	-1.376028	
	<i>ppπ</i>	6.0	0.957978	-3.294865	1.757472	-0.541900	0.005503	

Table B.5. Carbon-carbon CF-TB Hamilton matrix parameters for the different basis sets of Table IV.2. The vacuum level dimer on-site elements were used to gauge the bond integrals.

basis	bond	r^c	α	a_0	a_1
4.0	$ss\sigma$	6.5	1.298103	$1.076784 \cdot 10^1$	$-1.303527 \cdot 10^1$
	$sp\sigma$	7.0	1.085945	-8.517249	9.683750
	$pp\sigma$	6.5	$1.394109 \cdot 10^{-1}$	$1.409809 \cdot 10^3$	$8.502823 \cdot 10^1$
	$pp\pi$	7.0	$4.089812 \cdot 10^{-1}$	1.271455	2.309498
5.0	$ss\sigma$	7.0	$1.903143 \cdot 10^{-2}$	$4.015539 \cdot 10^5$	$2.693245 \cdot 10^3$
	$sp\sigma$	7.6	$7.187493 \cdot 10^{-1}$	$8.904034 \cdot 10^{-1}$	4.026769
	$pp\sigma$	7.4	$3.348607 \cdot 10^{-2}$	$1.836302 \cdot 10^5$	$2.191033 \cdot 10^3$
	$pp\pi$	7.0	$5.552709 \cdot 10^{-1}$	-3.064865	$8.800754 \cdot 10^{-1}$
6.0	$ss\sigma$	7.5	1.043576	$9.714240 \cdot 10^{-1}$	-5.818512
	$sp\sigma$	8.0	$2.431984 \cdot 10^{-1}$	$1.844986 \cdot 10^1$	$-1.814326 \cdot 10^{-1}$
	$pp\sigma$	8.5	$3.859269 \cdot 10^{-1}$	$3.866213 \cdot 10^1$	$1.082056 \cdot 10^1$
	$pp\pi$	7.0	$3.864343 \cdot 10^{-1}$	$-3.469823 \cdot 10^1$	-5.562221
					-1.281225

Table B.6. Asymptotic atomic eigenvalues of titanium (Rydberg units) for the 5.5 Bohr basis set of Table IV.4. The values listed here are the asymptotic dimer on-site levels.

level	ε (Ry)
$3d$	-0.19724237
$4s$	-0.12547622
$4p$	0.22769111

Table B.7. Titanium–titanium overlap matrix parameters for the 5.5 Bohr basis of Table IV.4.

bond	r^c	α	a_0	a_1
$ss\sigma$	9.0	$2.794948 \cdot 10^{-1}$	$2.171521 \cdot 10^{+1}$	4.551077
$sp\sigma$	9.0	$3.721474 \cdot 10^{-2}$	$-6.635016 \cdot 10^{+4}$	$-9.024315 \cdot 10^{+2}$
$sd\sigma$	9.0	$3.890365 \cdot 10^{-1}$	4.503248	6.305605
$pp\sigma$	9.3	$3.400831 \cdot 10^{-2}$	$-1.691743 \cdot 10^{+5}$	$-2.099935 \cdot 10^{+3}$
$pp\pi$	9.0	$8.632969 \cdot 10^{-1}$	-8.241099	6.070320
$pd\sigma$	8.8	$4.405740 \cdot 10^{-2}$	$6.333488 \cdot 10^{+4}$	$1.044869 \cdot 10^{+3}$
$pd\pi$	9.0	1.104278	$4.628924 \cdot 10^{+1}$	$-1.771658 \cdot 10^{+1}$
$dd\sigma$	8.8	$2.926792 \cdot 10^{-1}$	$2.670904 \cdot 10^{+1}$	8.455301
$dd\pi$	9.0	1.256986	$7.827095 \cdot 10^{+1}$	$-2.824005 \cdot 10^{+1}$
$dd\delta$	9.0	1.769584	$-1.019427 \cdot 10^{+2}$	$4.087898 \cdot 10^{+1}$

Table B.8. Titanium–titanium crystal-field parameters for the constant s level gauge (Sec. V.4) calculated using the 5.5 Bohr basis of Table IV.4. The asymptotic values are the atomic eigenvalues.

bond	r^c	α	a_0	a_1	a_2	a_3
$ss\sigma$	7.0	0.0	0.0			
$sp\sigma$	7.0	0.72895844	-0.09663143	1.92912601	5.70750207	-0.19023690
$sd\sigma$	7.0	0.26176485	-2.14534567	1.50600295 · 10 ⁺¹	2.29294275	0.56149437
$pp\sigma$	7.0	5.39617705	1.31689733 · 10 ⁺⁵	4.52077989 · 10 ⁺⁵	1.36417011 · 10 ⁺⁶	2.95210493 · 10 ⁺⁶
$pp\pi$	7.0	0.30732532	2.61969511	-5.39511904	-0.17039448	-0.31041839
$pd\sigma$	7.0	0.63151429	-1.79204664 · 10 ⁺¹	-4.41653848 · 10 ⁺²	5.95994934 · 10 ⁺¹	-1.84927245 · 10 ⁺¹
$pd\pi$	7.0	2.25253384	-6.29218702 · 10 ⁺¹	-1.58639819 · 10 ⁺²	-2.39819127 · 10 ⁺²	8.34125762 · 10 ⁺¹
$dd\sigma$	7.0	0.75350451	1.06904530 · 10 ⁺¹	1.12513442 · 10 ⁺¹	-1.03928230	0.94298070
$dd\pi$	7.0	0.26545603	2.10158731	-3.39453019	-1.15964286	-0.20419978
$dd\delta$	7.0	0.28356260	1.19181292	0.63576460	-0.99244482	-0.11333145

Table B.9. Titanium–titanium Hamilton matrix parameters for the constant s level gauge (Sec. V.4) calculated using the 5.5 Bohr basis of Table IV.4.

bond	r^c	α	a_0	a_1
$ss\sigma$	10.0	$2.869123 \cdot 10^{-2}$	$-4.965661 \cdot 10^{+4}$	$-5.150134 \cdot 10^{+2}$
$sp\sigma$	10.0	$2.156450 \cdot 10^{-2}$	$3.376002 \cdot 10^{+5}$	$2.585704 \cdot 10^{+3}$
$sd\sigma$	10.0	$5.978868 \cdot 10^{-2}$	$-3.068560 \cdot 10^{+3}$	$-7.348511 \cdot 10^{+1}$
$pp\sigma$	11.0	$1.679339 \cdot 10^{-2}$	$7.452474 \cdot 10^{+5}$	$4.407254 \cdot 10^{+3}$
$pp\pi$	10.0	$2.282773 \cdot 10^{-2}$	$-2.481779 \cdot 10^{+4}$	$-2.001175 \cdot 10^{+2}$
$pd\sigma$	10.5	$2.212126 \cdot 10^{-2}$	$-1.642983 \cdot 10^{+5}$	$-1.297864 \cdot 10^{+3}$
$pd\pi$	10.0	$4.880766 \cdot 10^{-1}$	$-7.519091 \cdot 10^{-2}$	$7.625051 \cdot 10^{-1}$
$dd\sigma$	11.0	$4.161644 \cdot 10^{-2}$	$-1.928837 \cdot 10^{+3}$	$-3.025027 \cdot 10^{+1}$
$dd\pi$	10.0	$9.794532 \cdot 10^{-1}$	$-1.148878 \cdot 10^{+1}$	4.736235
$dd\delta$	10.0	1.280980	-9.032470	$-1.409751 \cdot 10^{-4}$

Table B.10. Titanium–titanium Hamilton matrix parameters for the vacuum level gauge (Sec. V.4) calculated using the 5.5 Bohr basis of Table IV.4.

bond	r^c	α	a_0	a_1
$ss\sigma$	10.0	$3.369936 \cdot 10^{-2}$	$-8.017207 \cdot 10^{+3}$	$-9.627212 \cdot 10^{+1}$
$sp\sigma$	10.0	$2.722366 \cdot 10^{-2}$	$1.149647 \cdot 10^{+5}$	$1.128442 \cdot 10^{+3}$
$sd\sigma$	10.0	$5.289592 \cdot 10^{-2}$	$-2.629362 \cdot 10^{+3}$	$-5.378035 \cdot 10^{+1}$
$pp\sigma$	10.5	$2.121426 \cdot 10^{-2}$	$3.971683 \cdot 10^{+5}$	$2.999889 \cdot 10^{+3}$
$pp\pi$	10.0	$1.739778 \cdot 10^{-1}$	-3.446840	$-1.859243 \cdot 10^{-5}$
$pd\sigma$	10.0	$3.167418 \cdot 10^{-2}$	$-5.753656 \cdot 10^{+4}$	$-6.674643 \cdot 10^{+2}$
$pd\pi$	10.0	$5.986011 \cdot 10^{-1}$	2.860792	$-1.699955 \cdot 10^{-6}$
$dd\sigma$	10.0	$3.071750 \cdot 10^{-2}$	$-3.303891 \cdot 10^{+3}$	$-3.487611 \cdot 10^{+1}$
$dd\pi$	10.0	$9.100875 \cdot 10^{-1}$	9.603299	$2.189680 \cdot 10^{-4}$
$dd\delta$	10.0	1.303322	$-1.213264 \cdot 10^{+1}$	$1.006250 \cdot 10^{-3}$

Table B.11. Titanium–titanium crystal-field parameters for the vacuum level gauge (Sec. V.4) calculated using the 5.5 Bohr basis of Table IV.4. The asymptotic values are the atomic eigenvalues.

bond	r^c	α	a_0	a_1	a_2	a_3
$ss\sigma$	7.0	0.63262355	-7.68657619	$7.014301024 \cdot 10^{+1}$	11.43488123	2.97612226
$sp\sigma$	7.0	0.72857338	0.39888919	1.42495050	3.31224929	-0.05645666
$sd\sigma$	7.0	0.33308320	-1.31579448	-0.10693290	0.41210473	0.21029743
$pp\sigma$	7.0	0.30101456	-1.86366778 · 10^{+1}	$8.43141241 \cdot 10^{+1}$	-2.25982758	3.05534375
$pp\pi$	7.0	0.72377131	8.10753717	9.61711985	-1.23651293	0.79705489
$pd\sigma$	7.0	0.61374126	0.60075767	1.44610196	3.21379618	-0.31868243
$pd\pi$	7.0	0.73010232	-6.04074207 · 10^{+1}	-7.27464004 · 10^{+1}	8.54608913	-5.57382626
$dd\sigma$	7.0	0.78721441	1.52598476	0.62153698	-2.01465315	0.10525566
$dd\pi$	7.0	0.69459467	7.17044083	10.60164981	-0.55677876	0.68952108
$dd\delta$	7.0	0.67855218	3.36149213	5.90308733	-0.11329383	0.33047242

Bibliography

- [1] E. Schrödinger, “[Quantisierung als Eigenwertproblem.](#)” *Ann. Phys.* **386** (1926) 109–139.
- [2] R. G. Parr and W. Yang, “[Density-Functional Theory of Atoms and Molecules.](#)” Oxford University Press, 1989.
- [3] G. C. Abell, “[Empirical chemical pseudopotential theory of molecular and metallic bonding.](#)” *Phys. Rev. B* **31** (1985) 6184–6196.
- [4] J. Tersoff, “[New empirical approach for the structure and energy of covalent systems.](#)” *Phys. Rev. B* **37** (1988) 6991–7000.
- [5] D. W. Brenner, “[Empirical potential for hydrocarbons for use in simulating the chemical vapor deposition of diamond films.](#)” *Phys. Rev. B* **42** (1990) 9458.
- [6] D. G. Pettifor and I. I. Oleinik, “[Analytic bond-order potentials beyond Tersoff-Brenner. I. Theory.](#)” *Phys. Rev. B* **59** (1999) 8487–8499.
- [7] M. W. Finnis and J. E. Sinclair, “[A simple empirical N-body potential for transition metals.](#)” *Phil. Mag. A* **50** (1984) 45–55.
- [8] M. S. Daw and M. I. Baskes, “[Embedded-atom method: Derivation and application to impurities, surfaces, and other defects in metals.](#)” *Phys. Rev. B* **29** (1984) 6443–6453.
- [9] F. H. Stillinger and T. A. Weber, “[Computer simulation of local order in condensed phases of silicon.](#)” *Phys. Rev. B* **31** (1985) 5262.
- [10] W. R. P. Scott, P. H. Hünenberger, I. G. Tironi, A. E. Mark, S. R. Billeter, J. Fennen, A. E. Torda, T. Huber, P. Krüger, and W. F. van Gunsteren, “[The GROMOS Biomolecular Simulation Program Package.](#)” *J. Phys. Chem. A* **103** (1999) 3596–3607.
- [11] M. T. Nelson, W. Humphrey, A. Gursoy, A. Dalke, L. V. Kalé, R. D. Skeel, and K. Schulten, “[NAMD: a Parallel, Object-Oriented Molecular Dynamics Program.](#)” *Int. J. High Perform. C.* **10** (1996) 251–268.
- [12] W. D. Cornell, P. Cieplak, C. I. Bayly, I. R. Gould, K. M. Merz, D. M. Ferguson, D. C. Spellmeyer, T. Fox, J. W. Caldwell, and P. A. Kollman, “[A Second Generation Force Field for the Simulation of Proteins, Nucleic Acids, and Organic Molecules.](#)” *J. Am. Chem. Soc.* **117** (1995) 5179–5197.

- [13] E. Hückel, "Quantentheoretische Beiträge zum Benzolproblem." *Z. Phys. A-Hadron. Nucl.* **70** (1931) 204–286.
- [14] J. C. Slater and G. F. Koster, "Simplified LCAO Method for the Periodic Potential Problem." *Phys. Rev.* **94** (1954) 1498–1524.
- [15] R. Hoffmann, "An Extended Hückel Theory. I. Hydrocarbons." *J. Chem. Phys.* **39** (1963) 1397–1412.
- [16] R. C. Bingham, M. J. S. Dewar, and D. H. Lo, "Ground states of molecules. XXV. MINDO/3. Improved version of the MINDO semiempirical SCF-MO method." *J. Am. Chem. Soc.* **97** (1975) 1285–1293.
- [17] M. J. S. Dewar and W. Thiel, "Ground states of molecules. 38. The MNDO method. Approximations and parameters." *J. Am. Chem. Soc.* **99** (1977) 4899–4907.
- [18] M. J. S. Dewar, E. G. Zoebisch, E. F. Healy, and J. J. P. Stewart, "AM1: a new general purpose quantum mechanical molecular model." *J. Am. Chem. Soc.* **107** (1985) 3902–3909.
- [19] M. Finnis, "Interatomic Forces in Condensed Matter." Oxford University Press, 2010.
- [20] C. M. Goringe, D. R. Bowler, and E. Hernández, "Tight-binding modelling of materials." *Rep. Prog. Phys.* **60** (1997) 1447.
- [21] D. A. Papaconstantopoulos and M. J. Mehl, "The Slater–Koster tight-binding method: a computationally efficient and accurate approach." *J. Phys.: Condens. Matter* **15** (2003) R413.
- [22] H. Amara, C. Bichara, and F. Ducastelle, "Formation of carbon nanostructures on nickel surfaces: A tight-binding grand canonical Monte Carlo study." *Phys. Rev. B* **73** (2006) 113404.
- [23] J. J. P. Stewart, "Optimization of parameters for semiempirical methods I. Method." *J. Comput. Chem.* **10** (1989) 209–220.
- [24] M. F. Montemor, M. G. S. Ferreira, N. E. Hakiki, and M. D. C. Belo, "Chemical composition and electronic structure of the oxide films formed on 316L stainless steel and nickel based alloys in high temperature aqueous environments." *Corros. Sci.* **42** (2000) 1635–1650.
- [25] M. H. Abd Elhamid, Y. M. Mikhail, G. V. Dadheech, F. Zhong, R. H. Blunk, and D. J. Lisi, "Corrosion resistant metal composite for electrochemical devices and methods of producing the same." Patent US 7,972,449 B2. 2011.
- [26] J. Harris, "Simplified method for calculating the energy of weakly interacting fragments." *Phys. Rev. B* **31** (1985) 1770–1779.

- [27] W. M. C. Foulkes, "Interatomic forces in solids." PhD thesis. University of Cambridge, 1987.
- [28] W. M. C. Foulkes and R. Haydock, "Tight-binding models and density-functional theory." *Phys. Rev. B* **39** (1989) 12520–12536.
- [29] A. Horsfield, A. Bratkovsky, D. Pettifor, and M. Aoki, "Bond order potential and cluster recursion for the description of chemical bonds: Efficient real-space methods for tight-binding molecular dynamics." *Phys. Rev. B* **53** (1996) 1656–1665.
- [30] M. Finnis, "Bond-order potentials through the ages." *Prog. Mater. Sci.* **52** (2007) 133–153.
- [31] A. Horsfield and A. Bratkovsky, "Ab initio tight binding." *J. Phys.: Condens. Matter* **12** (2000) R1–R24.
- [32] D. Porezag, T. Frauenheim, T. Köhler, G. Seifert, and R. Kaschner, "Construction of tight-binding-like potentials on the basis of density-functional theory: Application to carbon." *Phys. Rev. B* **51** (1995) 12947–12957.
- [33] M. Elstner, D. Porezag, G. Jungnickel, J. Elsner, M. Haugk, T. Frauenheim, S. Suhai, and G. Seifert, "Self-consistent-charge density-functional tight-binding method for simulations of complex materials properties." *Phys. Rev. B* **58** (1998) 7260–7268.
- [34] P. Koskinen and V. Mäkinen, "Density-functional tight-binding for beginners." *Comput. Mater. Sci.* **47** (2009) 237–253.
- [35] G. Seifert and J.-O. Joswig, "Density-functional tight binding – an approximate density-functional theory method." *Wiley Interdiscip. Rev. Comput. Mol. Sci.* **2** (2012) 456–465.
- [36] O. K. Andersen and O. Jepsen, "Explicit, First-Principles Tight-Binding Theory." *Phys. Rev. Lett.* **53** (1984) 2571.
- [37] D. Nguyen-Manh, D. G. Pettifor, and V. Vitek, "Analytic Environment-Dependent Tight-Binding Bond Integrals: Application to MoSi₂." *Phys. Rev. Lett.* **85** (2000) 4136.
- [38] M. Mrovec, D. Nguyen-Manh, D. G. Pettifor, and V. Vitek, "Bond-order potential for molybdenum: Application to dislocation behavior." *Phys. Rev. B* **69** (2004) 094115.
- [39] M. Mrovec, R. Gröger, A. G. Bailey, D. Nguyen-Manh, C. Elsässer, and V. Vitek, "Bond-order potential for simulations of extended defects in tungsten." *Phys. Rev. B* **75** (2007) 104119.
- [40] W. C. Lu, C. Z. Wang, M. W. Schmidt, L. Bytautas, K. M. Ho, and K. Ruedenberg, "Molecule intrinsic minimal basis sets. I. Exact resolution of ab initio optimized molecular orbitals in terms of deformed atomic minimal-basis orbitals." *J. Chem. Phys.* **120** (2004) 2629.

- [41] W. C. Lu, C. Z. Wang, T. L. Chan, K. Ruedenberg, and K. M. Ho, "Representation of electronic structures in crystals in terms of highly localized quasiautomatic minimal basis orbitals." *Phys. Rev. B* **70** (2004) 041101.
- [42] W. C. Lu, C. Z. Wang, K. Ruedenberg, and K. M. Ho, "Transferability of the Slater-Koster tight-binding scheme from an environment-dependent minimal-basis perspective." *Phys. Rev. B* **72** (2005) 205123.
- [43] T. Chan, Y. X. Yao, C. Z. Wang, W. C. Lu, J. Li, X. F. Qian, S. Yip, and K. M. Ho, "Highly localized quasiautomatic minimal basis orbitals for Mo from *ab initio* calculations." *Phys. Rev. B* **76** (2007) 205119.
- [44] X. Qian, J. Li, L. Qi, C.-Z. Wang, T.-L. Chan, Y.-X. Yao, K.-M. Ho, and S. Yip, "Quasiautomatic orbitals for *ab initio* tight-binding analysis." *Phys. Rev. B* **78** (2008) 245112.
- [45] N. Marzari and D. Vanderbilt, "Maximally localized generalized Wannier functions for composite energy bands." *Phys. Rev. B* **56** (1997) 12847–12865.
- [46] I. Souza, N. Marzari, and D. Vanderbilt, "Maximally localized Wannier functions for entangled energy bands." *Phys. Rev. B* **65** (2001) 035109.
- [47] N. Marzari, A. A. Mostofi, J. R. Yates, I. Souza, and D. Vanderbilt, "Maximally localized Wannier functions: Theory and applications." *ArXiv e-prints* (2011).
- [48] B. N. Figgis and M. A. Hitchman, "Ligand field theory and its applications." Vol. 67. Wiley, 2000 02.
- [49] H. Bethe, "Termaufspaltung in Kristallen." *Ann. Phys.* **395** (1929) 133–208.
- [50] J. H. V. Vleck, "Theory of the Variations in Paramagnetic Anisotropy Among Different Salts of the Iron Group." *Phys. Rev.* **41** (1932) 208–215.
- [51] A. Holleman and N. Wiberg, "Inorganic Chemistry." Ed. by B. J. Aylett. Academic Press, 2001.
- [52] D. J. Chadi, "Atomic Simulation of Materials Beyond Pair Potentials." In: ed. by V. Vitek and D. J. Srolovitz. Plenum, New York, 1988. Chap. Transferability of tight-binding matrix elements 309–315.
- [53] A. K. McMahan and J. E. Klepeis, "Direct calculation of Slater-Koster parameters: Fourfold-coordinated silicon/boron phases." *Phys. Rev. B* **56** (1997) 12250–12262.
- [54] M. Born and R. Oppenheimer, "Zur Quantentheorie der Molekeln." *Ann. Phys.* **389** (1927) 457–484.
- [55] F. Pilar, "Elementary Quantum Chemistry." Dover Publications, 2001.

- [56] A. Szabó and N. Ostlund, [“Modern Quantum Chemistry: Introduction to Advanced Electronic Structure Theory.”](#) Dover Publications, 1996.
- [57] F. Jensen, [“Introduction to Computational Chemistry.”](#) John Wiley & Sons, 2007.
- [58] P. Hohenberg and W. Kohn, [“Inhomogeneous Electron Gas.”](#) *Phys. Rev.* **136** (1964) B864–B871.
- [59] W. Kohn and L. J. Sham, [“Self-Consistent Equations Including Exchange and Correlation Effects.”](#) *Phys. Rev.* **140** (1965) A1133–A1138.
- [60] R. Drautz and D. G. Pettifor, [“Valence-dependent analytic bond-order potential for magnetic transition metals.”](#) *Phys. Rev. B* **84** (2011) 214114.
- [61] I. J. Robertson and B. Farid, [“Does the Harris energy functional possess a local maximum at the ground-state density?”](#) *Phys. Rev. Lett.* **66** (1991) 3265–3268.
- [62] B. Farid, V. Heine, G. E. Engel, and I. J. Robertson, [“Extremal properties of the Harris-Foulkes functional and an improved screening calculation for the electron gas.”](#) *Phys. Rev. B* **48** (1993) 11602–11621.
- [63] A. V. Podolskiy and P. Vogl, [“Compact expression for the angular dependence of tight-binding Hamiltonian matrix elements.”](#) *Phys. Rev. B* **69** (2004) 233101.
- [64] A. M. Elena and M. Meister, [“Automatic generation of matrix element derivatives for tight binding models.”](#) *Phys. Rev. B* **72** (2005) 165107.
- [65] P.-O. Löwdin, [“On the Non-Orthogonality Problem Connected with the Use of Atomic Wave Functions in the Theory of Molecules and Crystals.”](#) *J. Chem. Phys.* **18** (1950) 365.
- [66] D. J. Chadi, [“Energy-Minimization Approach to the Atomic Geometry of Semiconductor Surfaces.”](#) *Phys. Rev. Lett.* **41** (1978) 1062–1065.
- [67] D. G. Pettifor, [“Individual orbital contributions to the SCF virial in homonuclear diatomic molecules.”](#) *J. Chem. Phys.* **69** (1978) 2930–2931.
- [68] A. R. Mackintosh and O. K. Andersen, [“Electrons at the Fermi surface.”](#) In: ed. by M. Springford. Cambridge University Press, 1980. Chap. The electronic structure of transition metals 149–224.
- [69] D. G. Pettifor, [“The structures of binary compounds. I. Phenomenological structure maps.”](#) *J. Phys. C: Solid State* **19** (1986) 285.
- [70] D. Pettifor, [“Bonding and Structure of Molecules and Solids.”](#) Clarendon Press, 1995.
- [71] A. P. Sutton, M. W. Finnis, D. G. Pettifor, and Y. Ohta, [“The tight-binding bond model.”](#) *J. Phys. C: Solid State* **21** (1988) 35.

- [72] R. S. Mulliken, "Electronic Population Analysis on LCAO[Single Bond]MO Molecular Wave Functions. I." *J. Chem. Phys.* **23** (1955) 1833–1840.
- [73] D. G. Pettifor and R. Podloucky, "The structures of binary compounds. II. Theory of the *pd*-bonded AB compounds." *J. Phys. C: Solid State* **19** (1986) 315–330.
- [74] M. Elstner, "SCC-DFTB: What Is the Proper Degree of Self-Consistency." *J. Phys. Chem. A* **111** (2007) 5614–5621.
- [75] R. G. Parr and R. G. Pearson, "Absolute hardness: companion parameter to absolute electronegativity." *J. Am. Chem. Soc.* **105** (1983) 7512–7516.
- [76] P. P. Ewald, "Die Berechnung optischer und elektrostatischer Gitterpotentiale." *Ann. Phys.* **369** (1921) 253–287.
- [77] R. E. Cohen, M. J. Mehl, and D. A. Papaconstantopoulos, "Tight-binding total-energy method for transition and noble metals." *Phys. Rev. B* **50** (1994) 14694–14697.
- [78] M. J. Mehl and D. A. Papaconstantopoulos, "Applications of a tight-binding total-energy method for transition and noble metals: Elastic constants, vacancies, and surfaces of monatomic metals." *Phys. Rev. B* **54** (1996) 4519–4530.
- [79] B. Meyer, "Entwicklung eines neuen ab-initio "mixed-basis"-Pseudopotentialprogrammes und Untersuchung atomarer Fehlstellen in Molybdän und intermetallischen Verbindungen." PhD thesis. Universität Stuttgart, 1998.
- [80] B. Meyer, F. Lechermann, C. Elsässer, and M. Fähnle, *FORTTRAN 90 program for mixed-basis pseudopotential calculations for crystals*. Max-Planck-Institut für Metallforschung, Stuttgart.
- [81] D. R. Hamann, M. Schlüter, and C. Chiang, "Norm-Conserving Pseudopotentials." *Phys. Rev. Lett.* **43** (1979) 1494–1497.
- [82] D. Vanderbilt, "Optimally smooth norm-conserving pseudopotentials." *Phys. Rev. B* **32** (1985) 8412–8415.
- [83] J. Perdew, K. Burke, and M. Ernzerhof, "Generalized Gradient Approximation Made Simple." *Phys. Rev. Lett.* **77** (1996) 3865–3868.
- [84] J. P. Perdew, K. Burke, and M. Ernzerhof, "ERRATA: Generalized Gradient Approximation Made Simple." *Phys. Rev. Lett.* **78** (1997) 1396.
- [85] O. Sinanoğlu, "A principle of linear covariance for quantum mechanics and the electronic structure theory of molecules and other atom clusters." *Theor. Chim. Acta* **65** (1984) 233–242.
- [86] L. E. Ballentine and M. Kolar, "Recursion, non-orthogonal basis vectors, and the computation of electronic properties." *J. Phys. C: Solid State* **19** (1986) 981.

- [87] E. Artacho and L. M. del Bosch, "Nonorthogonal basis sets in quantum mechanics: Representations and second quantization." *Phys. Rev. A* **43** (1991) 5770–5777.
- [88] M. Head-Gordon, P. E. Maslen, and C. A. White, "A tensor formulation of many-electron theory in a nonorthogonal single-particle basis." *J. Chem. Phys.* **108** (1998) 616–625.
- [89] D. Sánchez-Portal, E. Artacho, and J. Soler, "Projection of Plane-Wave Calculations into Atomic Orbitals." *Solid State Comm.* **95** (1995) 685–690.
- [90] D. Sánchez-Portal, E. Artacho, and J. Soler, "Analysis of atomic orbital basis sets from the projection of plane-wave results." *J. Phys.: Condens. Matter* **8** (1996) 3859–3880.
- [91] O. F. Sankey and D. J. Niklewski, "Ab initio multicenter tight-binding model for molecular-dynamics simulations and other applications in covalent systems." *Phys. Rev. B* **40** (1989) 3979.
- [92] B. Lange, C. Freysoldt, and J. Neugebauer, "Construction and performance of fully numerical optimum atomic basis sets." *Phys. Rev. B* **84** (2011) 085101.
- [93] E. Francisco, L. Seijo, and L. Pueyo, "The maximum overlap method: A general and efficient scheme for reducing basis sets. Application to the generation of approximate AO's for the 3d transition metal atoms and ions." *J. Solid State Chem.* **63** (1986) 391–400.
- [94] G. K. H. Madsen, E. J. McEniry, and R. Drautz, "Optimized orthogonal tight-binding basis: Application to iron." *Phys. Rev. B* **83** (2011) 184119.
- [95] A. Urban, M. Reese, M. Mrovec, C. Elsässer, and B. Meyer, "Parameterization of tight-binding models from density functional theory calculations." *Phys. Rev. B* **84** (2011) 155119.
- [96] E. Artacho, D. Sánchez-Portal, P. Ordejón, A. García, and J. M. Soler, "Linear-Scaling ab-initio Calculations for Large and Complex Systems." *Phys. Status Solidi (b)* **215** (1999) 809–817.
- [97] J. Junquera, O. Paz, D. Sánchez-Portal, and E. Artacho, "Numerical atomic orbitals for linear-scaling calculations." *Phys. Rev. B* **64** (2001) 235111.
- [98] E. Anglada, J. M. Soler, J. Junquera, and E. Artacho, "Systematic generation of finite-range atomic basis sets for linear-scaling calculations." *Phys. Rev. B* **66** (2002) 205101.
- [99] A. H. Larsen, M. Vanin, J. J. Mortensen, K. S. Thygesen, and K. W. Jacobsen, "Localized atomic basis set in the projector augmented wave method." *Phys. Rev. B* **80** (2009) 195112.
- [100] G. Lippert, J. Hutter, P. Ballone, and M. Parrinello, "Response Function Basis Sets: Application to Density Functional Calculations." *J. Phys. Chem.* **100** (1996) 6231–6235.

- [101] E. R. Margine, A. N. Kolmogorov, M. Reese, M. Mrovec, C. Elsässer, B. Meyer, R. Drautz, and D. G. Pettifor, “Development of orthogonal tight-binding models for Ti-C and Ti-N systems.” *Phys. Rev. B* **84** (2011) 155120.
- [102] L. Goodwin, A. J. Skinner, and D. G. Pettifor, “Generating Transferable Tight-Binding Parameters: Application to Silicon.” *Europhys. Lett.* **9** (1989) 701–706.
- [103] W. Press, B. Flannery, S. Teukolsky, and W. Vetterling, “Fortran Numerical Recipes: The Art of Scientific Computing.” 2nd ed. Vol. 1. Cambridge University Press, 1992 992.
- [104] T. Williams, C. Kelley, and many others, *Gnuplot 4.4: an interactive plotting program*. <http://gnuplot.sourceforge.net/>.
- [105] M. J. Mehl and D. A. Papaconstantopoulos, “Tight-binding study of high-pressure phase transitions in titanium: Alpha to omega and beyond.” *Europhys. Lett.* **60** (2002) 248–254.
- [106] D. R. Trinkle, M. D. Jones, R. G. Hennig, S. P. Rudin, R. C. Albers, and J. W. Wilkins, “Empirical tight-binding model for titanium phase transformations.” *Phys. Rev. B* **73** (2006) 094123.
- [107] N. Börnsen, B. Meyer, O. Grotheer, and M. Fähnle, “E cov - a new tool for the analysis of electronic structure data in a chemical language.” *J. Phys.: Condens. Matter* **11** (1999) L287.
- [108] G. Bester and M. Fähnle, “Interpretation of ab initio total energy results in a chemical language: I. Formalism and implementation into a mixed-basis pseudopotential code.” *J. Phys.: Condens. Matter* **13** (2001) 11541.
- [109] R. Peierls, “More Surprises in Theoretical Physics.” Princeton University Press, 1991 126.
- [110] H. A. Jahn and E. Teller, “Stability of Polyatomic Molecules in Degenerate Electronic States. I. Orbital Degeneracy.” *P. Roy. Soc. Lond. A Mat.* **161** (1937) 220–235.

Curriculum vitae

Name	Alexander Urban
Date of birth	July 26, 1983
Place of birth	Duisburg, Germany

Education

2008–2012	PhD student in the group of Bernd Meyer at the ICMM, Department of Chemistry, Friedrich–Alexander–Universität Erlangen–Nürnberg, Germany
2011 Oct–Dec	Visiting PhD student in the group of Nicola Marzari, École Polytechnique Fédérale de Lausanne, Switzerland
2006–2008	Master of Science (Chemistry), Ruhr-Universität Bochum, Germany
2003–2006	Bachelor of Science (Chemistry), Ruhr-Universität Bochum, Germany

Honors

since 2009	Member of the Graduate School Molecular Science (GSMS), Friedrich–Alexander–Universität Erlangen–Nürnberg, Germany
2009–2012	Kekulé fellowship of the <i>Fonds der Chemischen Industrie</i>
2008	Wilke prize of the <i>Verein zur Förderung der Chemie und Biochemie</i> , Ruhr–Universität Bochum, Germany